TWO PHASE FLOW ANALYSIS IN ELECTROCHEMICAL MACHINING FOR L-SHAPED TOOL: A CFD APPROACH

A thesis
Submitted by

Usharani Rath
(211ME2202)

In partial fulfillment of the requirements
for the award of the degree of

Master of Technology
In
Mechanical Engineering
(Production Engineering)

Department of Mechanical Engineering
National Institute of Technology Rourkela
Orissa -769008, India
June 2013

TWO PHASE FLOW ANALYSIS IN ELECTROCHEMICAL MACHINING FOR L-SHAPED TOOL: A CFD APPROACH

A thesis
Submitted by

Usharani Rath
(211ME2202)

In partial fulfillment of the requirements
for the award of the degree of

Master of Technology
In
Mechanical Engineering
(Production Engineering)

Under The Guidance of
Dr. C.K. Biswas

Department of Mechanical Engineering
National Institute of Technology Rourkela
Orissa -769008, India
June 2013

NATIONAL INSTITUTE OF TECHNOLOGY
ROURKELA – 769008, ORISSA
INDIA

This is to certify that the thesis entitled, "TWO PHASE FLOW ANALYSIS IN ELECTROCHEMICAL MACHINING FOR L-SHAPED TOOL: A CFD APPROACH" submitted by **Usharani Rath** in partial fulfillment of the requirement for the award of **Master of Technology** degree in **Mechanical Engineering** with specialization in **Production Engineering** at the National Institute of Technology, Rourkela is an authentic work carried out by her under my supervision and guidance. To the best of my knowledge, the matter embodied in the thesis has not been submitted to any other University/Institute for the award of any degree or diploma.

Research Guide

Place: Rourkela

Date:

Dr. C.K. Biswas
Associate Professor
Department of Mechanical Engineering
NIT Rourkela

ACKNOWLEDGEMENTS

First and foremost, I would like to thank the almighty for his blessings without which I may not be able to reach at this juncture of life. My parents have played a major role in my career and their unparalleled love and support has been a major inspiring force till this moment.

I am deeply indebted to **Dr. C.K. Biswas,** my advisor and guide, for the motivation, guidance, tutelage and patience extended throughout the research work. I appreciate his broad range of expertise and attention to even minute detail, as well as the constant encouragement he has given me over the year.

I am grateful to **Prof. K.P. Maity**, Head, Department of Mechanical Engineering for his valuable suggestions during my project work and the unyielding support over the year.

I am also very grateful to **Mr. Kunal Nayak**, for supporting me a lot during my experimental work.

Last but not the least, my friends, **Mr. Chinmaya Mishra and Mr. Shailesh Dewangan,** played a pivotal role during both computational studies and finalizing the thesis work

USHARANI RATH

ABSTRACT

Electrochemical machining (ECM) is a non-conventional machining process based on the principle of reverse electroplating. Some genuine characteristics like negligible tool wear, high precision machining in difficult to cut materials, lower thermal and mechanical stress on work piece etc. makes ECM advantageous over other non-conventional machining processes. Still there are some challenges in ECM like generation of hydrogen bubbles and its effect on Material Removal Rate (MRR), complexity of tool geometry and its effect on various process parameters, prediction of electrolyte flow pattern and its impact etc.

In the present study, three dimensional two phase flow pattern of ECM process has been simulated using Computational Fluid Dynamics (CFD) in three different L-shaped tool models. The software used for the analysis was ANSYS 13.0 CFX. Various process parameters like volume fraction profile, velocity profile, and turbulent pattern of electrolyte flow in the Inter Electrode Gap (IEG) etc. have been evaluated from the simulated environment in all the three models. The results indicated generation of hydrogen bubbles in all three cases which in turn reduced the volume fraction of brine at varied rate depending upon the tool geometry. Reduced brine volume fraction led to reduction in MRR. It was also inferred that the same would affect the surface finish as well. As a result of hydrogen bubble formation, temperature towards the boundaries were increased rapidly as gaseous hydrogen bubbles possess sufficiently lower convective heat transfer coefficient as compared to liquid brine. Similarly, the results of static pressure and velocity profiles across tool work piece interface provided a varying pattern depending upon the tool geometry. For validating the simulation results, a set of experiments have been carried out on ECM by fabricating the three tool geometries. The experimental results were analyzed by using MINITAB 16 software.

Key Words: Computational Fluid Dynamics; Convective Heat Transfer; Electrochemical Machining; Electrolyte; Two Phase Flow

TABLE OF CONTENTS

Title **Page No**

LIST OF TABLES

Title **Page No.**

LIST OF FIGURES

Title **Page No.**

ABBREVIATIONS

ECD	Electrochemical Drilling
STEM	Shaped Tube Electrolytic Machining
DAROC	Depth Averaged Radial Overcut
PECM	Pulse Electrochemical Machining
CAE-ECM	Computer Aided Engineering System for ECM
FDM	Finite Difference Method
FEM	Finite Element Method
BEM	Boundary Element Method
FLC	Fuzzy Logic Control
EMM	Electrochemical Micromachining
CFD	Computational Fluid Dynamics
SOFC	Solid Oxide Fuel Cell
LCMM	Localized Collocation Meshles Method
ANOVA	Analysis of Variance

NOMENCLATURES

α_G	Gas volume fraction
ρ_G	Density of gas phase.
$\vec{u}_{\mathrm{G}}$	Velocity of gas phase.
CG	Diffusion coefficient (used for equation of mass conservation).
DG	Diffusion coefficient (used for equation of momentum)
α_L	Liquid volume fraction
Γ	Source of mass per unit volume depending on the phase change on the cathode.
$\vec{u}_{\mathrm{L}}$	Velocity of liquid phase.
μ_L	Viscosity coefficient of liquid phase
ρ_{mix}	Density of combined phase
$\vec{u}_{\mathrm{mix}}$	Velocity of combined phase
ρ_L	Density of liquid phase.
P	Pressure.
Q'	Volume flow rate
A	Area of flow
v	Velocity of flow
J	Current density
y	Inter Electrode Gap
k	Thermal conductivity
Q	Heat generated in the IEG
I	Current

CHAPTER I

Introduction

1.1 OVERVIEW OF ECM PROCESS

Electrochemical machining (ECM) is a non-conventional machining process based on the principle of electrolysis and hence it can be called as the reverse process of electroplating or anodizing. Thus ECM can be thought of a controlled anodic dissolution at atomic level of the electrically conductive work-piece by a desired shaped tool due to flow of high current at relatively low potential difference through an electrolyte which is quite often water based neutral salt solution. ECM is one of advanced machining technologies and has been applied in highly specialized fields, such as aerospace, aeronautics, defence and medical industries [1]. In recent years, ECM is used in other industries such as automobile and turbo-machinery because of its various advantages. Some genuine characteristics like negligible tool wear, high precision machining in difficult to cut materials, lower thermal and mechanical stress on work piece etc. makes ECM advantageous over other non-conventional machining processes. Still there are some challenges in ECM like generation of hydrogen bubbles and its effect on Material Removal Rate (MRR), complexity of tool geometry and its effect on various process parameters, prediction of electrolyte flow pattern and its impact etc. which have been investigated by various researchers. In case of complicated shapes of work-piece it's very difficult to know the machining variables distribution within the inter electrode gap (IEG). By studying the flow pattern of electrolyte, we can predict the machining variable distribution accurately and thus can avoid the passivation which is the major problem in ECM in complicated shape cases. Again, two phase effect (hydrogen bubble generation) has a major role on the machining variables as well as on the material removal rate and surface roughness. The flowing electrolyte collects the evolving hydrogen gas generated at the cathode. The presence of hydrogen in the electrolyte reduces the specific conductivity of the solution and thereby the overall effect is a reduced MRR and a deterioration of the surface finish. So we need to study the sources, effects and pattern of hydrogen bubble generation and its impact on various critical parameters and overall machining performance. So, these are the motivating factors behind this project work.

1.2 MACHINING SET UP AND CRITICAL PARAMETERS

1.2.1 Electrochemical Machining Set Up

Electrochemical Machining (ECM) is the controlled removal of metal by anodic dissolution in an electrolytic cell in which the work piece is the anode and the tool is cathode. The electrolyte is pumped through the gap between the tool and the work piece, while direct current is passed through the cell, to dissolve metal from the work piece. Thus the ECM set up comprises of several components which is clearly seen in the figure 1.1

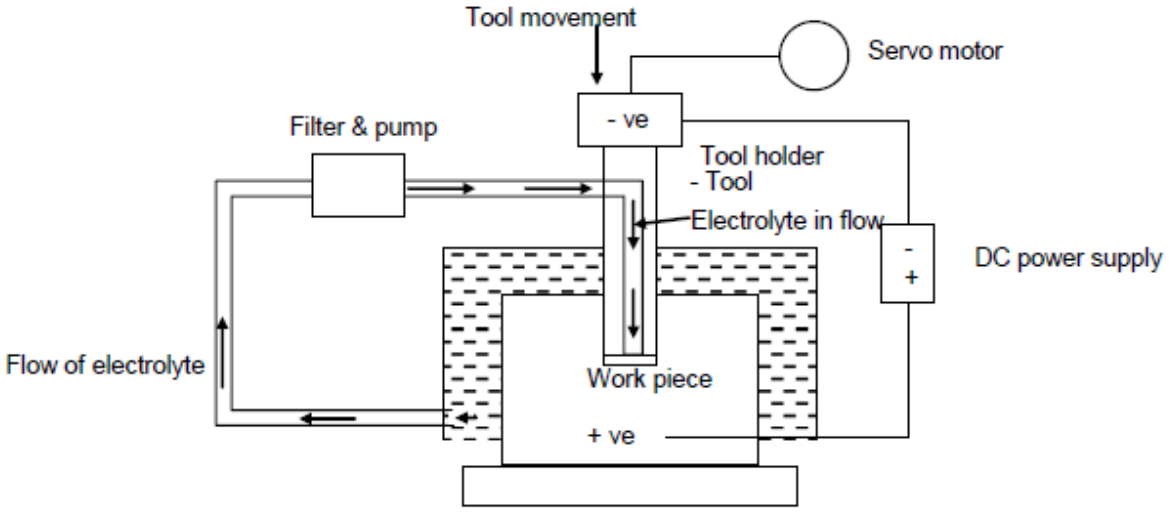

Fig. 1.1: Electrochemical machining set-up

1.2.1.1 Work-Piece

In electrochemical machining, work-piece is a conducting material and acts as an anode. This anode is connected with the positive terminal of the direct current (DC) power supply. The selective anodic dissolution will remove the material from the work-piece in the presence of pressurized electrolyte between the electrodes in a pre-set temperature. Generally materials with very high value of hardness or a very low value of machinability are used as work-piece materials in ECM, because it removes material independent of the hardness.

1.2.1.2 Tool

Tool which acts as cathode is connected to the negative terminal of the DC power supply. No tool wear makes ECM advantageous over other machining methods. During the machining, the tool is given a downward motion, so that the work-piece tends to take the shape of the tool and at a steady state the inter-electrode gap is uniform. Generally tool is made with copper, brass, stainless steel etc. Proper allowances are given for avoiding the taper and over cut etc.

1.2.1.3 Electrolyte

Electrolyte is a conducting fluid that plays a very vital role in ECM. An electrolyte in ECM performs three basic functions as follows

1. Completing the electrical circuits and allowing the large currents to pass,
2. Sustaining the required electrochemical reactions,
3. Carrying away the heat generated the metal sludge and the waste products.

The first function requires the electrolyte, ideally, to have a large electrical conductivity. The second function requires the electrolyte to be such that at the anode the work-piece material is continuously dissolved, and a discharge of the metal ion on the cathode should not occur. Generally, the cationic constituent of the electrolyte is hydrogen, ammonia, or alkali metals. The dissolution of the anode should be sustained at a high level of efficiency. Also, the electrolyte must have a good chemical stability. Apart from all these, the electrolyte should be inexpensive, safe, and as noncorrosive as possible. Generally, an aqueous solution of the inorganic compound is used. Table 1.1 lists the electrolytes used for various types of alloys.

Table.1.1: Types of electrolytes

Sl. No	Alloy	Electrolyte
1	Iron based	Chloride solutions in water (mostly 20% NaCl)
2	Ni based	HCl or mixture of brine and H_2SO_4
3	Ti based	10% hydrofluoric acid+10% HCl+10% HNO_3
4	Co-Cr-W based	NaCl
5	WC based	Strong alkaline solutions

1.2.1.4 Power Supply

DC power supply is required with low value of voltage and high value of current. Current of the order of 1000-40,000 A is generally required and 5-25 V is applied to overcome the resistance at the gap.

1.2.1.5 Pumps

Single or multi-stage centrifugal pumps are used in ECM set up. A minimum flow rate of Litres/ min is required for each 1000 A. Electrolyzing current is generally required. A pressure of 5-30 kg/cm^2 may be sufficient for most of the requirements of ECM application.

1.2.1.6 Filtration and Storage Tanks

Generally, small particles of grit, metal, plastics and products of machining are present in the electrolyte which may cause interference in the machining process thereby affecting the parameters of machining. Therefore, the filtration of electrolyte is required to prevent these particles from entering the machining gap and producing any harmful effect. These filters get clogged and need cleaning once in 30 hrs. For better results, we can use more than one filter.

1.2.1.7 Valves and Pipings

The control valves and piping which supply electrolyte to the ECM tooling, must not introduce any foreign matter into the electrolyte which will be applied to the machining gap. Stainless steel is the most suitable material for valves and Piping. Materials like fibre glass and reinforced plastics can be used with some degree of success.

1.2.1.8 Servo System

The servo system controls the tool motion relative to the work piece to follow the desired path. It also controls the gap width within such a range that the discharge process can continue. If tool moves too fast and touches the work piece, short circuit occurs. Short circuit contributes little to material removal because the voltage drop between electrodes is small and the current is limited by the generator. If tool electrode moves very slowly, the gap becomes too wide and electrical discharge never occurs. Another function of servo system is to retract the tool electrode when deterioration of inter electrode gap condition is detected. The width cannot be measured during machining; other measurable variables are required for servo control.

1.2.2 Critical Parameters

1.2.2.1 Tool Feed Rate

In ECM process, an inter electrode gap of about 0.01 to 0.07 mm is maintained between the tool and work piece. For smaller gap, the electrical resistance between the tool and work-piece is least and the current is the maximum and accordingly maximum metal is removed. The tool is feed in to the work-piece depending upon how fast the metal is to be removed. The movement of the tool slide is controlled by a hydraulic cylinder giving some range of feed rate.

1.2.2.2 Electrolyte Flow Rate

Electrolyte flow is a very important and critical parameter in the analysis of electrochemical machining. Insufficient and improper electrolyte flow in the IEG may cause poor machining. The effect of cavitation, stagnation, and vortex flow can avoid up to a certain extent by avoiding sharp corner. The entire flow path has an approximate radius of 0.7 to 0.8 mm. Flow will not cover all area of the work-piece initially. These difficulties can be avoided by using restriction techniques. Fig. 1.2 shows a tool with no sharp corners.

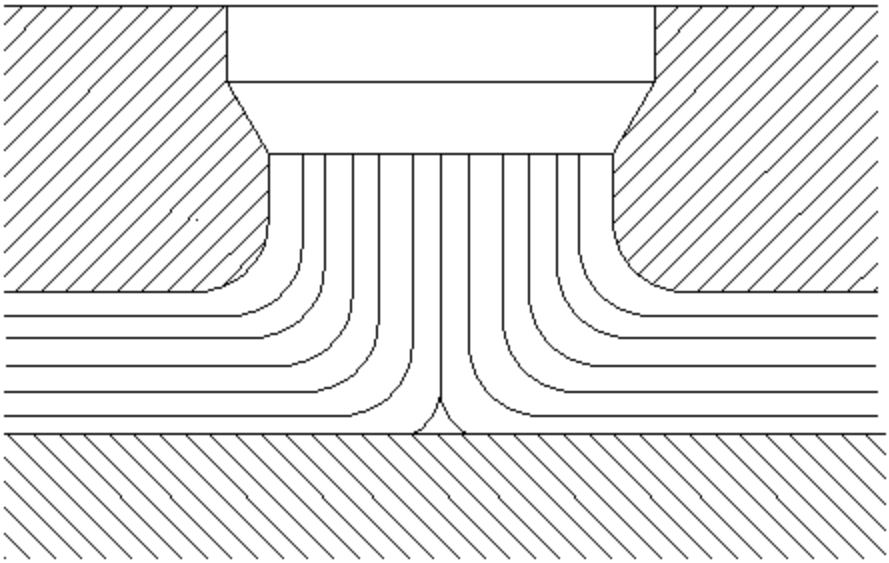

Fig.1.2: Tool with no sharp corners

1.2.2.3 Material Removal Rate

Material removal rate (MRR) is the rate at which the work-piece material is dissolved per unit time. It is primarily a function of feed rate which signifies the current passed between the work-piece and the tool. As the tool advances towards work, inter electrode gap decreases and current increases which cause more metal removal at a rate corresponding to the tool advance. A stable spacing between the tool and work is thus established. It may be noted that high feed rate not only is productive but also produces best quality of surface finish. However feed rate is limited by removal of hydrogen gas and products of machining. Metal removal rate is lower with low voltage, low electrolyte concentration and low temperature.

MRR in case of electrochemical machining is based on the principle of electrolysis which is given by Michel Faraday. Faraday proposed two laws of electrolysis.

According to the first law "The amount of chemical change produced by an electric current, that is, the amount of any material dissolved or deposited, is proportional to the quantity of electricity passed".

According to the second law "The amounts of different substances dissolved or deposited by the same quantity of electricity are proportional to their chemical equivalent weights".

Quantitatively, the Faraday's law (MRR in electrochemical machining) is given by the formula 1.1.

$$m = ItA/\rho FZ \quad (1.1)$$

If the work-piece or anode is an alloy instead of pure metal then metal removal rate can be found out by considering the rate required to remove a unit volume of each element. If atomic weight and the valences are A_1, A_2, $A3$ etc. and Z_1, Z_2, Z_3 etc. respectively and composition by weight of the alloy x_1% of alloy 1, x_2 % of alloy 2 etc. then a volume v cm_3 of the alloy contains $v\rho x_i/100$ gram of the i_{th} element. Charge required to remove the entire i_{th} element in the volume v is given by the Equation 2.2.

$$Q = 100/\rho F\left(\frac{1}{\sum i\left(\frac{X_i Z_i}{A_i}\right)}\right) \quad (1.2)$$

In actual ECM process many factors affects the material removal rate. But the theoretical removal rate based on divalent dissolution only. When the current is more, sometimes the dissolution takes place at higher potential and trivalent dissolution is also happening. Therefore theoretical value tends to be more than actual one. Sometimes dissolution valance is also affecting the material removal rate. For example in the case of copper dissolved in chloride solution in monovalent form and in nitrate solutions it is in the divalent state. The primary advantages of the processes involving material removal rate are that they hardly cause certain undesirable surface effects which occurs in conventional machining processes. The main advantages are that they produce stress free machining, burr free surfaces, reduced tool wear and elimination of thermal damage to the work-piece. These processes have no effect on physical and mechanical properties such as yield strength, ultimate tensile strength, ductility, hardness etc.

1.2.2.4 Tool Design

As no tool wear takes place, any good conductor can be used as a satisfactory tool material, but it must be strong enough to withstand the hydrostatic force, caused by the electrolyte being forced at high velocity through the gap between the tool and work-piece. The tool is made hollow for drilling holes so that electrolyte can pass along the bore within the tool. Cavitation, stagnation and vortex formation in electrolyte flow must be avoided because these result a poor surface finish. It should be given such a shape that the desired shape of job is achieved for the given machining condition. Both external and internal geometries can be machined with an electrochemical machine. Copper is often used as the electrode material. Brass, graphite, stainless steel and copper-tungsten are also used because of their ability to be easily machined, non-corroding nature.

1.2.2.5 Temperature Control

The temperature of the electrolyte must be constant so that variation in conductivity will not occur. If the temperature of the electrolyte is low it means lower rate of metal removal and if it is higher, it may lead to the vaporization of the electrolyte which can cause the formation of hydrogen bubbles. Therefore temperature of electrolyte must be maintained between 25° and 60°.

1.2.2.6 Voltage Drop

For electrochemical reaction to take place, voltage required is around 2 to 30V. This applied voltage is necessary to overcome the potential drop or voltage drop between the electrodes and is shown in the Fig. 1.3[2]. This potential drop consists of the following four types.

i) Electrode potential

Electrode potential is nothing but cathode and anode potential.

ii) Over voltage due to activation polarization

The minimum potential difference needed to break the equilibrium condition or steady state to start current flow in the circuit is called activation polarization.

iii) Concentration polarization

Ions are accumulated near the electrodes and they act as a barrier. The extra voltage required for breaking this barrier is called concentration polarization.

iv) Ohmic overvoltage.

Thin films formed in the electrodes during the machining because of the impurities will offer extra resistance. This effect is called ohimc overvoltage.

v) Ohmic resistance of electrolyte.

Electrical resistance offered by the electrolyte is called ohmic resistance of electrolyte.

This is the main voltage drop obey Ohm's law.

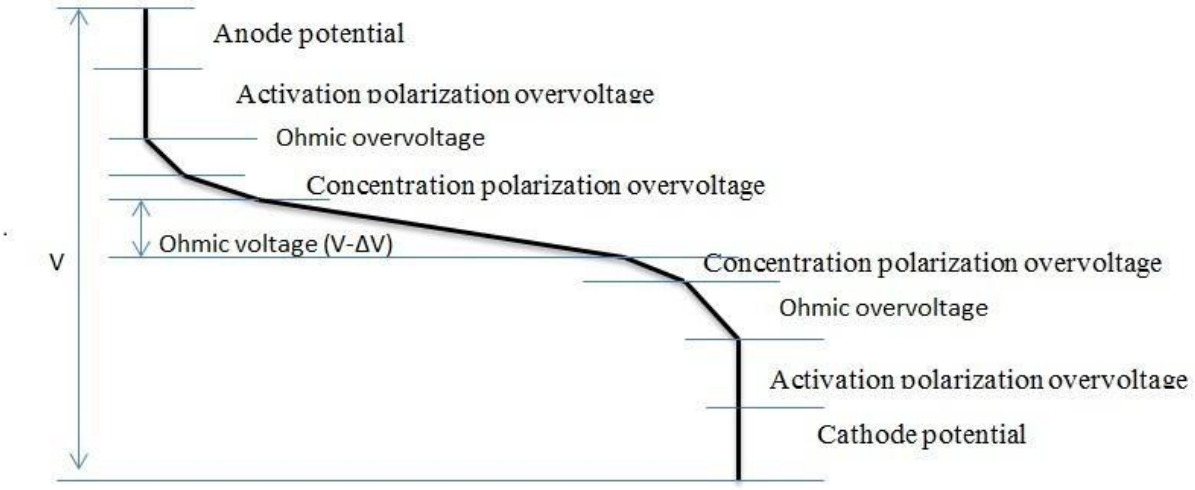

Fig. 1.3: Potential drop profile in ECM process [2]

1.2.2.7 Surface Finish

Electrochemical machining process can produce surface finish of the order of 0.4 µm by movement of tool. Any defect on tool face produces replica on the work piece surface. Tool surface should therefore be polished. The finish is better in harder materials. For optimum surface finish, careful electrode design, maximum feed rate, and surface improving additives in electrolyte are selected. Low voltage decreases the equilibrium machining gap and results in better surface finish and tolerance control. Low electrolyte concentration decreases the machining gap and gives a better surface finish. Low electrolytic temperature also promotes better surface finish.

1.2.2.8 Three Phase Effect

Three phase effect is nothing but an effect produced because of the combination of three separate phases in the electrolyte such as brine solution, hydrogen bubbles and metal sludge. Hydrogen bubbles are produced because of the electrochemical reaction taking place at the cathode and also because of the boiling of the electrolyte due to improper flow. Metal sludge is the precipitation of metal produced. Hydrogen bubbles have more impact on the critical parameters of machining rather than metal sludge. So, care must be taken in order to decrease

the amount of hydrogen bubbles and metal sludge. The generation of hydrogen gas at cathode during the electrochemical reaction is shown by the figure 1.4.

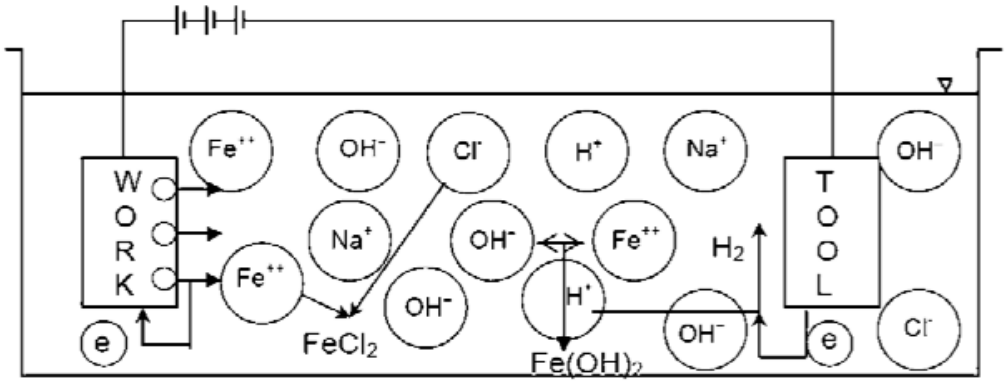

Fig .1.4: Schematic representation of ECM process showing hydrogen bubble generation

1.2.3 Characteristics of ECM Process

The characteristics of electrochemical machining process is given by the table 1.2

Table 1.2: ECM specification

Tool	Copper, brass or steel
Power Supply	Constant voltage 5-25 DC voltage
Current	50-40,000 A
Material Removal Rate	1600 mm^3/min
Specific Power Consumption	7 W/mm^3/min
Electrolytic Solution	Neutral salt, brine solution
Accuracy and surface finish	0.02 mm, 0.4µm
Application	Machining hard materials
Limitation	High specific energy consumption
Mechanical properties	Stress free machining, reduced tool wear
Surface properties	No thermal damage

1.3 WORKING PRINCIPLE

Electrochemical machining process is developed on the principles of Faradays and Ohm. In this process, an electrolytic cell is formed by the anode (work piece) and the cathode (tool) in the midst of a flowing electrolyte. The metal is removed by the controlled dissolution of the anode according to the well-known Faradays laws of electrolysis. When the electrodes are connected to about 20 V DC electric supply source, flow of current in the electrolyte is established due to positively charged ions being attracted towards cathode and negatively charged ions towards anode. Due to electrolysis process at cathode hydroxyl ion are released which combine with the metal ions of anode to form insoluble metal hydroxide. Thus the metal is removed in the form of sludge and precipitated in electrolytic cell. This process continues till

the tool has produced its shape on the work piece surface. The principle and process detailing of ECM for steel is shown in Figures 1.5.

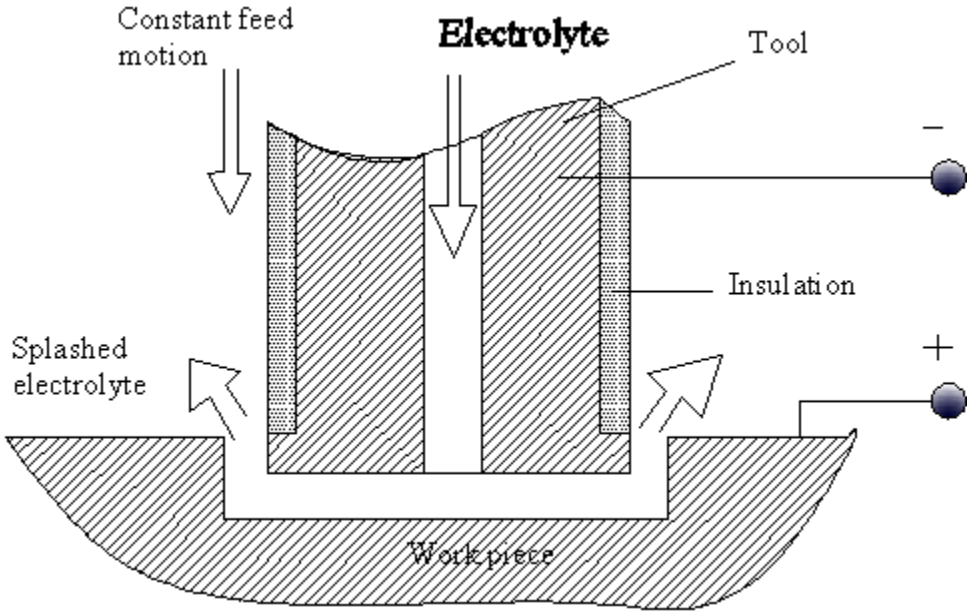

Fig. 1.5: Schematic diagram of the principle of electrochemical machining process

Let us take an example of machining of low carbon steel which is primarily a ferrous alloy mainly containing iron. For electrochemical machining of steel, generally a neutral salt solution of sodium chloride (NaCl) is used as the electrolyte. The electrolyte and water undergoes ionic dissociation as shown below as potential difference is applied.

Reactions occurring at the anode are given as

$$Fe \leftrightarrow Fe^{2+} + 2e^{-}$$

$$Fe^{2+} + 2Cl \leftrightarrow FeCl_2$$

$$Fe^{2+} + 2OH^{-} \leftrightarrow Fe(OH)_2$$

$$FeCl_2 + 2OH^{-} \leftrightarrow Fe(OH)_2 + 2Cl^{-}$$

$$2Cl^{-} \leftrightarrow Cl_2 \uparrow + 2e^{-}$$

$$2FeCl_2 + Cl_2 \leftrightarrow 2FeCl_3 \downarrow$$

$$H^{+} + Cl^{-} \leftrightarrow HCl$$

$$2Fe(OH)_2 + H_2 + O_2 \leftrightarrow 2Fe(OH)_3 \downarrow$$

$$Fe(OH)_3 + 3HCl \leftrightarrow FeCl_3 + 3H_2O$$

$$FeCl_3 + 3NaOH \leftrightarrow Fe(OH)_3 \downarrow + 3NaCl$$

Reactions occurring at the cathode are given as

$$Na^+ + e^- \leftrightarrow Na$$

$$Na + H_2O \leftrightarrow NaOH + H^+ \uparrow$$

$$2H^+ + 2e^- \leftrightarrow H_2 \uparrow$$

The above reaction shows that only hydrogen gas is evolved at cathode and there is no deposition on the tool. This generated hydrogen gases give rise to the two phase effect affecting the overall machining performance of ECM which is to be studied through this project work.

1.4 ADVANTAGES OF ECM

1. There is no mechanical stress impact on the processed work-piece.
2. There is no thermal impact of the work piece.
3. The material removal rate is independent of the hardness and toughness of the material.
4. There is no process related tool wear.
5. There is great versatility for machining of geometrical complex shapes.
6. During machining process, there is no burr formation.

1.5 LIMITATIONS OF ECM

1. High specific energy consumption is desired.
2. It is not suited for non-conducting pieces.
3. It has high initial and working cost.

1.6 APPLICATIONS OF ECM

ECM is widely used in machining of jobs involving intricate shapes and to machine very hard or tough materials those are difficult or impossible to machine by conventional machining. It is now frequently used for the machining of aerospace components, critical deburring, Fuel injection system components, ordnance components etc.

1. It is used for die sinking, profiling, contouring, grinding, drilling, trepanning
2. It is most suitable for manufacturing various types of dies and moulds.
3. It can be used for making complex shapes of turbine blades.
4. ECM is used for making polishing of gun barrels etc.

Various ECM processes are shown in the figures 1.6, 1.7, 1.8 and 1.9.

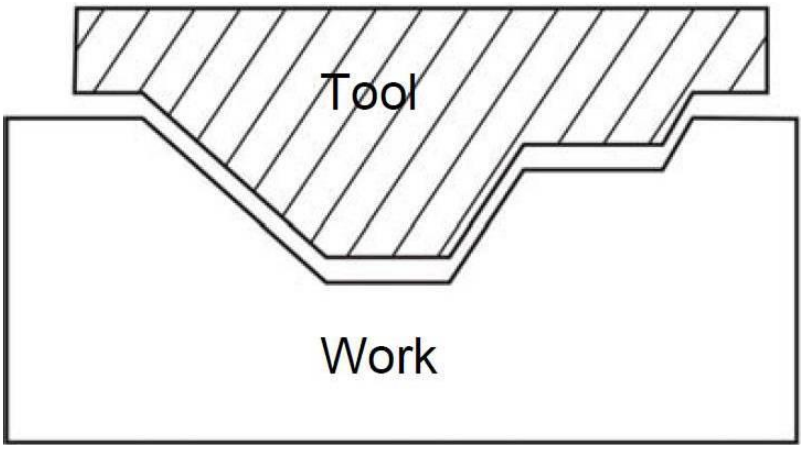

Fig.1.6: Die sinking operation

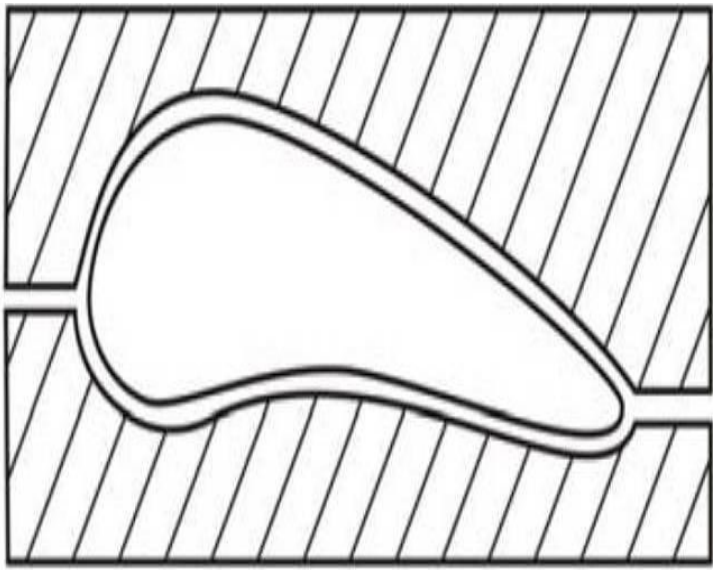

Fig. 1.7: 3D profiling operation

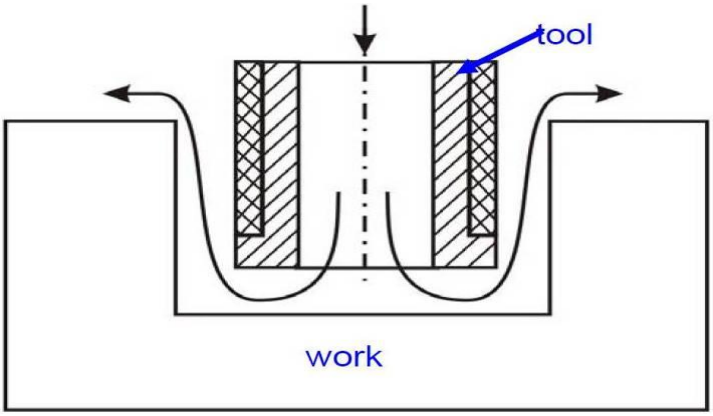

Fig. 1.8: Drilling operation

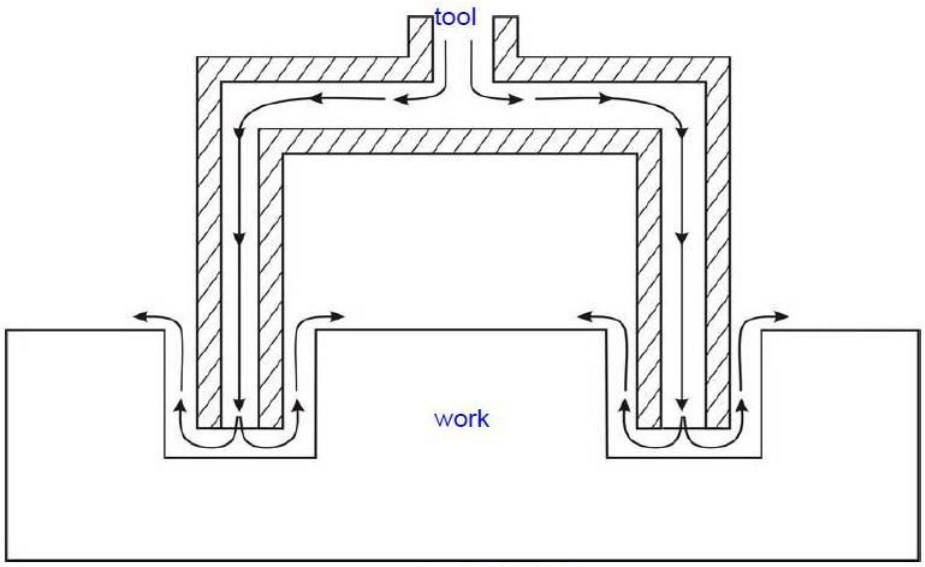

Fig. 1.9: Trepanning operation

1.7 SAFETY IN ECM

The electrochemical machining of metals is associated with a lot of risk factors. The effect of the toxic gases and aerosols produced in the course of ECM.

1. Chemical attack by electrolytes.

2. The risk of an electric shock.

3. The danger of a burn in the case of a short circuit between the positive and negative leads.

4. Mechanical factors.

5. The danger of a fire damp explosion.

6. The effects of the electromagnetic field.

The gases and aerosols produced in the course of ECM, when inhaled, may cause severe injuries to the internal organs. They may also produce an overall poisoning and local irritations.

1.8 ORGANIZATION OF THESIS

This first introductory chapter deals with the overview of electrochemical machining along with its principles. It also focussed on the critical parameters, materials and structure of the machining set up. It also discussed various advantages, disadvantages and applications of ECM. Safety precautions were also included in this chapter to avoid any risk factor during machining operations.

The second chapter deals with the literature reviews which is based on the previous research works done by various researchers, scholars etc. It gives us a basic idea regarding the type of research, extent of flexibility, validation of work, accuracy of results, use of materials in my project fields that is ECM and CFD. After exhaustive literature studies, the scope and objective of the proposed study can be identified and predicted accurately and satisfactorily.

The third chapter deals with the computational modelling of the selected shape of the geometrical system of tool & work-piece. It includes the formation of geometry by selecting appropriate dimensions with the help of design modeller. After the formation of geometry, meshing is done with the appropriate mesh size by conducting the grid independence study. Then the meshed model is allowed for run by giving a certain convergence criteria.

The fourth chapter discusses the experimental work done for this selected geometry. It covers the selection of tool and work-piece materials, procurement of tool material, entire fabrication process of tool, fabrication of work-piece. After the complete fabrication of tool and work-piece, machining is done in ECM.

The fifth chapter presents various results obtained from the above computational modelling as well as the experimental work done with the selected desired geometry. These results show the critical parameters of machining and the effect of hydrogen bubbles on these critical parameters.
The experimental results are plotted with the help of MINITAB 16 software which shows the effect of critical parameters on MRR.

The sixth chapter deals with the summary and conclusions of the present work

CHAPTER 2

LITERATURE REVIEW

An exhaustive literature survey has been carried out on electrochemical machining. The research and studies on ECM started a long back on 1969. A few of this research works is presented in this chapter. The review can be divided into various modules or sub-reviews such as parameters of ECM, experimentation on ECM, Modelling on ECM, ECM using CFD and CFD in other fields. Based on this important review papers, scope and objective of the present study is established.

2.1 ECM PARAMETERS

Neto et al. [3] suggested the study of the intervening variables in electrochemical machining (ECM) of SAE-XEV-F Valve-Steel. A prototype developed at the Federal University of Uberlandia was used. The material removal rate (MRR), roughness and over-cut were investigated. Feed rate, electrolyte, flow rate of the electrolyte and voltage are the parameters thoses are varied during the experiment. The intervening factors of the work-piece accuracy are shown by the figure 2.1. Forty-eight experiments were carried out in the equipment developed. Two electrolytic solutions were used such as sodium chloride (NaCl) and sodium nitrate (NaNO3). The results show that feed rate is the main parameter affecting the MRR. The electrochemical machining with sodium nitrate presented the best results of surface roughness and overcut. It has been seen that MRR increases with tool feed rate because of the decrease in machining time. NaCl results higher MRR than $NaNO_3$ as NaCl solution is a non-passivator electrolyte and has constant current efficiency.$NaNO_3$ electrolyte resulted in better surface roughness and overcut as compared to NaCl electrolyte as shown by the figure 2.2.

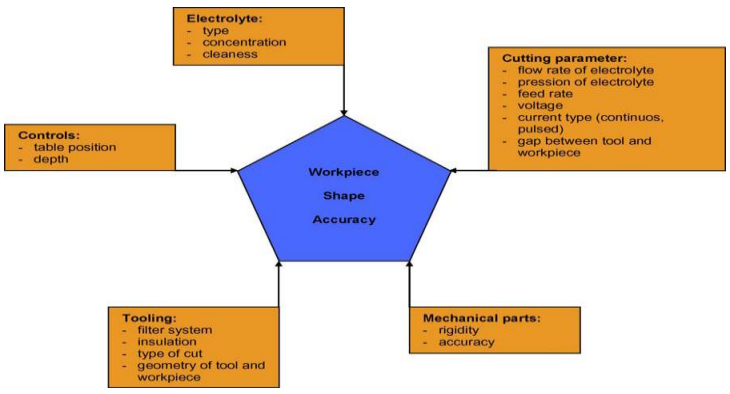

Fig. 2.1: Intervening factors in the work-piece accuracy [3]

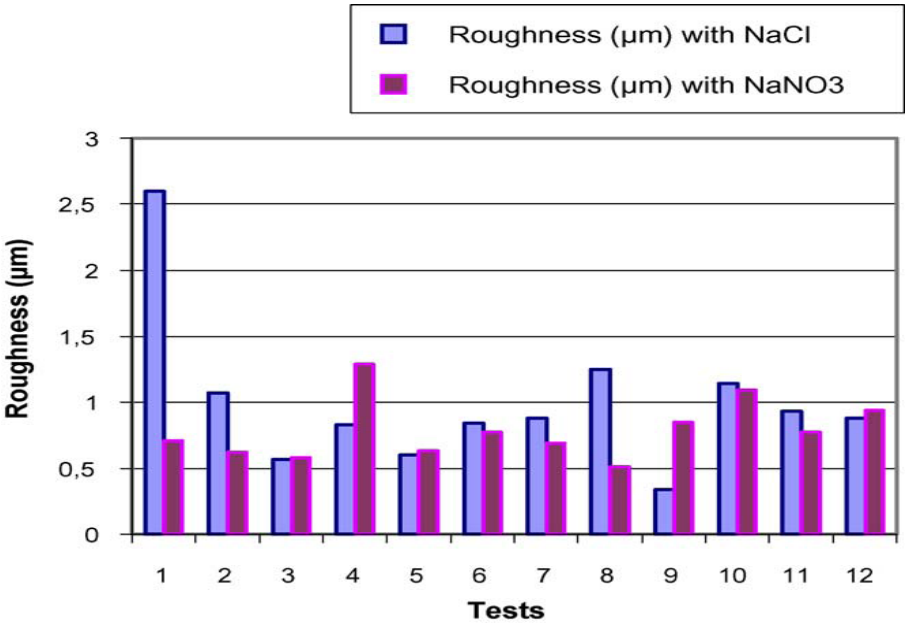

Fig. 2.2: Comparative study of roughness between NaCl and $NaNO_3$ [3]

Mukherjee et al. [4] in his paper Suggested that Material removal rate (MRR) of aluminium work piece has been obtained by electrochemical machining using NaCl electrolyte at different current densities. It has been observed that resistance of the electrolyte solution decrease sharply with increase in current density values. Initially, the over-voltage of the system increases and attains a saturation value with increasing current densities as shown in figure 2.3. The MRR, determined experimentally, becomes similar to the theoretical value with Al^{3+} state. On the other hand, taking into account over-voltage, MRR comes out be 72%. It appears that removal of a fraction of aluminium occurs in Al^{+} which subsequently gets converted into Al^{3+} through a series of chemical reaction.

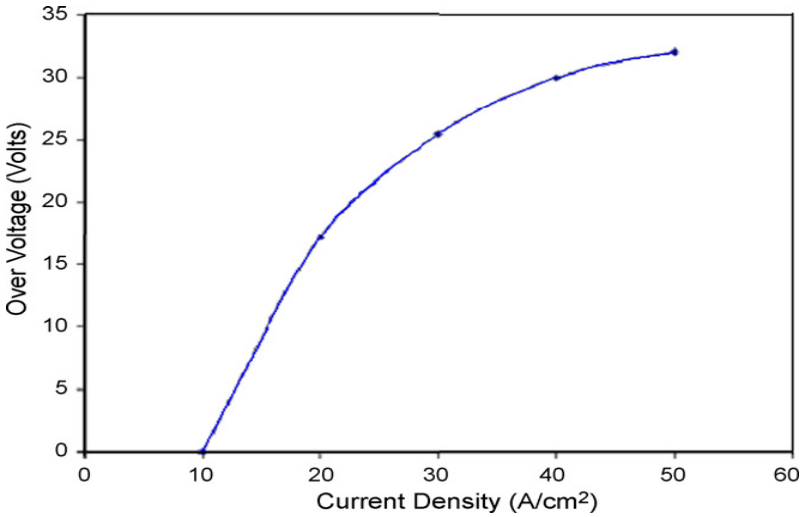

Fig. 2.3: Plot of current density against over-voltage. *A*= 26.97, *Z*=3, *V*=40V, *F* = 96500, *K*= 0.184Ohm−1 cm−1,*T*=20◦C and *f* = 0.000667 cm/s (fixed) [4].

Theoretical material removal rate for given valency was calculated by Eq.(2.1) and is shown in Fig. 2.4(a) for different current densities.

$$\text{MRR} = {}^{AI}/_{ZF} = (\frac{26.97}{3})\frac{1}{96500} I \text{ g/s} \quad (2.1)$$

Experimental material removal rate is determined by machining the pure aluminium work piece with brass tool having circular completely flat surface and is shown in Fig. 2.4(b). The corrected current density was calculated as

$$\text{Ic} = \text{VcKc} \quad (2.2)$$

Where *I*c is the corrected current density, *K*c is the conductivity = 1/*R*c, where (*R*c is the corrected specific resistance). And corresponding corrected material removal rate (MRRc) was calculated by Eq. 2.3 is shown in Fig. 2.4(c).

$$\text{MRRc} = 0.0000932 \text{ Ic g/s} \quad (2.3)$$

The efficiency of MRRc to MRRth (material removal rate theoretical) is determined by Eq. (2.4).

$$\text{Efficiency} = \text{MRR}_C / \text{MRR}_{th} \quad (2.4)$$

This comes out to be 72%.

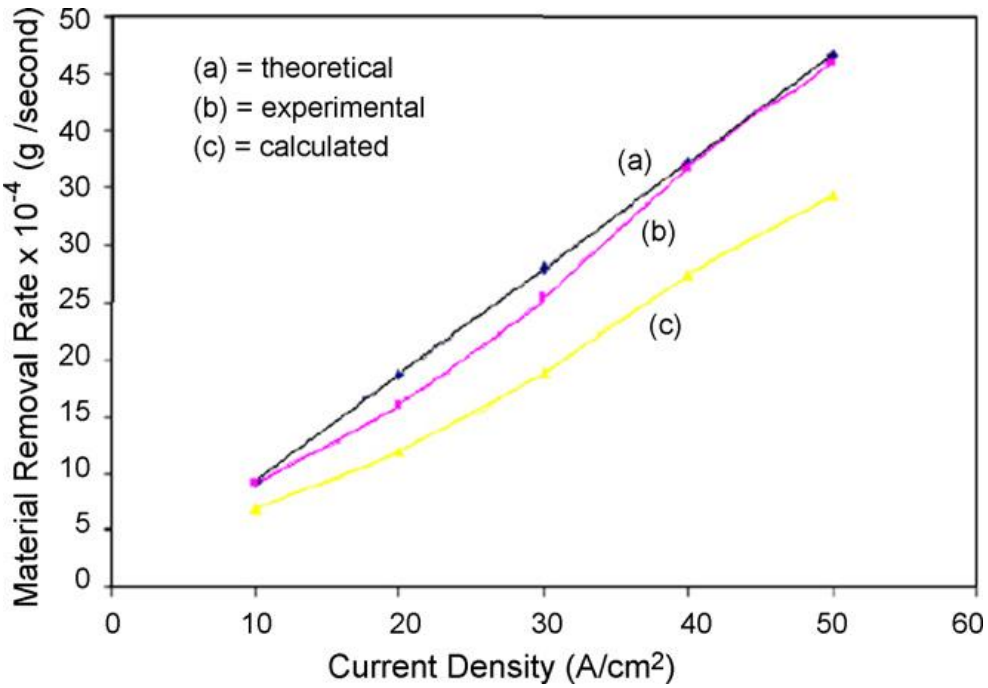

Fig. 2.4: Plot of material removal rate against current density [4]

Jain et al. [5] in his paper suggested that electrochemical drilling is a complex phenomenon involving two phase fluid dynamics, heat transfer at unsteady state etc. taking place in between moving boundaries. Therefore prediction and determination of the work-piece shape is always difficult. These models are difficult and complicated because they ignore the analysis of the stray current attack zone and stagnation zone. A modified anode shape prediction model has been proposed which can predict the zones like stagnation, front, transition, side, and stray current attack. Computational and experimental anode profiles suggest a satisfactory agreement between the two. For the prediction of a complete anode profile, and to develop a comprehensive tool design procedure for electrochemical drilling (ECD), a study of the stray current zone and the stagnation zone as shown in figure 2.5 becomes unavoidable. The two dimensional finite element model STZFET-22 used in this study is capable of predicting an anode profile in all the five zones identified in an electrochemically drilled hole. This method is also capable of designing tools for electrochemical drilling. The accuracy of the correction method depends upon the accuracy of the anode shape prediction model. Any inaccuracy in anode shape prediction model will be reflected as the poor accuracy in the designed tool profile.

.

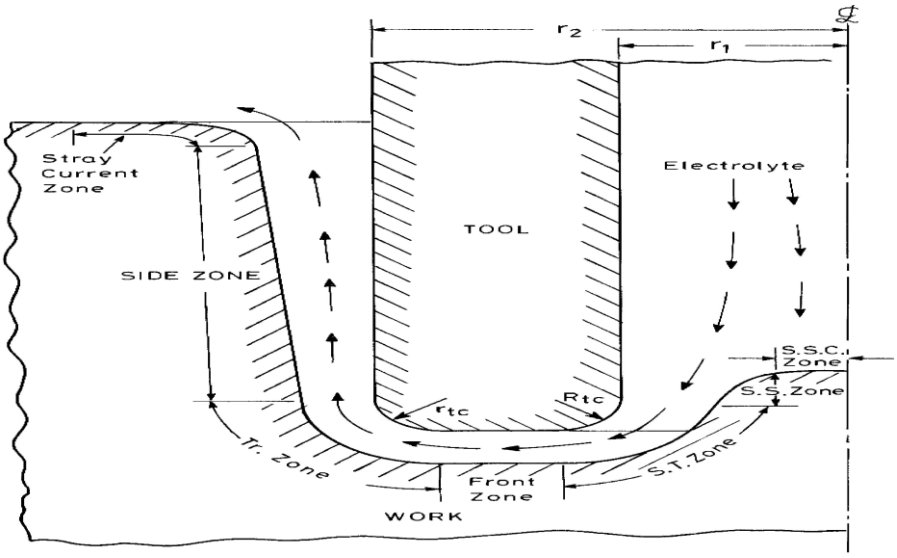

Fig. 2.5: Various zones identified in electrochemical drilling [5]

2.2 EXPERIMENTATION ON ECM

Davydov et al. [6] determined experimentally the limiting diffusion currents for the anodic dissolution of tungsten rotating disc electrode in alkaline solution under rectangular current pulses. In aqueous solutions, a WO_3 anodic film, which passivates the metal and hinders its dissolution, is formed on tungsten surfaces. This film is highly soluble only in alkaline solutions; therefore, a high rate of electrochemical dissolution of tungsten occurs only in these solutions. Consequently, all processes, which are based on the anodic dissolution of tungsten and are of practical importance, are conducted in alkaline solutions. This is true for electrochemical machining, electrochemical polishing and etching, and the processing of metal tungsten scrap. The anodic dissolution of tungsten proceeds according to the overall reaction as given in the equation 2.5. The anodic dissolution of tungsten in alkaline medium is improved because of the use of bipolar voltage pulses. Application of bipolar potential pulses enhances the anodic dissolution of tungsten in alkali due to the hydrogen bubble evolution during the cathodic half period; these bubbles stir the solution in the vicinity of the electrode and raise the anodic current. There is an optimal value of cathodic pulse amplitude for increasing the rate of tungsten dissolution under bipolar voltage pulses.

$$W+8OH^- \rightarrow WO_4^{2-}+4H_2O+6e^- \qquad (2.5)$$

Bilgi et al. [7] in his paper suggested that shaped tube electrolytic machining (STEM) as shown in the figure 2.6, is a versatile and relatively low cost process that can drill deep as well as high aspect ratio holes. Radial overcut is very important from the dimensional accuracy point of view as the radius of a drilled hole can be found out by summing up the tool radius and radial

overcut. But, overcut models till now are very rare and have been used only as shallow holes. Again, these models are very much restricted in broader aspect as these are purely empirical. A fundamental mathematical model that uses STEM operating parameters (voltage, tool diameter and feed rate, bare tip length and electrolyte composition) as inputs to predict radial overcut has been developed. The proposed radial overcut model is giving much similar results with the experimental data in comparison with the literature. This study formulates a methodology to determine the magnitude of current flowing radially from the bare tip length using total current values those are measured experimentally. Depth-averaged radial overcut (DAROC) is a more appropriate parameter for overcut in deep holes and the variation of DAROC with bare tip length is shown in the figure 2.7.

.

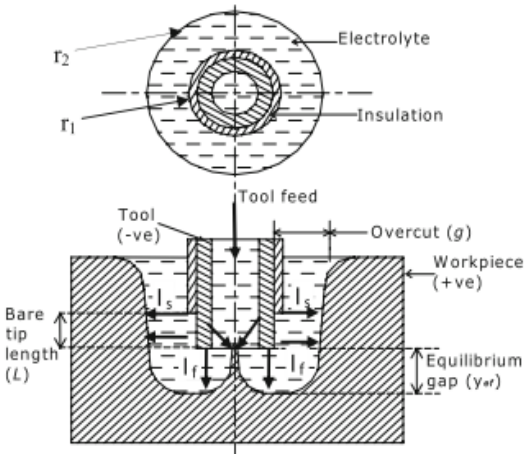

Fig. 2.6: Schematic diagram of STEM [7]

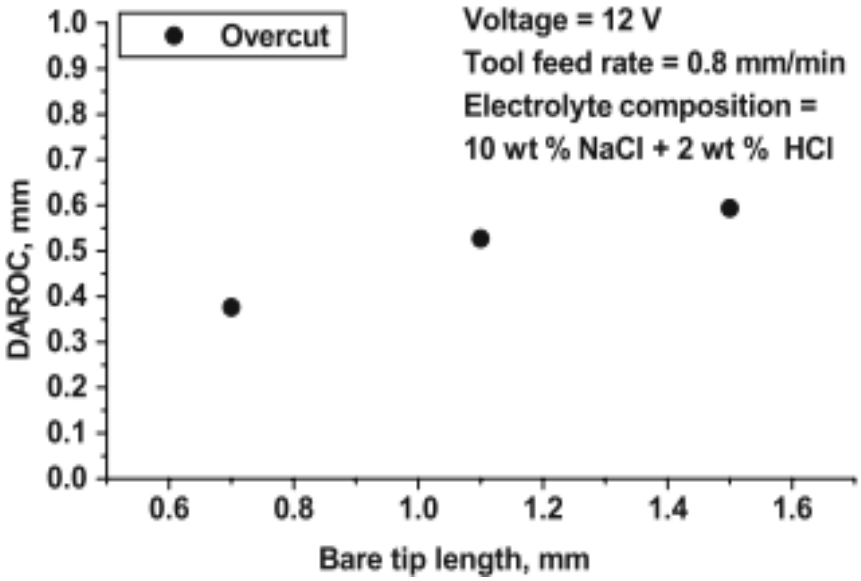

Fig. 2.7: Variation of DAROC with bare tip length [7]

Hocheng et al. [8] suggested that electrochemical machining is recognized for its potential of machining complicated shapes, but the precision of the profile machined is a concern of its application. In this paper, processes those involve machining in the micrometer range are analyzed. Both theoretical and computational models are described to demonstrate how the machined profile generates as the time passes. The fundamental laws of electrolysis and the integral of a finite-width tool are the basic concept behind this. Effect of experimental variables such as time of electrolysis, voltage, molar concentration of electrolyte and electrode gap on the MRR and diameter of machined hole is discussed. Experimental results show that MRR increases with increase in the values of electrical voltage, molar concentration of electrolyte, time of electrolysis and reduced initial gap as shown in the figures (2.8-2.10). The time of electrolysis is the most influential factor on the produced diameter of hole. The iteration integral method well simulates the development of the machined profile with elapsed time. The simulation agrees with the experimental results.. The produced diameter of hole can be controlled mostly with machining time, while other conditions apply mild effects.

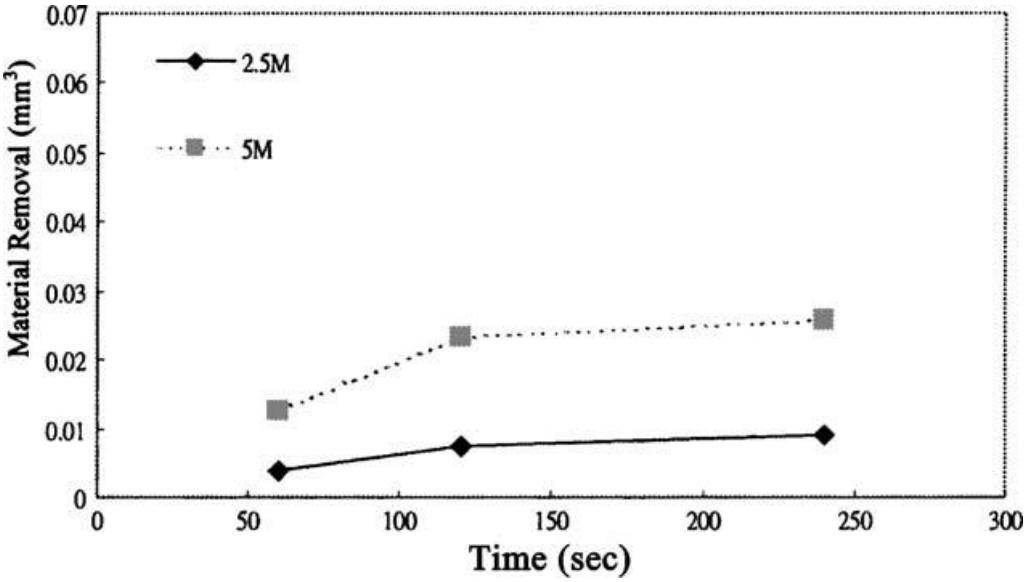

Fig. 2.8: Effect of machining time on material removal rate [8]

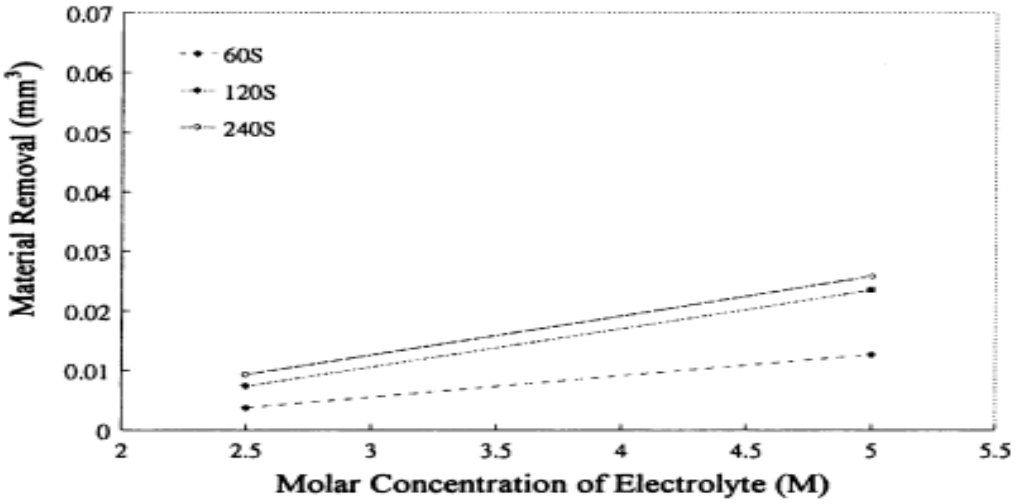

Fig. 2.9: Effect of electrolyte concentration on material removal [8]

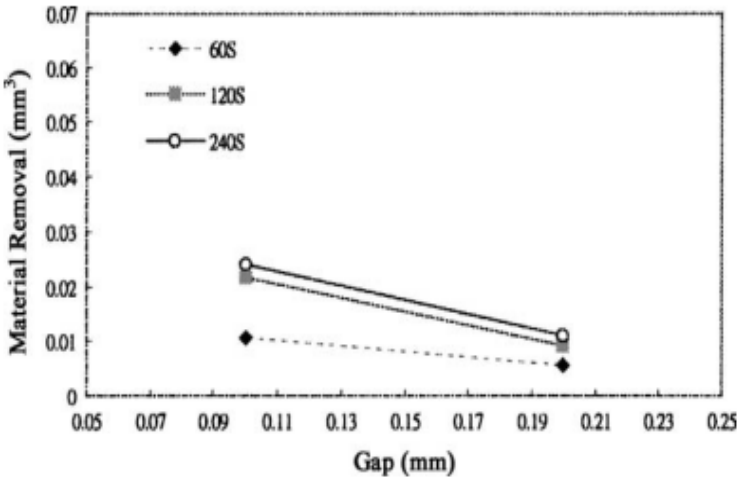

Fig. 2.10: Effect of initial gap on material removal [8]

Clifton et al. [9] suggested that during electrochemical machining, the dependency of IEG with time and process parameters can be utilized to determine process characteristics of ECM process and to describe the shape of the work-piece surface relative to the tool surface. Process variables are defined to map out the required gap-time function which requires the use of time-consuming iterative trials. Process control and tool to work-piece transfer characteristics can be achieved without the requirement to generate such parameter maps by in-line monitoring of the gap. The use of ultrasound used as a passive, nonintrusive and in-line gap measurement system for ECM can be explored from this work. The experimental sensor/ECM cell configuration, in which the ultrasound transmit/receive transducer, a CLF4 (Buehler Krautkramer Ltd) piezoelectric/Perspex delay line system operating at a frequency of 15 MHz, is sprung loaded against the lower face of the work-piece is shown in the figure 2.11. The accuracy of this

technique was confirmed through correspondence between the generated gap-time and current time data and theoretical models applicable to ideal conditions. Gap measurements are also used to demonstrate and quantify the degree of departure from ideal behavior for an In718/chloride system as the electrolyte flow rate is reduced from 16 to 41 min^{-1}. When determining the shape convergence under ideal conditions, for the example case of a 2D sinusoidal profile, the use of ultrasound has also been proven to be effective. One significant advantage of this approach is that it should be possible to extend these measurements to the non-ideal conditions which often apply in practical ECM, due to the need for long flow path length and multi-flow fields.

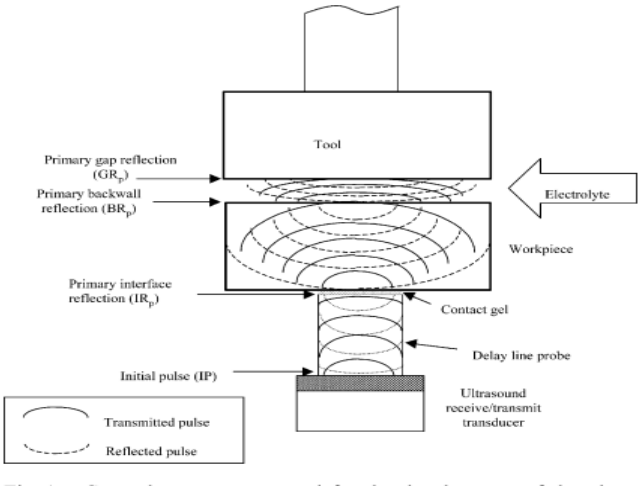

Fig. 2.11: General arrangement used for the development of the ultra-sonic gap measurement system [9]

Smet et al. [10] proposed that during the pulse electrochemical machining (PECM) process, simulation of the species concentrations can provide vital information on system design and guidelines for its real time use. Due to mutual dependencies, the concentrations can be calculated simultaneously with the temperature in the case of detailed numerical calculations. The pulses that are given to the PECM system need to be described on a timescale that can be orders of magnitude less than the physical timescales in the system. The time accurate calculation of the variable distributions evolutions in PECM can become computationally very expensive, if the full details of the applied pulses have to be taken into account. A different approach is used by time averaging the pulses applied to the system. Performing this, the time steps used during the calculations are no longer dictated by the pulse characteristics. The assumptions of the models, used to derive the analytical solutions, are very much strict for real-life ECM conditions. The results also apply very well as practical rules of thumb, when using the hybrid technique during complex numerical calculations.

Pa [11] suggested that process of ultrasonic aided electrochemical finishing using a low-cost high efficiency electrode requires no expensive special purpose equipment or high material removal as that in case of conventional ECM. Surface roughness can be improved rapidly by this newly developed technique of ECM. In the current study, the electrochemical finishing is categorized into electrochemical smoothing and electro-brightening. Higher electrical current is not required when an effective plate-shape electrode is used to reduce the response area. For various turning operations including profiling, form turning, and flute and thread cutting, this process can be used. Through simple equipment attachment, electrochemical smoothing and electro-brightening can follow the cutting on the same machine and chuck. There are some controlled factors that include the chemical composition and concentration of the electrolyte, the initial gap width, and the flow rate of electrolyte. Current density, rotational speed of the work-piece, on/off period of pulsed current, frequency and power level of ultrasonic, and the electrode geometry are taken as the experimental parameters. Smaller end radius and smaller angle of declination are associated with higher current density and provides larger discharge space and better polishing effect. The equipment of electro-polishing includes DC power supply, pulse generators, pump, flow meter, electrolytic & ultrasonic tank, and filter as shown in the figure 2.12. The electrode of inclined plane with slant discharge flute performs the best. The average effect of the ultrasonic is better than the pulsed current while the machining time needs not to be prolonged by the off-time. It was found that electro-brightening after precise turning needs quite a short time to make the work-piece smoothing and bright, and the electrochemical smoothing saves the need for precise turning, making the total process time less than the electro-brightening.

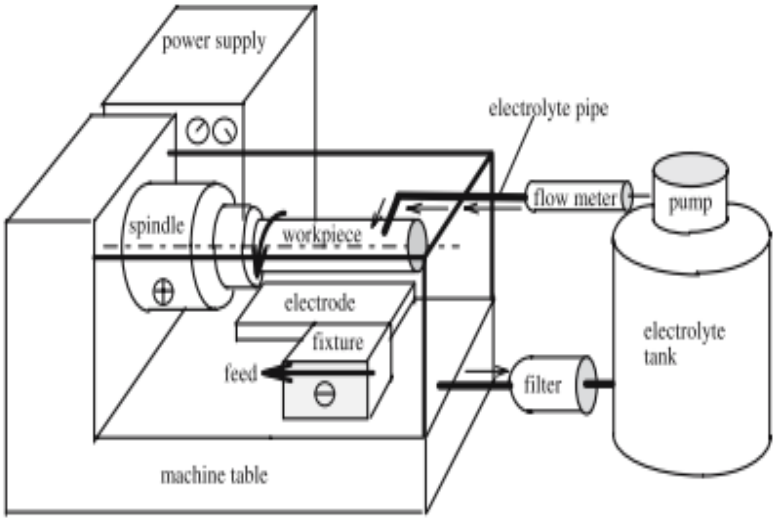

Fig. 2.12: Experimental set-up for electro-polishing [11]

Zhitnikov et al. [12] suggested about the transient processes occurring in electrochemical machining that lead to stationary, self-similar or other modes. These modes can be applied for a limited time to a part of the surface during a process. The problem is formulated as a Hele-Shaw problem. To solve it, highly specialized analytical-numerical method was developed and used. The singularities of the solution are eliminated by representing it as the sum of a known

function that includes the singularities and an unknown function without singularities. The unknown functions are determined by splines and a Schwarz integral. This method differs from the usual ones by using analytical solutions of the Hele-Shaw problem to obtain the partial time derivative of the work-piece-surface coordinates. It allows raising the accuracy up to order 3 and limit the rate of computational time increase to n^2 (n is the number of nodes). Moreover, it allows control of the node positions, thus increasing the stability of the numerical solution. The choice of the parametrical domain shape (a strip) and removing the singularities of the solution also improve the method.

.

Ramaswamy et al. [13] proposed that any surface generated by a manufacturing process bears a number of 'scars' due to the inherent nature of the process. In case of electro discharge machining process, very high temperature generated and the quenching effect of the dielectric at the end of each discharge lead to the formation of a hard and brittle white layer. To improve the functionality of the component/part, it is necessary to remove the defects introduced by a manufacturing process. To study the effect of parameters of electrochemical polishing on the 3D surface texture parameters of EDM surfaces of tool steel specimens is the objective of this paper. A dominating effect due to the direct current of the cell is observed, and there is a limiting value of the IEG for any given value of current density. A high influence of the interactive effect of current density and electrode gap is also observed. To meet the in-service requirements, this information would be very useful in selecting the appropriate magnitude of the process parameters in order to engineer the surface. This is because, 3D surface texture parameters, and the volume parameters can give quantitative information with respect to the functionality of a surface, such as the load bearing and fluid retention capabilities as well as running in wear etc.

2.3 MODELLING IN ECM

2.3.1 Finite Element Method And Finite Difference Method

Filatov et al. [14] carried out the machining of a two dimensional surface by ECM where the electrolyte in the machining gap is simulated as the two phase continuum-mixture of an incompressible fluid and gas. For a two dimensional domain, the system of unsteady conservation equations, averaged across the IEG is proposed. This equation was solved by finite difference method. Unsteady technological factors affecting the accuracy of ECM is studied. Mathematical simulation of ECM is needed for controlling the process and fast

designing the cathode tool and optimizing the technological parameters when ECM works in a pulsing mode, vibration of cathode tool is used frequently to increase the processing accuracy, and program of voltage switching on and off can be coordinated with a mode of vibration.

It is assumed that part of the processed component surface to be taken in investigation is bounded by closed continuous contour L. Part L1 of the contour is the feeding section, the electrolyte inlet in the working gap. Part L2 of the contour L is the place of electrolyte outlet from the working space. Part L3 is impermeable or semi-impermeable.

Mount et al. [15] in his paper suggested that the analysis of current transients during electrochemical machining at a planar work-piece planar tool configuration gives rise to the determination of the vital parameters for the ECM process. These are used in finite difference simulation of the ECM process, which allows simulation of the current transients and tool and work-piece configurations at any time for non-planar configurations that can be utilized for industrial ECM. Variation of the combined ECM parameter with current and electrolyte flow path length is observed due to Small differences in the simulated and experimentally observed current transients. These variations were measured for In718 by current transient analysis of experimental data obtained from the ECM of a planar work-piece planar segmented tool configuration. Using this configuration, variations in valency have also been measured for SS316. This information has then been used to improve the finite difference simulation. To increase the accuracy of both materials characterization and process simulation in ECM, this approach is used .The schematic of the configuration used in this study is shown by the figure 2.13. At slower flow rates and higher ECM currents, the consumption and production of ions during ECM would be expected to change significantly the composition of the electrolyte, which may result in variation in the ECM parameters along the flow path. In order to study this, a planar segmented tool system has been constructed, as shown in Figure 2.14.

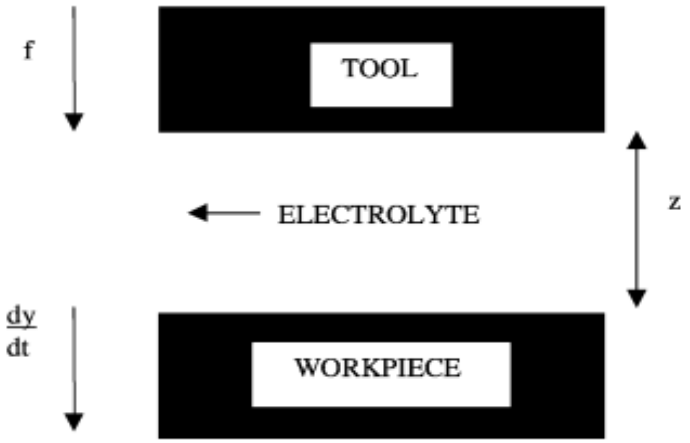

Fig. 2.13: Configuration of ECM [15]

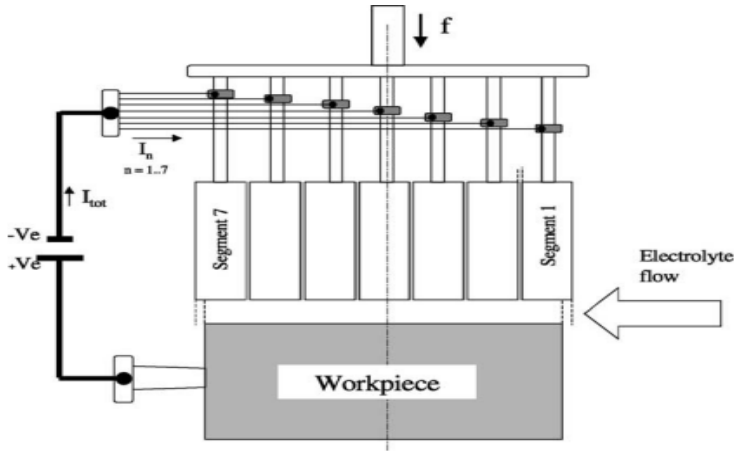

Fig. 2.14: The planar segmented tool-planar work-piece system [15]

Kozak [16] suggested that electrochemical machining is an important manufacture technology to machine difficult-to-cut and hard materials and to shape complicated contours and profiles with high MRR without any tool wear and residual stress. This paper presents the physical and mathematical models on the basis of which of the simulation process module in the computer-aided engineering system for ECM (CAE-ECM) has been developed. The jobs relating to this purpose can be reduced directly or indirectly to a problem searching for a boundary of the area within which the machining i.e. to a value boundary problem (moving boundary problem, free boundary problem or inverse boundary problem) is carried out. The CAE-ECM system is based on the conventional concepts of the expert system, i.e. the user interface, knowledge base, working data base and inference engine. Also used are the concepts of CAE/CAD/CAM system in the synthetic part of the CAE-ECM. Various numerical techniques including the finite difference method FDM, the finite element method FEM and the boundary element method BEM are used to solve different problems in electrochemical manufacturing using the CAE-ECM system. The general structure of CAE/ECM structure is shown in the figure 2.15.

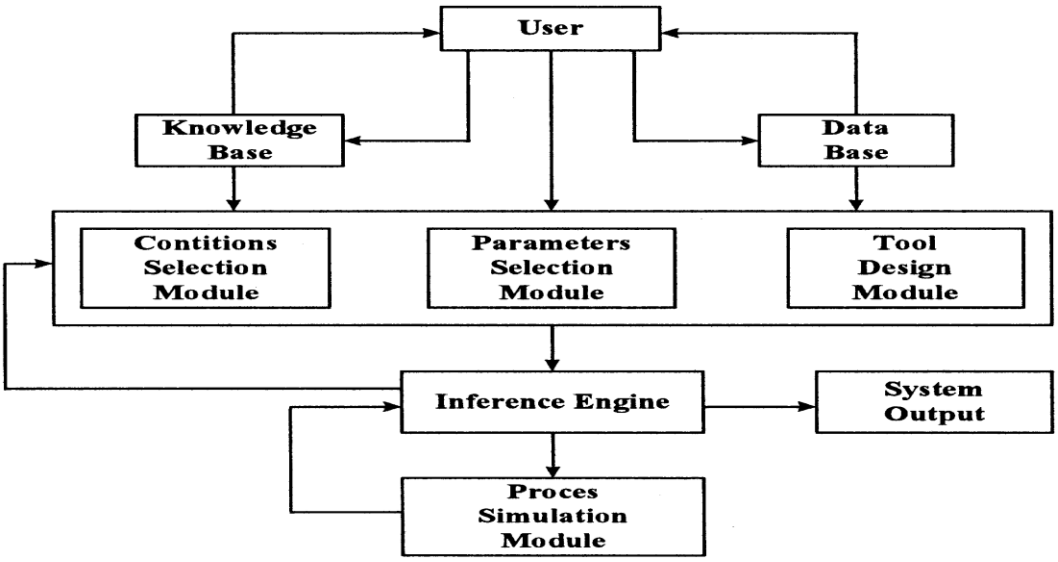

Fig. 2.15: Architecture of CAE/ECM software [16]

Kozak et al. [17] suggested a mathematical model along with the results of computer simulation with a spherical tool-electrode. Experimental investigations of electrochemical machining were also done. The experimental investigations were carried out in order to investigate the influence of working voltage, velocity of electrode displacement, initial IEG size, tool-electrode cross feed and electrode radius on removed material excess thickness, machined surface height of waviness, surface roughness and metal removal rate. Accuracy of computer simulation evaluated by differences between results of experimental tests and computer simulation depends on accuracy of a preliminary estimation of electrochemical machining coefficient, total over potential of electrode processes, electrical conductivity of electrolyte, etc. The results of application of neural network were used to predict the height of surface waviness and thickness of removed allowance which depend on setting parameters of electrochemical machining. Thus it was established that, the developed software for simulation of the ECM process with universal spherical tool-electrode and trained neural networks are useful for process analysis, machined surface prediction and optimization.

2.3.2 Boundary Element Method

Purcar et al. [18] suggested a general applicable numerical method for the simulation of 3D electrode shape changes obtained during electrochemical machining processes based on the "marker" method. The electrode shape change is found by displacing each node proportional

with, and in the direction of the local current density according to Faraday's law. The local growth rate is obtained by numerically solving the potential model using the boundary element method. Results related to 3D electrochemical machining of the letter "E" are presented. The electrode shape change is found by displacing each node in proportional with and in the direction of local current density according to Faraday's laws. The local growth rate is obtained by numerically solving the potential model using the boundary element method. In order to compute the current density distribution at the electrodes a numerical method is applied. When the BEM is applied, only the domain surfaces need to be discretized. Another advantage, in particular for electrochemical systems, is that the current density distribution along the electrodes is a direct unknown of the problem, rather than a variable that has to be computed afterwards from the derivative of the potential field perpendicularly to the electrodes. This implicates that the BEM is the more accurate method to solve potential problems, compared to the FEM and the FDM.

Bortels et al. [19] suggested new and general applicable simulation software for three dimensional ECM calculations. The software is fully integrated within the CAD package SolidWorks and enables to perform ECM design directly starting from scratch or by reading in existing CAD files (STEP, AutoCad, IGES, etc.). A hybrid structured-unstructured grid generator is incorporated within this software that produces the high quality meshes needed to perform the 3D ECM calculations. The software is very user-friendly with full windows interface and can visualize results using color plots, isoclines and streamlines in 3D and on random 2D cross-sections. The model takes into account the internal electrical resistivity of the electrodes and the interaction with the external electrical equipment. In this paper, the numerical model and solution method behind the software are presented and applied in case of the manufacturing of a die and the formation of a cavity. The model for the ECM calculations applied in this presentation combines a 3D boundary element method (BEM) for the potential distribution in the electrolyte with a 2D finite element method (FEM) that takes into account the ohmic potential drop in the electrode(s). Both models are coupled with each other via the current densities that flow from the electrolyte to the electrode(s) or vice versa. To demonstrate the software, the manufacturing of a die and the formation of a cavity has been treated. From these calculations it can be concluded that powerful 3D simulation software can significantly reduce the design time of ECM processes

Pattavanitch et al. [20] proposed the development and application of the boundary element method to model the machining of simple milling and turning features. Linear triangular

elements are used by the 3D model to discretize the work-piece and tool surfaces. The effective use of analytical integration to calculate the element matrices is the main objective of this program rather than numerical, and the automatic refinement of the mesh is done as the work-piece is progressively machined. To test and verify the program, milling slots using a rectangular tool and turning a thin-walled tube was done. It is found that there is good agreement between the predicted and experimental results. To model the tool and work-piece by BEM, the domain must be a closed shell of faces. The rectangular tool and Work-piece are modeled as a hollow open-topped box and an inverted U-shaped channel, respectively .To form a closed shell, virtual surface are added to the open box and channel. EC machining is a potential problem and therefore the current density distribution on the tool and work-piece surface can be represented by Laplace's equations as shown in the equation 2.6

$$\nabla^2 u = 0 \qquad (2.6)$$

2.3.3 Other Modelling Methods

Labib et al. [21] proposed a fuzzy logic controller to add intelligence to the ECM process. By the integration of a fuzzy logic controller into the existing control system, an experimental ECM drilling rig, at University of Manchester, was improved as shown in the figure 2.16. To build a fuzzy logic controller system, which can control the feed rate of the tool and the flow rate of the electrolyte, Fuzzy Logic Toolbox was used. The objective of the fuzzy logic controller was to improve machining performance and accuracy by controlling the ECM process variables. The results depict innovative possibilities and provide potential for future applications of fuzzy logic control (FLC) in ECM. Hybrid controllers that integrate fuzzy logic into the control system allow for ''human like'' decision-making intelligence to be incorporated into ECM controllers. The aim of this paper is the feasibility of FLC in ECM, but the results have the potential of being applied to EMM. As the future of ECM moves towards electrochemical micromachining (EMM), the need for process uncertainty control in this area may be met by FLC, which has advantages over conventional methods of process control.

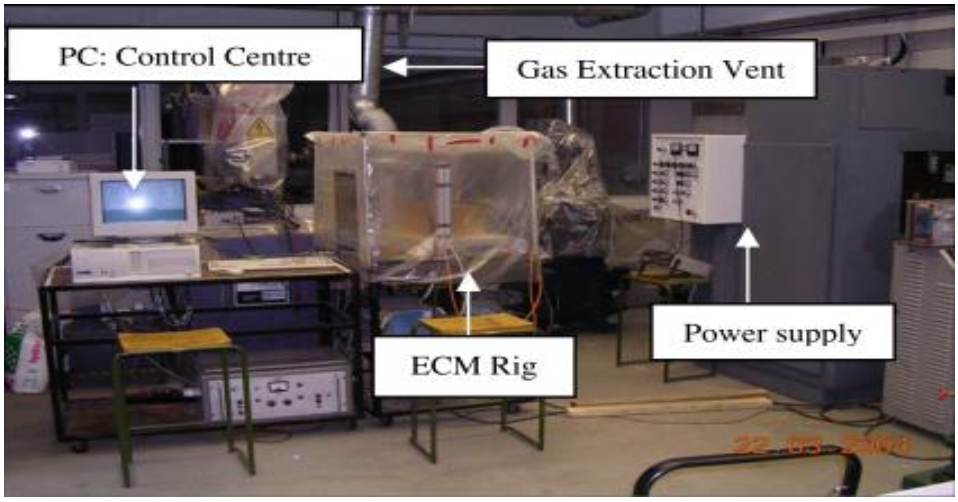

Fig. 2.16: picture showing the whole ECM drilling rig [21]

Hewidy et al. [22] determined that application of low frequency vibration to the tool electrode in electrochemical machining is one of the effective techniques for improving accuracy and quality of the machined surface. An analytical approach to establish mathematical model in an endeavor to assess the mechanism of metal removal for this novel and hybrid technique is presented in this paper. The effect of input parameters and machining conditions on the effectiveness of tool vibration during ECM has been fully investigated. The analytical model reveals that there could be a great complexity in the relationship between the tool amplitude and the equilibrium gap size, which could lead to tool damage, if the problem has not been carefully considered. Low frequency vibration of the tool represents an effective method to produce a flushing action. To study the behaviour of the tool during the ECM process under low frequency vibration, the case of ECM with plane parallel electrodes is considered. It has been assumed that the tool vibration follows a simple harmonic motion. Figure 2.17(a) and 2.17(b) shows the displacement–time and velocity–time relationships of the tool vibration, respectively.

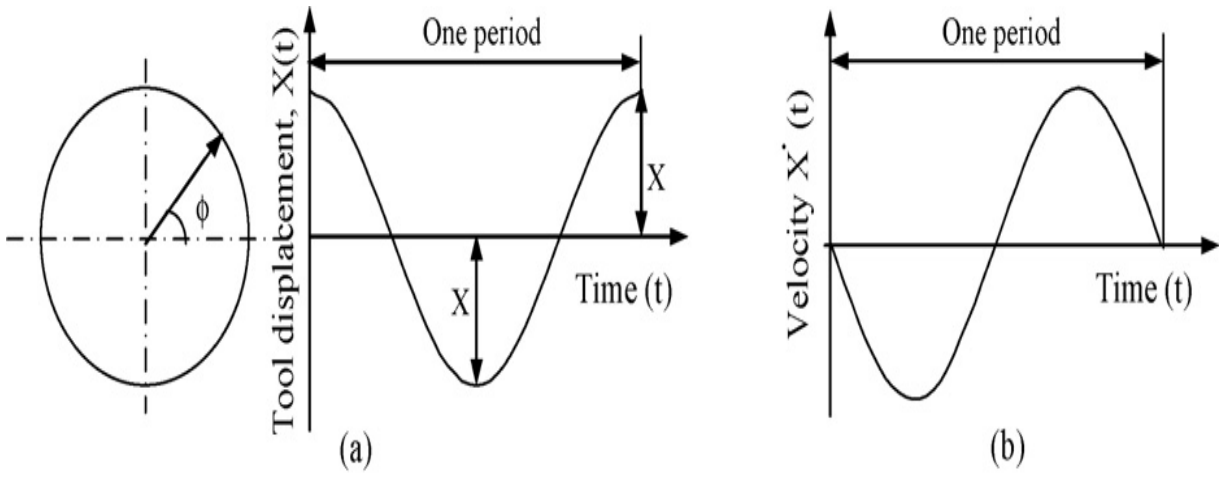

Fig. 2.17: Displacement–time (a) and velocity–time relationships (b) of the tool vibration [22]

2.4 ECM USING CFD

Ratkovich et al. [23] developed a computational fluid dynamics (CFD) model to study the effect of slug flow on the surface shear stress in a vertical tubular membrane. The model was validated by using surface shear stresses that can be measured using an electrochemical shear probe and gas slug (Taylor bubble) rising velocities that can be measured using a high speed camera. Due to the coalescing of gas slugs as they travelled up the tube, the length of the gas slugs and, therefore, the duration of a shear event, were observed to vary substantially. However, the magnitude of the peak surface shear stress does not vary largely. The experimental conditions affected the extent to which the gas slugs coalesced. For the experiments performed with higher gas flow rates and lower liquid flow rates, more coalescing between gas slugs was typically observed. Therefore, the results implied that the frequency of shear events decreases at higher gas flow rates and lower liquid flow rates. Shear stress histograms (SSH) were used as a simple approach to compare the different experimental conditions investigated. All conditions resulted in bi-modal distributions: a positive surface shear peak, caused by the liquid slug, and a negative shear peak caused by the gas slugs. At high gas flow rates and at low liquid flow rates, the frequencies of the shear stresses in both the negative and positive peaks were more evenly distributed. For all cases, increasing the liquid flow rate and decreasing the gas flow rate tends to result in a predominant positive peak. These results are of importance since conditions that promote evenly distributed positive and negative peaks, are likely to promote better fouling control in membrane system. At high liquid and low gas flow rates, the frequencies obtained numerically and experimentally were found to be similar, deviating by less than approximately 10%. However, at high gas and low liquid flow

rates, the differences were slightly higher, exceeding 20%. The shear stresses induced by gas slugs were over predicted by CFD model simulations, under these conditions. Thus, the results indicate that the CFD model was able to accurately simulate shear stresses induced by gas slugs for conditions of high liquid and low gas flow rates.

Tsuboi et al. [1] modeled ECM process taking into account metal dissolution, electrolyte flow, void fraction distribution of hydrogen bubbles generated from the tool cathode, thermal, electric potential, and electric conductivity. Especially, two types of method are used for the coupling between gas- and liquid-phase in electrolyte. One is one-way coupling method; only the electrolyte flow affects the void fraction distribution of hydrogen bubbles. The other is two-way coupling method; considering the interaction between the electrolyte flow and the void fraction distribution. In the two-way coupling method, considering bulk density distribution in the electrolyte flow path due to hydrogen bubble, Low-Mach-Number approximation is used for simulations. The one way and two way coupling simulations are shown in the figures 2.18 and 2.19 respectively. For applications with our numerical code, simulations for machining 3-D compressor blade are performed. Blade geometry is successfully predicted and we can obtain some guideline of ECM process.

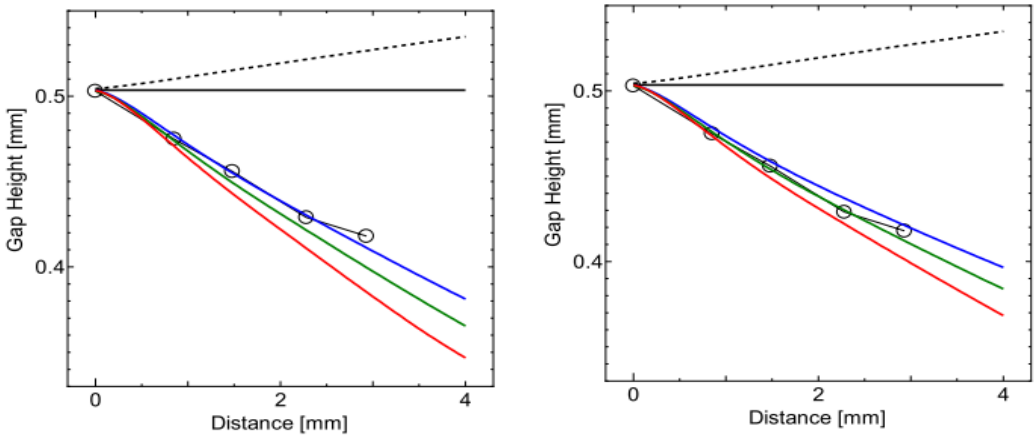

Fig. 2.18: One-way coupling simulation [1] Fig. 2.19: Two-way coupling simulation [1]

2.5 CFD IN OTHER FIELDS

Conner et al. [24] suggested the CFD modeling methodology and validation for steady-state, normal operation in a PWR fuel assembly. The program used here is developing a CFD methodology for modeling and predicting single-phase and two-phase flow conditions downstream of structural grids that contain mixing devices. The purpose of the mixing devices

(mixing vanes in this case) is to increase turbulence and improve heat transfer characteristics of the fuel assembly. STAR-CD CFD code was used to develop the detailed CFD modeling methodology for single-phase flow conditions in PWR fuel assemblies. The details of the computational mesh, the used turbulence model, and the boundary conditions applied to the model are included in this methodology. This methodology was developed by taking in to account CFD results versus small-scale experiments. The experiments use PIV to measure the lateral flow field downstream of the grid, and thermal testing to determine the heat transfer characteristics of the rods downstream of the grid. The CFD results and experimental data presented in the paper provide validation of the single-phase flow modeling methodology. Two-phase flow CFD models are being developed to investigate two-phase conditions in PWR fuel assemblies, and these can be presented at a future CFD Workshop.

.

Frank et al. [25] presented multiphase flow models for the description of mono- and poly-disperse bubbly flows in the Eulerian framework of multiphase flow modeling in ANSYS CFX. The models are taking into account interphase momentum transfer due to governing drag and non-drag forces. Furthermore in case of a poly-disperse air–water or water–steam bubbly flow the bubble size distribution, bubble break-up and coalescence processes as well as different gas velocities in dependency on the bubble diameter are taken into account in the newly developed inhomogeneous MUSIG model. Both multiphase flow models for mono- and poly-disperse bubbly flows have thoroughly been validated and compared to experiments of MT-Loop and TOPFLOW test facilities (FZ Dresden-Rossendorf, Germany). Best practice guidelines (Menter, 2002) have been applied in order to allow for a systematic error quantification and thoroughly assessment of model formulations.

Li et al. [26] developed a transient computational fluid dynamics model to depict the hydraulics of a full open valve tray. It focused on the three-dimensional two-phase flow of gas and liquid in the Eulerian framework. A new correlation of liquid hold-up was developed, and the interphase momentum transfer term was determined, based on the clear liquid height measured on a full open valve tray. Various simulations were carried out for the rectangular full open valve tray with different characters of system. The CFD simulations demonstrate chaotic tray hydrodynamics. Predicted results were in good agreement with the experimental data.

.

Gerogiorgis et al. [27] discussed on a finite element (FE) computational fluid dynamics model developed for a candidate carbothermic aluminium reactor for the application in industrial carbothermic Al production. This process is an alternative to the conventional Hall–Heroult electrolysis process and is cheaper in cost and useful in environmental point of view. This Process technology encompasses a wide spectrum of phenomena (convection, diffusion, reaction, evaporation, electric field) that occur simultaneously in a multiphase configuration, the geometry of which is an open design problem and remains to be determined without prior experience or even abundance of experimental data. The strong interaction among Joule heating, endothermic reaction, natural Bossiness convection and turbulent flow phenomena is of paramount importance for understanding reactor performance; conducting CFD simulations is an efficient way to advance with the latter goal, since reliable high-temperature measurements of state variables are remarkably laborious, uncertain and expensive. The quadruple partial differential equation (PDE) problem (electric charge, heat, momentum and gas volume balances) for the slag flow in the ARP reactor is solved via a commercial CFD software suite (FEMLABw v.2.3) to obtain potential, temperature, velocity and gas volume fraction distributions in a two-dimensional domain, representing in detail the complete second stage of the proposed carbothermic reactor. To accurately calculate the volume fraction of the gas generated within the molten slag and define how the proposed geometry affects production is the main challenging factor. To extract conclusions regarding the reactive slag flow, the extent of space utilization and the existence of dead volumes, and to provide design guidelines are some of the vital objective of this CFD study.

Kasat et al. [28] developed a comprehensive CFD model to gain an insight into solid suspension and its implications on the liquid-phase mixing process in a solid--liquid stirred reactor. The turbulent solid--liquid flow in a stirred reactor was simulated using a two-fluid model with the standard k-ϵ turbulence model with mixture properties. The multiple reference frames (MRFs) approach was used to simulate impeller rotation in a fully baffled reactor. The computational model with necessary sub-models was mapped on to a commercial solver FLUENT 6.2 (of Fluent Inc., USA). The predicted solid concentration distribution was compared with the experimental data of Yamazaki et al. Concentration profiles of solids suspended in a stirred tank. The computational model was then further extended to simulate and understand the implications of the suspension quality on liquid-phase mixing process. The computational model and the predicted results discussed here will be useful for understanding the liquid-phase mixing process in stirred slurry reactors in various stages of solid suspension.

.

Mimouni et al. [29] proposed modeling and the numerical simulation with the NEPTUNE CFD code of cavitation phenomena and boiling of bubbly flows. NEPTUNE CFD solver, developed jointly by EDF R&D and CEA is used to compute Compressible, unsteady, turbulent 3D two-phase flow. A finite-volume co-located cell-centered approach is used for the numerical simulation making use of an original pressure-based multi-field coupling algorithm. The cavitation nuclei either come from wall nucleation or are pre-existing in the flow. Formed vapour bubbles are advected by the flow and expand in the regions where the local pressure is below the saturation value with a tendency to agglomerate into slug bubbles. This model was compared with experimental data on enough selective local variables and found that satisfactory agreement could be obtained without any floating parameter to fit the data. The second part of the paper deals with boiling bubbly flow through a mixing device representing the effect of a fuel assembly spacer grid equipped with mixing blades (DEBORA-mixing experiment, CEA, Grenoble). The void fraction can be locally measured and are provided downstream the mixing enhancer. The computations compare favorably with the experimental results; in particular, the global effect of the mixing blades was observed. A modification of the classical nucleate boiling model is proposed to overcome the strong model sensitivity with respect to near wall grid refinement.

Prasser et al. [30] proposed the use of wire-mesh sensors to understand turbulent mixing processes in single-phase flow as well as to characterize the dynamics of the gas–liquid interface in a vertical pipe flow. For the development and test of closure relations describing bubble coalescence and break-up, interfacial momentum transfer and turbulence modulation for a multi-bubble-class model, experiments at a pipe of a nominal diameter of 200mm are taken as the basis. It is done by measuring the evolution of the flow structure along the pipe. The transferability of the extended CFD code to more complicated 3D flow situations is assessed against measured data from tests involving two-phase flow around an asymmetric obstacle placed in a vertical pipe. The obstacle, a half-moon-shaped diaphragm, is movable in the direction of the pipe axis; this allows the 3D gas fraction field to be recorded without changing the sensor position. In the outlook, the pressure chamber of TOPFLOW is presented, which will be used as the containment for a test facility, in which experiments can be conducted in pressure equilibrium with the inner atmosphere of the tank. In this way, flow structures can be observed by optical means through large-scale windows even at pressures of up to 5MPa. The so-called “Diving Chamber” technology will be used for Pressurized Thermal Shock (PTS)

tests. Finally, some important trends in instrumentation for multi-phase flows will be given. This includes the state-of-art of X-ray and gamma tomography, new multi-component wire-mesh sensors, and a discussion of the potential of other non-intrusive techniques, such as neutron radiography and magnetic resonance imaging (MRI)

Schepper et al. [31] compared the calculated gas/vapor–liquid two-phase co-current horizontal flow regimes with the experimental data, taken from the Baker chart. For the calculation of the two-phase flow regimes, the well-known volume of fluid (VOF) multiphase flow model that uses a piecewise linear interface calculation (PLIC) interface reconstruction method in each computational cell, implemented in a computational fluid dynamics (CFD) code was used. The flow regimes for water–air flow are reproduced. All simulations give good agreement with the flow regimes expected from the Baker chart. Horizontal flow regimes for two-phase liquid–vapour gas oil flow are also reproduced. To the best of our knowledge, this is the first time that the flow regimes for gasoil liquid–vapour flow as predicted by the Baker chart are simulated. Again, a good agreement between the simulated and expected flow regime is obtained. All horizontal flow regimes appearing in the Baker chart can thus be calculated using CFD.

Vallee et al. [32] investigated stratified two-phase flow, for which two horizontal channels with rectangular cross-section were built at Forschungszentrum Dresden-Rossendorf (FZD). The channels allow the investigation of air/water co-current flows, especially the slug behavior, at atmospheric pressure and room temperature. The test-sections are made of acrylic glass, so that optical techniques, like high-speed video observation or particle image velocimetry (PIV), can be applied for measurements. The rectangular cross-section was chosen to provide better observation possibilities. Moreover, dynamic pressure measurements were performed and synchronized with the high-speed camera system. CFD post-test simulations of stratified flows were performed using the code ANSYS CFX. The Euler–Euler two fluid models with the free surface option were applied on grids of minimum 4×105 control volumes. The turbulence was modeled separately for each phase using the k–ω-based shear stress transport (SST) turbulence model. The results compare very well in terms of slug formation, velocity, and breaking. The qualitative agreement between calculation and experiment is encouraging and shows that CFD can be a useful tool in studying horizontal two-phase flow.

Wang et al. [33] described a numerical simulation tool for calculating the planar solid oxide fuel cells. The finite volume method was employed for the simulation, which was on the basis of the fundamental conservation laws of mass, momentum, energy and electrical charge.

Temperature distributions, molar concentrations of gaseous species, current density and over potential were calculated using a single cell unit model with double channels of co-flow and counter-flow cases. The influences of operating conditions and anode structure on the performances of SOFC were also discussed. Simulation results show that the co-flow case has more uniform temperature and current density distributions and smaller temperature gradients, thus offers thermo-structural advantages than the counter-flow case. Moreover, in co-flow case, with the increasing of delivery rate, temperature and hydrogen mass fraction of fuel, average temperature of PEN, current density and activation potential also rise. However, with increasing the delivery rate of air, average temperature of PEN decreases. In particular, it is effective to improve the output voltage by reducing the thickness of anode or increasing its porosity.

Yun et al. [34] examined a mechanistic bubbles size model to enhance the prediction capability of sub-cooled boiling flows for the CFD code. In addition to this, advanced sub-cooled boiling models such as new wall boiling and two-phase logarithmic wall function models were also applied for an improvement of energy partitioning and two-phase turbulence models, respectively. The benchmark calculation against the DEBORA sub-cooled boiling data confirms that the bubble size model with the two advanced sub-cooled boiling models shows good prediction results and is applicable to the wide range of flow conditions that are expected in the nominal and postulated accidental conditions of a nuclear power plant.

Zahab et al. [35] reported on the development and validation of a localized collocation meshles method (LCMM) to model laminar incompressible flows. A high order unwinding scheme was devised to dampen the numerical oscillations arising in convection-dominated flows. Subsequently, the LCMM was analytically validated and demonstrated to yield third-order accurate solutions when compared to a benchmark analytical decaying vortex solution .Numerical validations are provided by comparison with the finite volume commercial (FVM) solver Fluent6.2. The flow geometry for the numerical validation arises from a biomedical application that consists of modeling blood flow in the inter-connection between a bypass graft and an artery. Very good agreement was found between the LCMM and the FVM.

2.6 OBJECTIVE

On the basis of the exhaustive literature review it was depicted that it is very difficult to know the machining variables within the IEG in case of complicated shapes of tool. So there is a need to understand about those parameters related to flow pattern. Once the flow pattern is

known, then it's easy to design the tool and avoid passivation which is the major problem in case of complicated shapes. Again, the two phase analysis in ECM which is the major aspect of this study involving electrode shape change and various critical parameters influencing the shape change may be comprehensively studied with the help of mathematical or computational models with a close proximity with real world processes.

2.7 SCOPE OF THE STUDY

In this study, a two phase flow pattern of L-shaped tool in ECM will be modelled by CFD analysis. The work-piece material is iron and the tool is copper. The electrolyte used is brine and the various parameters that will be determined from the simulation results are given as follows

1. Volume fraction of brine
2. Interphase mass transfer pattern of brine
3. Velocity pattern of electrolyte
4. Temperature pattern of electrolyte
5. Pressure pattern of electrolyte
6. Heat flux pattern of electrolyte
7. Current density distribution on the work-piece
8. Material removal rate pattern on the work-piece.

Partial verification of simulated results will be carried out in ECM setup. The various parameters that can be determined from the experimental results are

1. MRR
2. Profile of work-piece after machining
3. Effect of voltage, flow rate and electrolyte concentration on MRR.

CHAPTER 3

MODELLING AND SIMULATION

3.1 BRIEFING THE MODELLING

This chapter explains the shapes, dimensions, modelling, of three models used for the analysis. The analysis techniques and boundary conditions are also explained in this chapter. ECM set up consists of a work-piece, tool and an electrolyte solution. Work-piece should be electrically conducting material and the tool may or may not be. Commonly used electrolytes are NaCl solution and $NaNO_3$. To get required shape in the work-piece, tool should be designed properly. The shape of the tool affects the critical parameters of machining. Another important aspect in the modelling of ECM is the flow pattern of electrolyte and the various intervening factors those are affected by the two phase flow pattern of electrolyte.

3.2 GEOMETRICAL MODELLING

A finite element based commercial CFD software package, ANSYS 13.0 CFX, which operated under the Windows VISTA 32-bit operating system was used for the simulation study. In the present simulation process, the modelling is done with ANSYS Design modeller Module of ANSYS 13.0 CFX software. Three different models are used for this simulation study and are given as follows.

i. Model 1 - L shaped tool with central through hole.
ii. Model 2 - L shaped tool having slot in the tool face with rounded corners.
iii. Model 3 - L shaped model having intermediate chamber and slot in the tool face with rounded corners.

The initial shape of the work-piece in all the three models is same. It is circular in shape with 60 mm diameter and 20 mm height. Model of work-piece is shown in Figure 3.1. Electrolyte used for this simulation is NaCl solution (20%). The electrolyte starts flowing with a constant diameter of 3 mm from the inlet of the tool. The long side of the L-shape is having 30 mm length and short side of 15 mm length and the central hole has diameter of 3mm. Variation in the arrangement of slot make these models different from each other. Top view of the tool is shown in Figure 3.2 and is same for all the three models and 3D view is shown in Figure 3.3. Inter electrode gap (IEG) for all the models is kept constant at 0.5 mm that is shown in Figure

3.4.The key dimensional feature of the physical model is as shown in table 3.1. The complete physical model of work-piece-tool set up is as shown in figure 3.5.

..

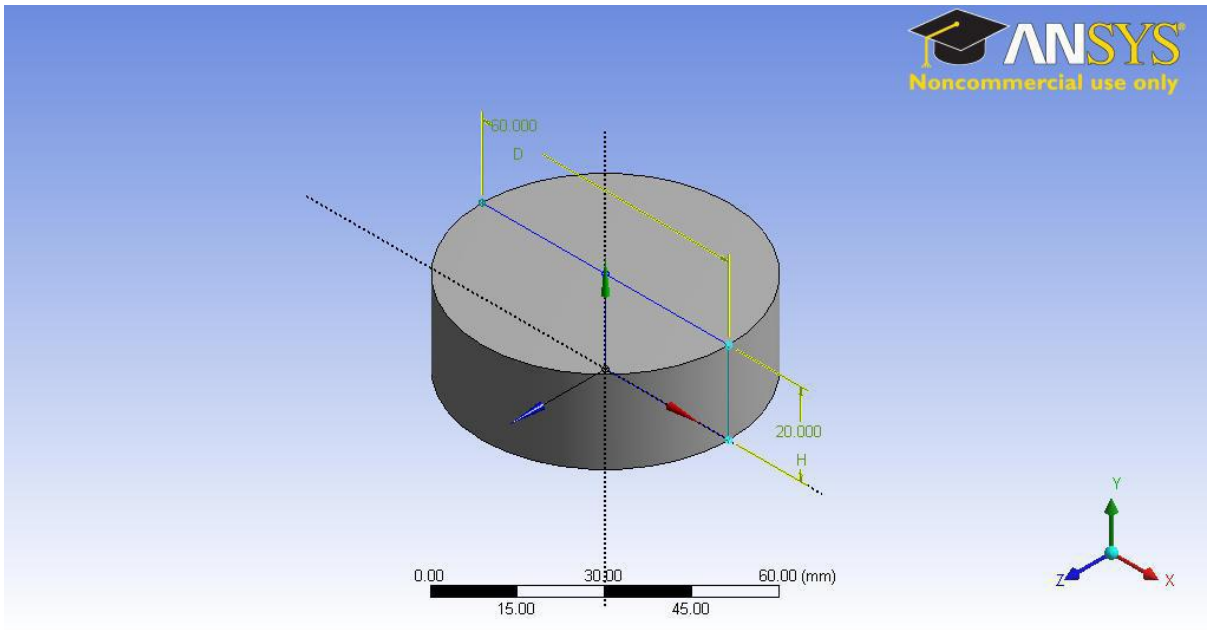

Fig. 3.1: Model of the work-piece used for simulation study

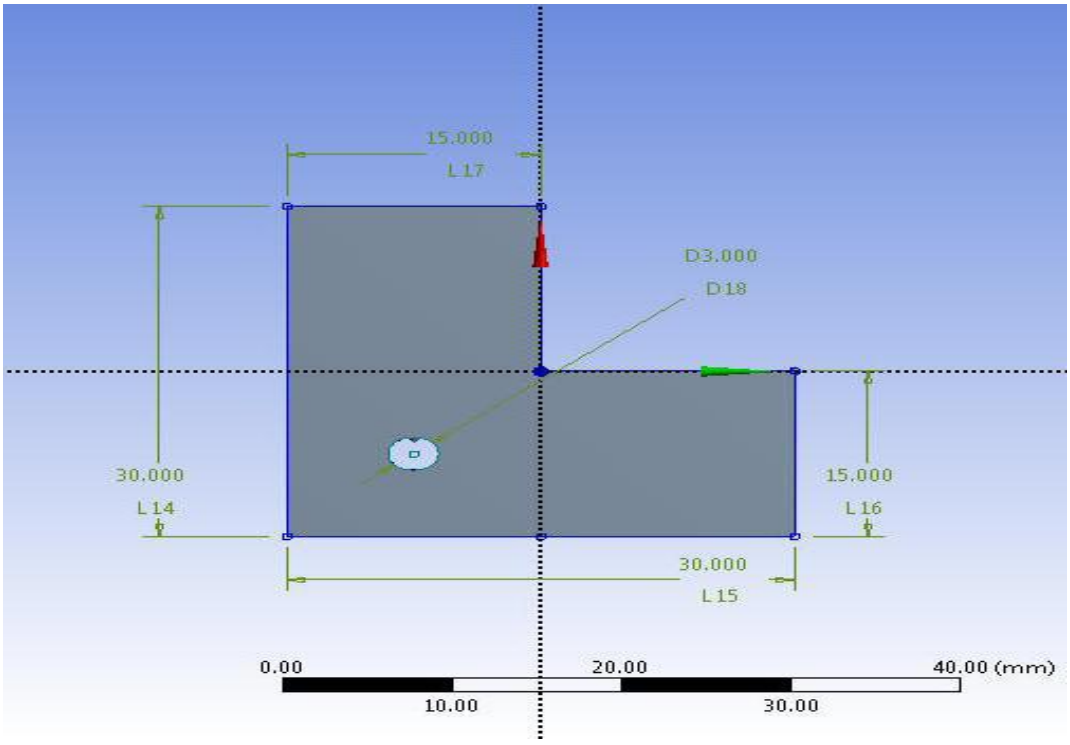

Fig. 3.2: Top view of tool for all models used for simulation study

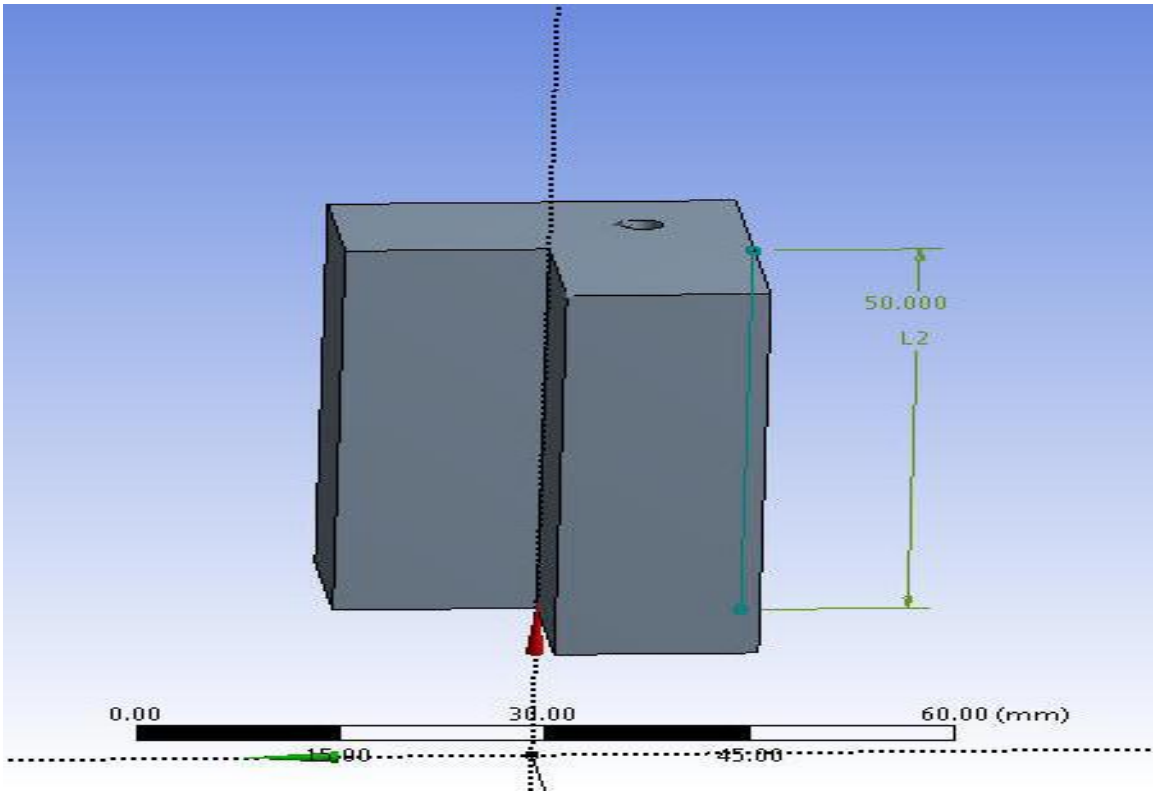

Fig. 3.3: 3D view of tool for all models used for simulation study

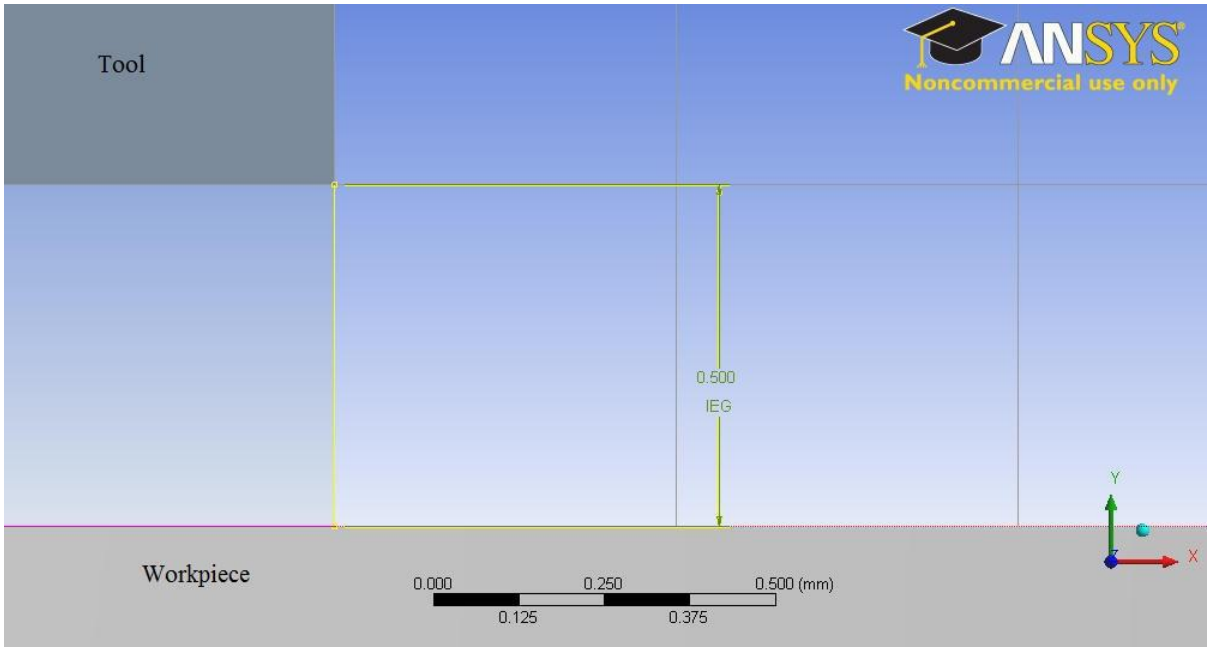

Fig. 3.4: IEG for the tool-work-piece model

Table 3.1: Element type

Sl no	Component	Material	Physical state	Shape	Dimension(mm)
1	Work-piece	Iron	Solid	Cylindrical	60 dia. X 20 ht.
2	Tool	Copper	Solid	L-shaped	Arm 30 X Width 15 X Height 50 X Central hole 3Ø
3	Medium	Brine	Fluid	-	

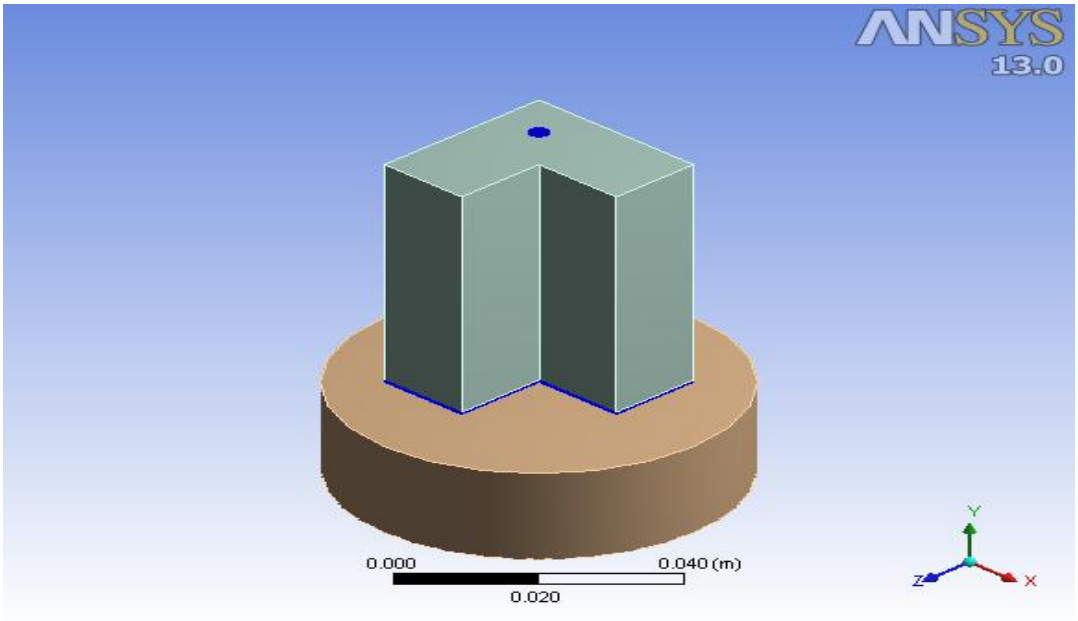

Fig. 3.5: Physical model

3.2.1 Model 1 – L Shaped Tool with Central Through Hole

Model 1 is a simple L shaped model having a central through hole with a diameter of 3mm and height of 50 mm. This centre of the hole is fixed on (-7.5,-7.5) coordinate in the XZ plane. Fluid is flowing through the through hole and flow out through the IEG. Top view of the tool is shown in Figure 3.2 and 3D view is shown in Figure 3.3. Inter electrode gap (IEG) is for all models kept constant is 0.5mm that is shown in Figure 3.4.

3.2.2 Model 2- L Shaped Tool Having Slot in the Tool Face with Rounded Corners

Unlike model 1, the bottoms face of the tool in model 2 is having grooves with rounded corners. In this model the central hole has 3 mm diameter and two grooves are connected with this. Those grooves are having a diameter of 0.8 mm and end corners of the grooves has a

diameter of 3 mm. Dimensions of this tool is presented in the Figure 3.5. Height of the tool is same as that of previous model. According to tool design for ECM, distance between the slot end and corners of work-piece should remain at least 1.5 mm and the width of the slots are 0.8 mm for best results. These conditions are taken in to account for all the tool designs.

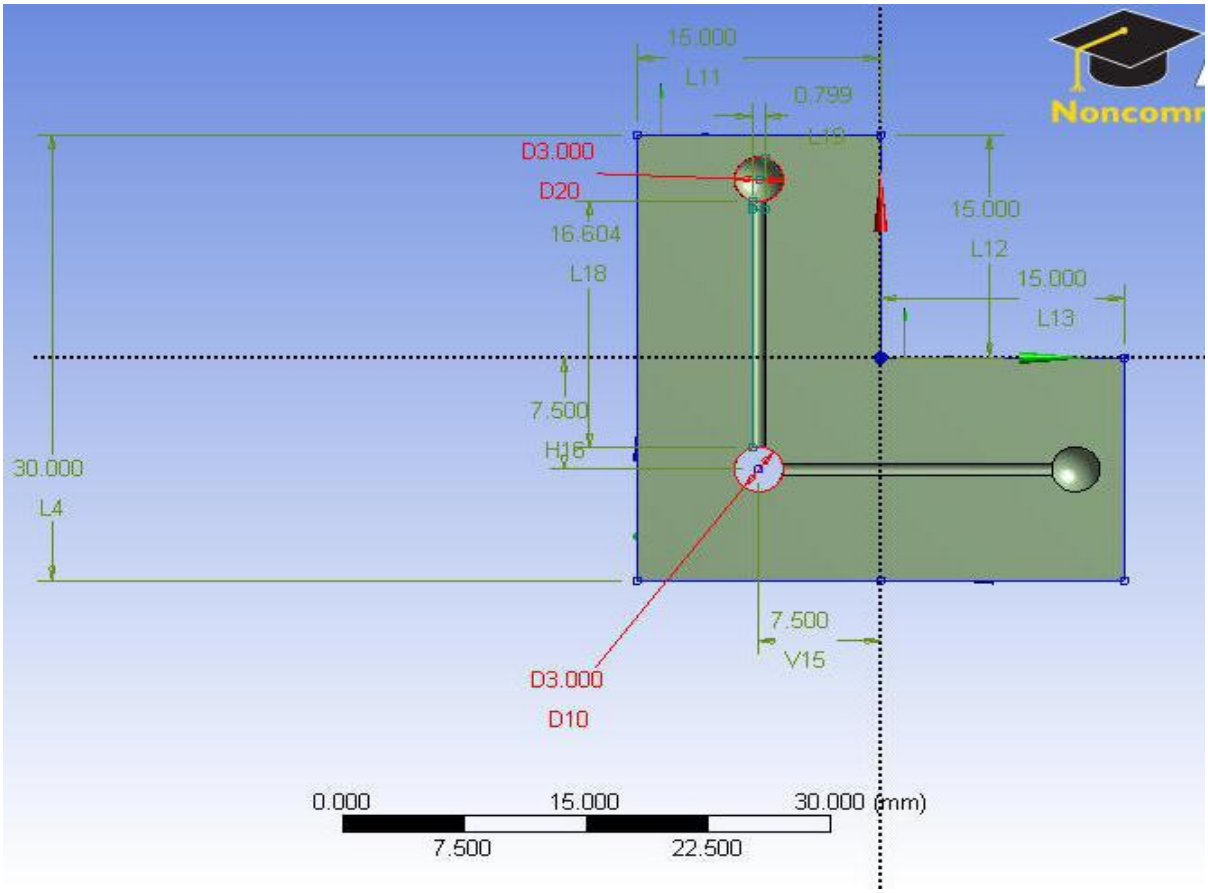

Fig. 3.6: Tool dimensions for model 2

3.2.3 Model 3 - L Shaped Model having Intermediate Chamber and Slot in the Tool fFace with Rounded Corners.

Model 3 is entirely different from other models. In other models fluid is coming from the inlet and distributed to the grooves at bottom face of the tool. In Model 3, fluid first come to the L-shaped chamber then it flows to the IEG through slots provided in the bottom of the tool. Here the inlet diameter is given same as like other models but rounded corners in the slot have different dimensions. That design is shown in Figure 3.6. In that slit is in the bottom portion of the chamber. Chamber face dimensions are shown in Figure 3.7 and have a thickness of 1 mm and a height of 5 mm. Chamber constructed for Model 3 is shown in Figure 3.7. Slits in the Model 2 had two rounded end each having a diameter of 3 mm and there is a central rounded portion with a diameter of 5 mm.

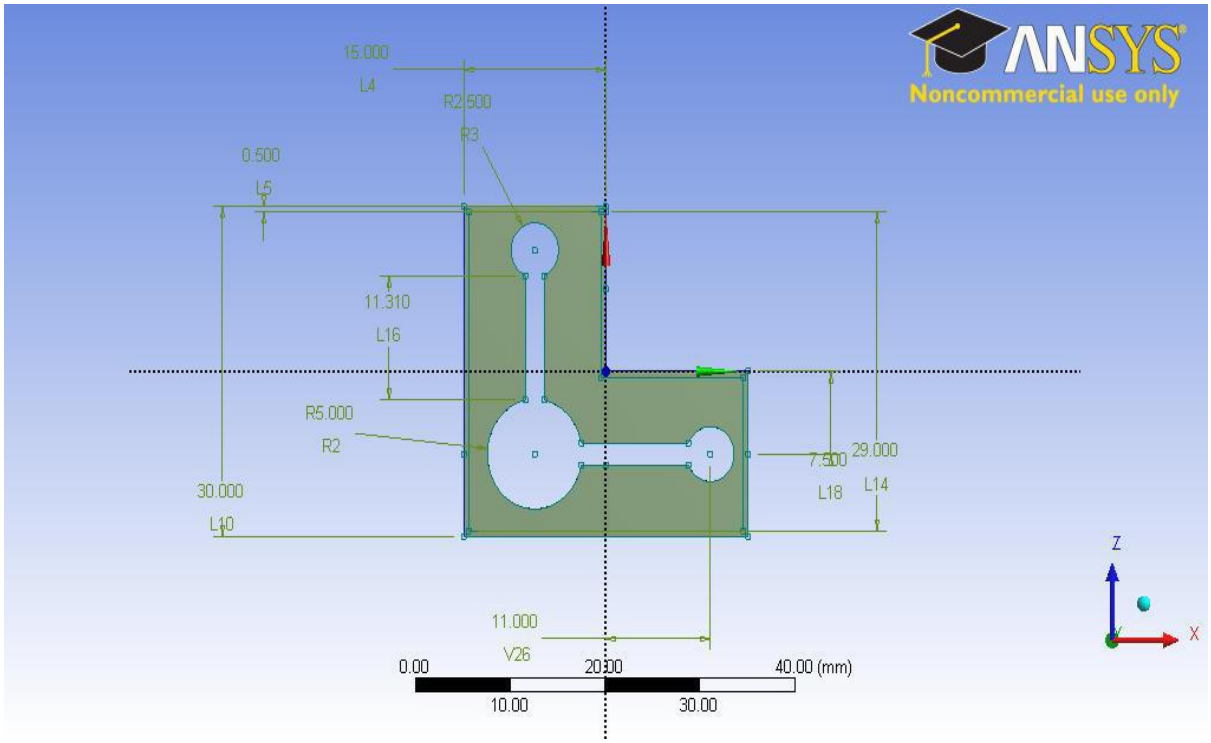

Fig. 3.7: Tool dimension for model 3

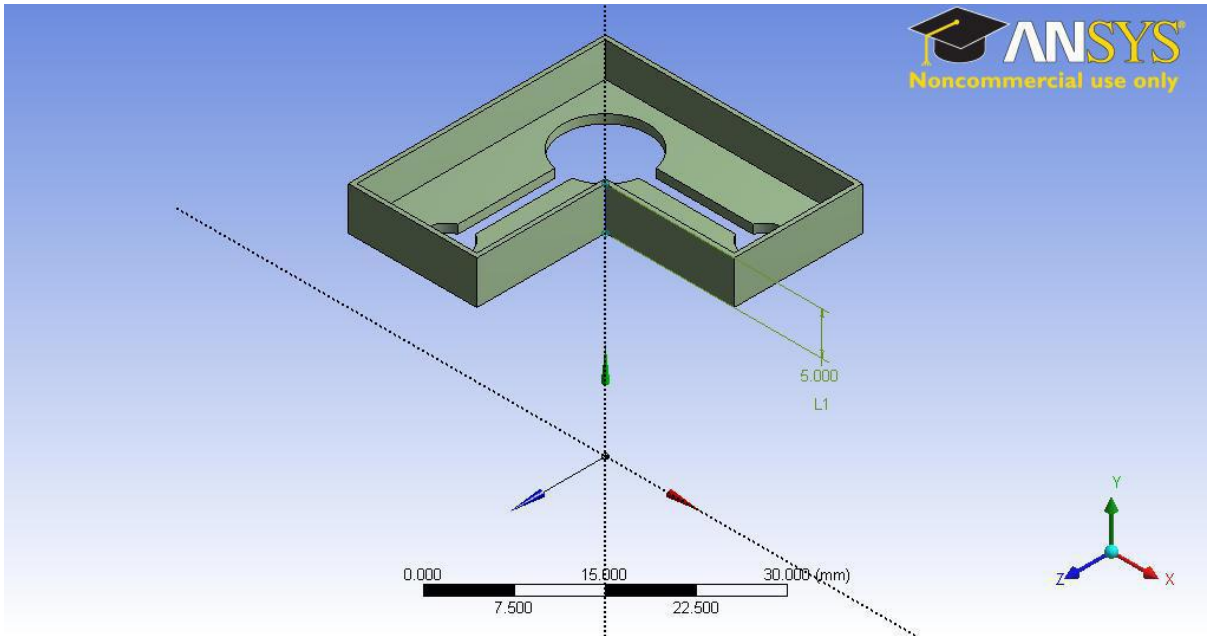

Fig. 3.8: Chamber in model 3

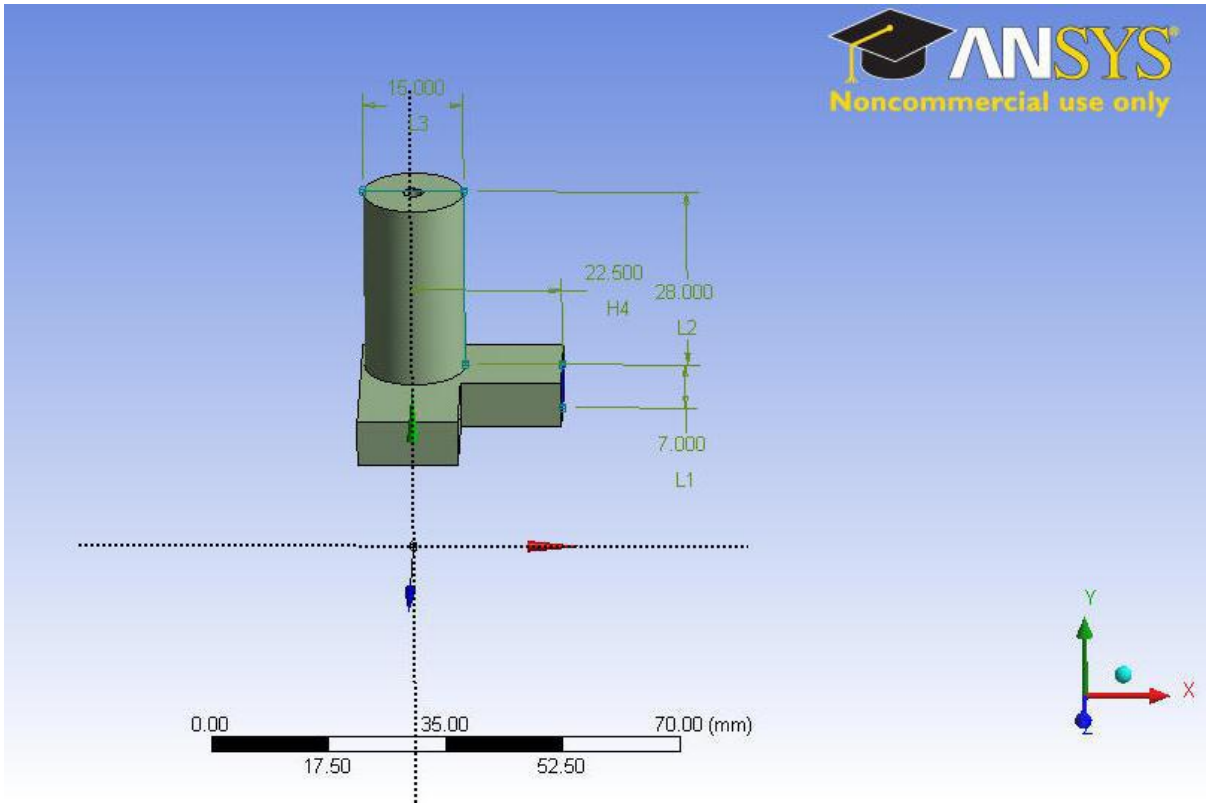

Fig. 3.9: External dimension for model 3

3.3 MESHING

Model is meshed using ANSYS Mesh Module in ANSYS commercial software. The quality of mesh is a relevant factor in the case of appropriate geometry of the model and accuracy of the results. This can be expressed in terms of orthogonal quality. If the value of orthogonal quality is coming near to '1' then our mesh quality is good and it gives better results. At the same time if it is coming near to zero, then the mesh gives bad results. Tetrahedral elements are used for meshing the geometry and elements have a minimum edge length 5×10^{-4} m. Tetrahedral meshes generally provides more automatic solutions with ability to add mesh controls to improve accuracy in critical region. Hexahedral meshes generally give more accurate results but it's very difficult to generate. Program controlled automatic inflation method is enabled for meshing. Mesh methods included in ANSYS are Patch conforming and Patch independent methods. Out of these, Patch independent meshing method is adopted for meshing present geometry model. Patch independent method uses top down approach which means, it creates volume mesh and extracts surface mesh from boundaries. Advantages of this method is that it uses the geometry only to associate the boundary faces of the mesh to the region of interest there by ignoring gaps, overlaps and other issues that present in other meshing tools.

For grid independence study three different types of mesh resolutions were investigated. The outcomes of the grid independence study are shown in Table 3.2. The best results in terms of consistency and validation was obtained using the fine resolution mesh of 2392617-cell. However, the required timing of simulation for the finer meshes was found to be 35% higher than intermediate mesh and 190% higher than the coarse mesh. Materials used are copper for tool, iron for work piece and brine (20% NaCl) as the electrolyte solution.

Table 3.2: Grid independence study

Sl no	Mesh resolution	Fine	Intermediate	Coarse
1	Interval size(mm)	1.5	2.0	2.5
2	Number of cells	23,92,617	16,81,790	3,48,861
3	Orthogonal quality	0.9878	0.8656	0.6789
4	Skewness	0.640137	0.638719	0.598314

Different sections in each of the models are named as follows

i) Work-piece

Work top - Top face surface of work-piece

Work bottom - Bottom face surface of work-piece

Work outer – Outer surfaces of work-piece.

ii) Tool

Tool top – Top face surface of tool

Tool bottom surface – bottom face surface of tool

Tool groove – Hollow surface in the tool

Tool outer – Outer surfaces of tool

iii) Electrolyte

Inlet – Starting region of electrolyte where electrolyte enters in to the tool

Outlet – The portion where electrolyte is flowing out of the tool

Brine top - Top face of brine which making contact with tool bottom

Brine bottom - Bottom face of brine which making contact with work-piece top

Brine groove – It is the portion of electrolyte inside the tool groove.

The meshed model of the model is as shown in the figure 3.6.

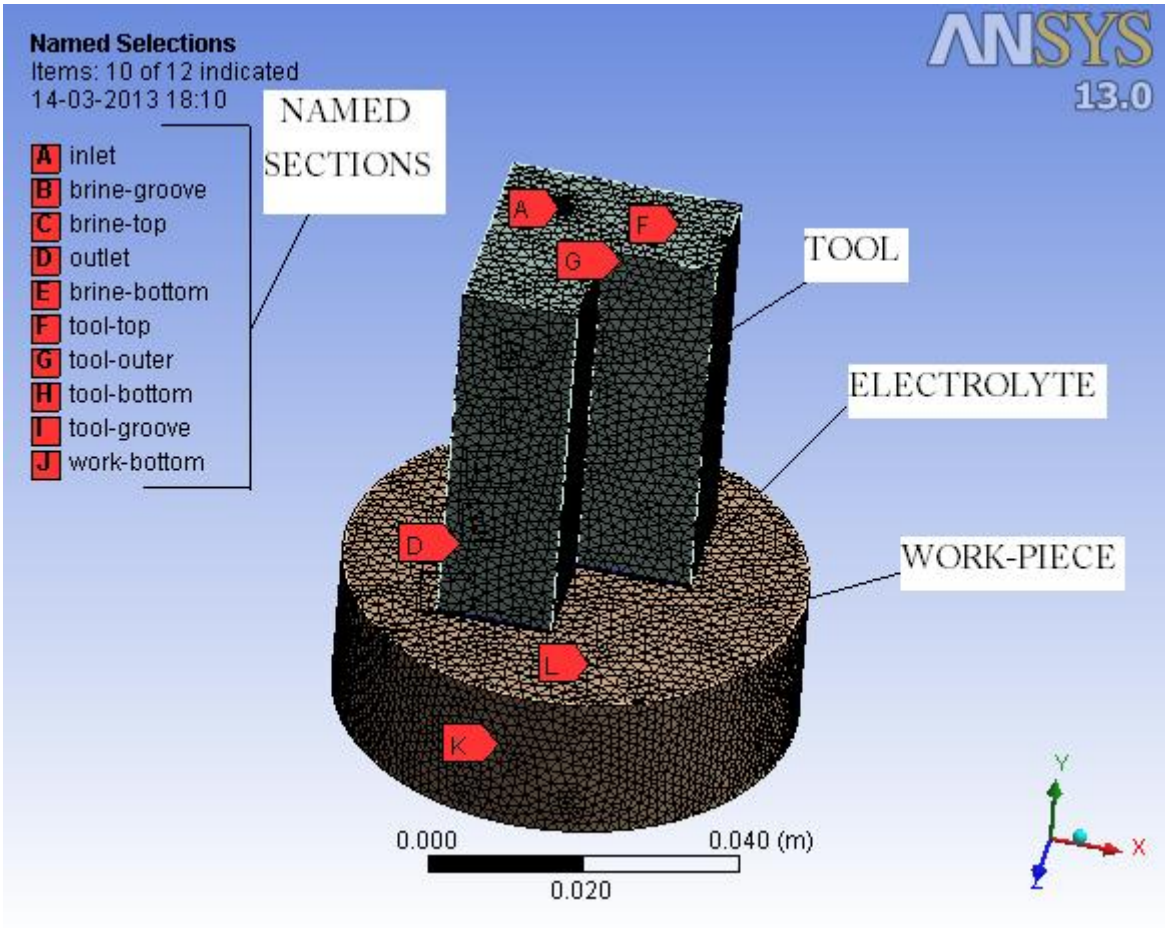

Fig. 3.10: Meshed model with sections naming

3.4 GOVERNING EQUATIONS

Simulations are carried out on the basis of governing equations. Generally, governing equations are of two types, first one is Computational Fluid Dynamic model equations and other is some user defined equations used for modelling. The CFD modelling equations are inbuilt in the software model of ANSYS 13.0 CFX and second types of equations are those defined by the user to carry out specific simulation tasks.

3.4.1 Computational Fluid Dynamics Governing Equations

Reynolds no in the inlet region is found to be more than 4000 which indicate that flow is in the turbulent region. So, there is a need of the turbulent model for this simulation. Here k-ε model is used for solving this problem. This model is a two equation model. It uses gradient based hypothesis for making relation between Reynolds stress to the mean velocity gradient and the turbulent viscosity.

Again, as we are simulating the electrolyte as two phase mixture of brine and hydrogen bubbles, so we must take the continuity and Navier-stokes equation for each phase separately and at the end we can add the equations of the two phases to make the phases homogenous.

Especially, two types of method are used for the coupling between gas- and liquid-phase in electrolyte [1]. First method is one-way coupling method where only the electrolyte flow affects the void fraction distribution of hydrogen bubbles. The other is two-way coupling method which considers the interaction between the electrolyte flow and the void fraction distribution. In the two-way coupling method, considering bulk density distribution in the electrolyte flow path due to hydrogen bubble, we assume the velocities of the both the phases equal. In this study, two way coupling method is taken in to account.

The continuity and Navier stokes equation for gas phase (hydrogen bubbles) is given by the equations (3.1) and (3.2) respectively.

$$\partial/_{\partial t}\,(\alpha_G\rho_G)+\nabla.\,(\alpha_G\,\rho_G\vec{u}_G)=\Gamma+C_G\nabla^2\alpha_G\rho_G \tag{3.1}$$

$$\partial/_{\partial t}\,(\alpha_G\rho_G\vec{u}_G)+\nabla.\,(\alpha_G\rho_G\vec{u}_G)=-\alpha_G\nabla P+\alpha_G D_G\nabla^2\vec{u}_G \tag{3.2}$$

The continuity and Navier stokes equation for the liquid phase (brine) is given by the equations (3.3) and (3.4) respectively

$$\partial/_{\partial t}(\alpha_L\rho_L)+\nabla.\,(\alpha_L\rho_L\vec{u}_L)=-\Gamma-C_G\nabla^2\alpha_G\rho_G \tag{3.3}$$

$$\partial/_{\partial t}(\alpha_L\rho_L\vec{u}_L)+\vec{u}_L.\nabla(\alpha_L\rho_L\vec{u}_L)=-\alpha_L\nabla P+\alpha_L\mu_L\nabla^2\vec{u}_L \tag{3.4}$$

Considering the gas phase velocity equal to liquid phase (Homogeneous flow) characterized by

$$\vec{u}_{mix}=\vec{u}_G=\vec{u}_L \tag{3.5}$$

Summing equations (3.1) and (3.3) & equations (3.2) and (3.5), equations (3.6) and (3.7) are obtained.

$$\partial/_{\partial t}\,\rho_{mix}+\nabla.\,(\rho_{mix}\vec{u}_{mix})=0 \tag{3.6}$$

$$\partial/_{\partial t}\,(\rho_{mix}\vec{u}_{\text{mix}})+\vec{u}_{\text{mix}}\nabla.\,(\rho_{mix}\vec{u}_{\text{mix}})=-\nabla P+\mu_{mix}\nabla^2\vec{u}_{\text{mix}} \quad (3.7)$$

$$\rho_{mix} = \alpha_G\rho_G+ \alpha_L\rho_L \quad (3.8)$$

$$\mu_{MIX}=\alpha_G D_G+\alpha_L\mu_L \quad (3.9)$$

Equation (3.6) is the continuity equation and Equation (3.7) is the Navier-Stokes equation for simulation of multi-phase flow in the ECM process.

Generally, in computing incompressible flow, we neglect the change in density, but in this model, the change in density depends on the void fraction distribution as in Equation (3.8).

3.4.2 User Defined Governing Equations

For finding out the velocities the desired parameter is volume flow rate range for the electrolyte. Using continuity equation shown in the Equation 3.10 it is ease to found the inlet velocities within that range. The inlet velocity is kept constant for that purpose. The inlet velocity is taken as 40 m/s.

$$Q = Av \quad (3.10)$$

Current density (J) changes as per the conductivity. Current density can be obtained from the Equation 3.11.

$$J = k(V - \Delta V)/y \quad (3.11)$$

From the above relation, it is understood that current density depends upon the thermal conductivity (k) and inter electrode gap (IEG). But in this simulation process *y* is kept constant as 0.5mm. Thermal conductivity is proportional to the temperature in the IEG as shown in the Equation 3.12.

$$k = k_0(1+\propto (T_b - T)) \quad (3.12)$$

Heat generated in the IEG due to Joule's heating can be obtained from the equation 3.13 as follows.

$$Q = I^2 R_e \quad (3.13)$$

3.5 MATERIAL PROPERTIES

Materials used for making this simulation are, Iron, Copper and brine. Iron is the material for work-piece, copper for the tool and 20% brine solution as electrolyte. Properties of air are taken instead of hydrogen for the simplicity of the process. Data's for this simulations are taken from reference [35] and [36]. Material properties are given in Table 3.3.

3.6 ANALYSIS

The analysis is done with the help of ANSYS 13.0 CFX software operated under the Windows VISTA 32-bit operating system. Analysis using CFX is much simpler than Fluent as the MHD option can be easily activated for the simulation. To start with the analysis, the problem needs to be categorized in either steady state or transient state. In this study, the problem is taken as a steady state problem.

3.6.1 Assumptions

To begin with any process, it may be theoretical or experimental, there are certain assumptions which are applied throughout the process. Similarly, the assumptions considered here are as follows.

i. The IEG remains constant.
ii. Material properties of the tool and work-piece never change throughout the analysis.
iii. Tool and work-piece materials are homogenous.
iv. Heat generation is only due to Joule's heating.
v. Material removal depends only on the current density.
vi. Electrolyte is considered to be a two phase mixture of an incompressible fluid and gas.
vii. Diameter of hydrogen bubbles produced is taken as 30µm universally.
viii. Velocities of the two phases in the electrolyte are equal (homogenous model).
ix. For the simplicity of the process, properties of air are considered instead of hydrogen.

Table 3.3: Material properties

Properties	Brine	Copper	Iron	Air
Molar mass(Kg/Kmol)	58.44	63.55	55.85	-
Density(Kg/m^3)	1050	8933	7860	-
Specific heat(J/KgK)	3760	385	460	-
Dynamic viscosity(Pa s)	0.001	-	-	-
Thermal Conductivity(W/mK)	0.6	401	80	-
Electrical Conductivity(S/m)	8.43	5.96E+07	1E+07	-
Convection coefficient (W/m^2K)	1000	-	-	100

3.6.2 Boundary Conditions

Before considering the boundary conditions, the computational domains should be specified. In this simulation three domains are being used such as two solid domains and a fluid domain. One solid domain for work-piece and other is for tool. Materials of solid domain are considered as pure solids. Morphology of materials in the solid domain is given as continuous solid and reference temperature is given 298K. Electric potential model with automatic value is chosen from Electromagnetic model. Fluid domain is constructed for electrolyte. Two materials are taken for fluid domain as it is a two phase flow analysis. Morphology for fluid domain is taken as continuous fluid for brine and dispersed fluid for hydrogen bubbles. The properties of the materials used in these domains are set as per the values in the Table 3.3. The conductivity of the electrolyte varies with respect to temperature according to the equation 3.12 and keeping other properties constant. This equation is written as CEL expression and directly assigned it as material property. α- value is taken as 0.01 K^{-1}. Boiling temperature for brine is taken as 373K.

Valence for iron is taken as 2. In this simulations Iron is used as the work-piece material, copper as the tool material and 20% Nacl brine with hydrogen bubbles as the electrolyte material.

The following boundary conditions are used for each domain for the simulation to be carried out as a two phase flow.

i) DOMAIN- BRINE

This domain is a fluid domain. The morphology consists of 2 types such as continuous fluid for brine and dispersed fluid for air. Minimum volume fraction for air is taken as 10^{-15}. The buoyancy model is not enabled here. For fluid pair, homogenous model is used for multiphase model whereas free surface model is deactivated in this simulation. Heat transfer is by thermal energy and for turbulence k-ϵ model is considered and medium intensity (5%) is considered for turbulence. The surface tension coefficient is taken as 0.33 N/m. The interphase transfer is by particle model and mass transfer is by cavitation which is Rayleigh plesset.

For cavitation model,

Mean diameter = 2.0×10^{-6} m,

Saturation pressure = 150 atm,

Cavitation condensation coefficient = 0.01

Cavitation vaporization coefficient = 50

Maximum density ratio = 1000

Nuclei volume fraction = 5.0×10^{-4}

Cavitation rate under relaxation factor = 0.25

Various boundaries those are present in the domain brine as given as follows

a. Inlet

Boundary type = inlet

Mass and Momentum = Normal speed = 40 m/s

Flow regime = Subsonic

Turbulence = Medium intensity (5%)

Fractional intensity =0.06

Heat transfer static temperature = 298K

Electric field = zero flux

Brine volume fraction = 1.0

Hydrogen volume fraction = 0.0

b. Outlet

Boundary type = opening

Mass and Momentum = Opening pressure and direction = 0 Pa and flow normal to the boundary

Flow regime = Subsonic

Turbulence = Medium intensity (5%) and auto computation length

Fractional intensity =0.06

ii) DOMAIN-TOOL

This domain is a solid domain with stationary domain motion. The morphology consists of a continuous solid and the material used is copper. Heat transfer is by thermal energy. Electromagnetic model is activated with electric potential as the concerned factor for electric model. For domain initialization, temperature is set at 298 K and electric potential is set as 0 V. Different boundaries present in the domain tool are given as follows.

a. Tool top

Boundary type = Wall

Location = Tool top

Heat transfer coefficient = 100 W/m^2K

Outside temperature = 298 K

b. Tool outer

Boundary type = Wall

Location = Tool outer

Heat transfer coefficient = 100 W/m^2K

Outside temperature = 298 K

Electric field = zero flux

iii) DOMAIN-WORK

This domain is a solid domain as that of domain tool with stationary domain motion. The morphology consists of a continuous solid and the material used is iron. Heat transfer is by

thermal energy. Electromagnetic model is activated with electric potential as the concerned factor for electric model. For domain initialization, temperature is set at 298 K and electric potential is set as 10 V. Different boundaries present in the domain tool are given as follows.

a. Work bottom

Boundary type = Wall

Location = Work bottom

Heat transfer coefficient = 100 W/m^2K

Outside temperature = 298 K

Electric field = Zero flux

b. Work outer

Boundary type = Wall

Location = Work bottom

Heat transfer coefficient = 100 W/m^2K

Outside temperature = 298 K

Electric field = Zero flux

iv) INTERFACES

It is the connection between two similar or dissimilar domains. Here we have considered two interfaces as follows.

a. Brine-Tool

Interface type = Fluid solid

Interface side 1 = brine top

Interface side 2 = Tool bottom

Interface model = general connection

Mesh connection = automatic

Heat transfer = conservative interface flux

b. Brine-Work

Interface type = Fluid solid

Interface side 1 = brine bottom

Interface side 2 = Work top

Interface model = general connection

Mesh connection = automatic

Heat transfer = conservative interface flux

After applying the above boundary conditions, High resolution advection scheme was taken with first order turbulence numeric. Auto time scale is taken and RMS value is taken for residual type. The residual target is 1×10^{-4}. For conservation target, value of 0.01 is taken. For running the program, multiphase control with segregated volume fraction coupling is enabled.

3.7 SUMMARY

Geometries of all the three Models are explained with proper figures and dimensions. A grid independence study was done while carrying out meshing in order to find the best mesh resolution. Governing equations are described for the two phase flow analysis which includes both computational fluid dynamics equations as well as user defined equations. Before doing the analysis, the material properties of all the three materials of tool, work-piece and brine are studied and presented. Assumptions as well as the boundary conditions are presented for the analysis of the simulation.

CHAPTER 4
EXPERIMENTATION

4.1 INTRODUCTION

This chapter deals with the experiment that has been conducted in the ECM set up available in the production engineering laboratory of N.I.T Rourkela. The experiments were conducted with three L-shaped tools as per the dimensions of model 1; model 2 and model 3 to find out the MRR to validate the simulation results.

4.2 ECM SET UP

The ECM set up used for the experiment is as shown in the Fig. 4.1 and the control panel is as shown in Fig. 4.2. The detailed specification of the machine is given below in the Table 4.1.

Fig. 4.1: ECM set up used for the experiment

Fig. 4.2: Control panel

4.3 FABRICATION OF TOOL AND WORK-PIECE

To carry out the experiment, we need to fabricate the tool and work-piece of exact dimension as that in the modelling. For fabricating the tool, we have procured a copper rod of nearly 800 gram weight as shown in the Fig. 4.3. After procurement, we cut the rod into three pieces for producing the models 1, 2 and 3. Then facing and turning operation was done in each of the pieces. After then, a marker was used to draw lines on the pieces so that we can file them properly as per the required size and shape. Hence, L-shape is produced by filing as shown in Fig. 4.4 and to polish it, we have used grinding operation as shown in Fig. 4.5. Again, for the groove, a through hole is drilled on the tool by the help of the drilling machine. Then, as per the requirement of the design, either slot or chamber is made on the bottom of the tool for model 2 and 3 respectively. Model 1 only contains the groove. Now, the L-shape is ready. A pipe having one side threaded end is used for connecting the tool with the tool holder. The pipe is fabricated with a through hole of same dimension as that of the groove in the tool. The pipe is shown in the Fig. 4.6. After generation of L-shape and the pipe, both of them are aligned properly and brazed as shown in the Fig. 4.7. After brazing, the required tool is ready as shown on Fig. 4.8. Bottom of the tools for the model 1, 2 and 3 are as shown in Fig. 4.9, 4.10 and 4.11

respectively. The work-piece material used is mild steel which is procured and is cut in to 18 circular pieces of diameter 60 mm.

Table 4.1: Detailed specification of ECM set up

Sl. No	Parameters	Specification
1	Working gap	0.05-0.8 mm
2	Current density	5-100 A/cm^2
3	Voltage	5-30 V
4	Current	50-40,00 A
5	Temperature	30-80 ^0C
6	Velocity	5-50 m/s
7	MRR	15×10^3 mm^3/min
8	Inlet pressure	0.15-3 MPa
9	Outlet pressure	0.1-0.3 MPa
10	Feed rate	0.1-20 mm/min
11	Electrolyte used	NaCl solution or $NaNo_3$ solution
12	Specific power consumption	7 W/mm^3/min
13	Accuracy and surface finish	0.02 mm, 0.4 µm
14	Critical parameters	Voltage, current, feed rate, electrolyte conductivity
15	Applications	Machining hard material, machining complex shaped parts like blind complex cavities, curved surface through cutting etc
16	Limitations	High specific energy consumption, Not applicable to electrically non- conducting materials and for jobs with very small dimensions.
17	Mechanical properties	Stress free machining reduced tool wear
18	Surface properties	No thermal damage

Fig. 4.3: Copper rod with dia. = 60 mm

Fig. 4.4: L-shape after filing

Fig. 4.5: Grinding operation on L-shape

Fig. 4.6: Threaded pipe

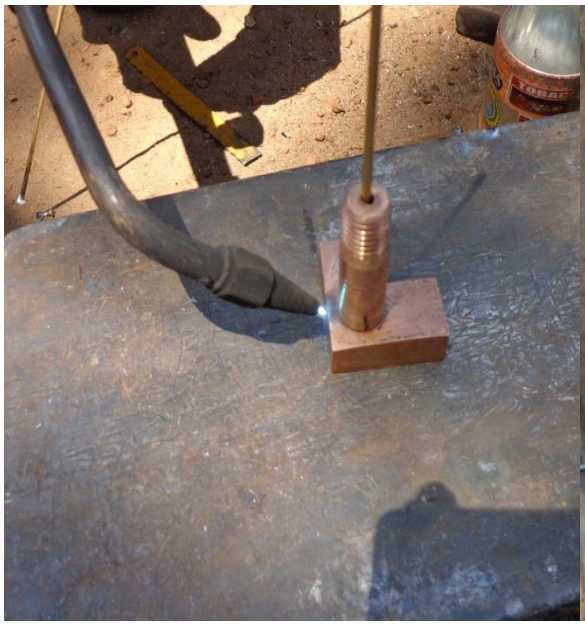

Fig. 4.7: Brazing of tool

Fig. 4.8: Final desired tool

Fig. 4.9: Bottom of model 1

Fig. 4.10: Bottom of model 2

Fig. 4.11: Bottom of model 3

4.4 TAGUCHI EXPERIMENTAL DESIGN AND ANALYSIS

4.4.1 Taguchi Philosophy

Taguchi's unparalleled work in the field of quality engineering is one of the engineering achievements of the 20th century. Effective and specialized application of engineering strategies was the main motive behind his work. Both upstream and shop-floor quality engineering systems are included in these strategies. Upstream methods effectively use small-scale experiments to reduce variability and to improve cost effectiveness. Shop-floor techniques are real time techniques which are used for monitoring and maintaining quality in production. Taguchi's philosophy is based on the following three fundamental principles:

1. Quality should be designed into the product and not inspected into it.
2. Quality is best achieved by minimizing the deviations from the target. The product or process should be so designed that it is immune to uncontrollable environmental variables.

3. The cost of quality should be measured as a function of deviation from the standard and the losses should be measured system-wide.

Taguchi realized that the best way to eliminate variation is during the initial stages of the product which means during the design of a product and its manufacturing process. Consequently, he developed a strategy in quality engineering that can be used in both contexts. The process has three stages:

1. System design

This is the conceptual level design which involves creativity and innovation.

2. Parametric design

This design is called as robustification. After the concept is established, nominal values of various parameters are set in this stage.

3. Tolerance design

After the completion of parametric design, the effect of various parameters on performance is studied and the variations in the critical parameters on the performance are reduced.

In the present work, Taguchi's design approach is used to study the effect of process parameters on the material removal rate of the ECM process.

4.4.2 DESIGN STRATEGY

Taguchi's design focused at greater understanding of variations of parameters. Taguchi proposed to extend each experiment with an "outer array" called the orthogonal array. Use of linear graphs and triangular tables proposed by Taguchi has made the assignment of parameters simple. Taguchi introduced many methods for analyzing experimental results. ANOVA (Analysis of Variance) is one of them. ANOVA is a type of statistical hypothesis testing used in the analysis of experimental data. A statistical hypothesis test is a method of making decisions using data. In the present work, ANOVA has been performed. The effect of the selected ECM process parameters on the response have been investigated through the main effect plots based on ANOVA. The optimum condition for each of the parameter in order to improve the response has been estimated. In this experiment, Minitab 14 software for Taguchi

design was used. In this study, 3 level designs (3 factors) with total of 9 numbers of experiments has been conducted and hence the OA L9 was chosen. The machining parameters and their level with details are shown in Table 4.2. The experimental observations for models 1, 2 and 3 are shown in the Tables 4.3, 4.4 and 4.5 respectively.

Table 4.2: Machining parameters and their levels

Machining parameters	Symbol	Unit	Levels		
			Level 1	Level 2	Level 3
Voltage	V	V	10	12.5	15
Flow rate	F	m/s	30	35	40
Concentration	C	g/L	60	85	110

Table 4.3: Experimental observation table for model 1 using L9 orthogonal array

Run	Voltage, V	Flow rate, m/s	Concentration, g/L	Initial weight (W_i)g	Final weight (W_f) g	Time (t) min	MRR, mm^3/min
1	10	30	60	419	418	10	12.7226
2	10	35	85	379	377	10	25.4453
3	10	40	110	418	416	5	50.8906
4	12.5	30	85	538	535	10	38.1679
5	12.5	35	110	454	452	10	25.4453
6	12.5	40	60	455	454	5	25.4453
7	15	30	110	413	411	10	25.4453
8	15	35	60	414	413	10	12.7226
9	15	40	85	514	512	5	50.8906

Table 4.4: Experimental observation table for model 2 using L9 orthogonal array

Run	Voltage, V	Flow rate, m/s	Concentration, g/L	Initial weight (W_i) g	Final weight (W_f) g	Time (t) min	MRR, mm^3/min
1	10	30	60	407	405	10	25.4453
2	10	35	85	419	418	10	12.7226
3	10	40	110	405	402	5	76.3359
4	12.5	30	85	487	485	10	25.4453
5	12.5	35	110	368	366	10	25.4453
6	12.5	40	60	371	368	5	76.3359
7	15	30	110	361	359	10	25.4453
8	15	35	60	362	361	10	12.7226
9	15	40	85	480	477	5	76.3359

Table 4.5: Experimental observation table for model 3 using L9 orthogonal array

Run	Voltage, V	Flow rate, m/s	Concentration g/L	Initial weight (W_i) g	Final weight (W_f) g	Time (t) min	MRR, mm^3/min
1	10	30	60	301	299	5	50.8906
2	10	35	85	401	399	5	50.8906
3	10	40	110	299	296	5	76.3359
4	12.5	30	85	490	487	5	76.3359
5	12.5	35	110	351	349	5	50.8906
6	12.5	40	60	354	351	5	76.3359
7	15	30	110	370	368	5	50.8906
8	15	35	60	373	370	5	76.3359
9	15	40	85	381	379	5	50.8906

Sample calculation (For run 1) for MRR:

$$MRR = \frac{Initial\ weight(Wi) - Final\ weight(Wf)}{density \times Time(t)} \qquad (4.1)$$

$$MRR = \frac{419 - 418}{7.86 \times 10}\ cm^3/_{min}$$

$$= 0.0127226 \times 10^3\ mm^3/_{min}$$

$$= 12.7226\ mm^3/_{min}$$

The iron work-pieces after machining for all the runs in models 1, 2 and 3 are as shown in Figs. 4.12- 4.16.

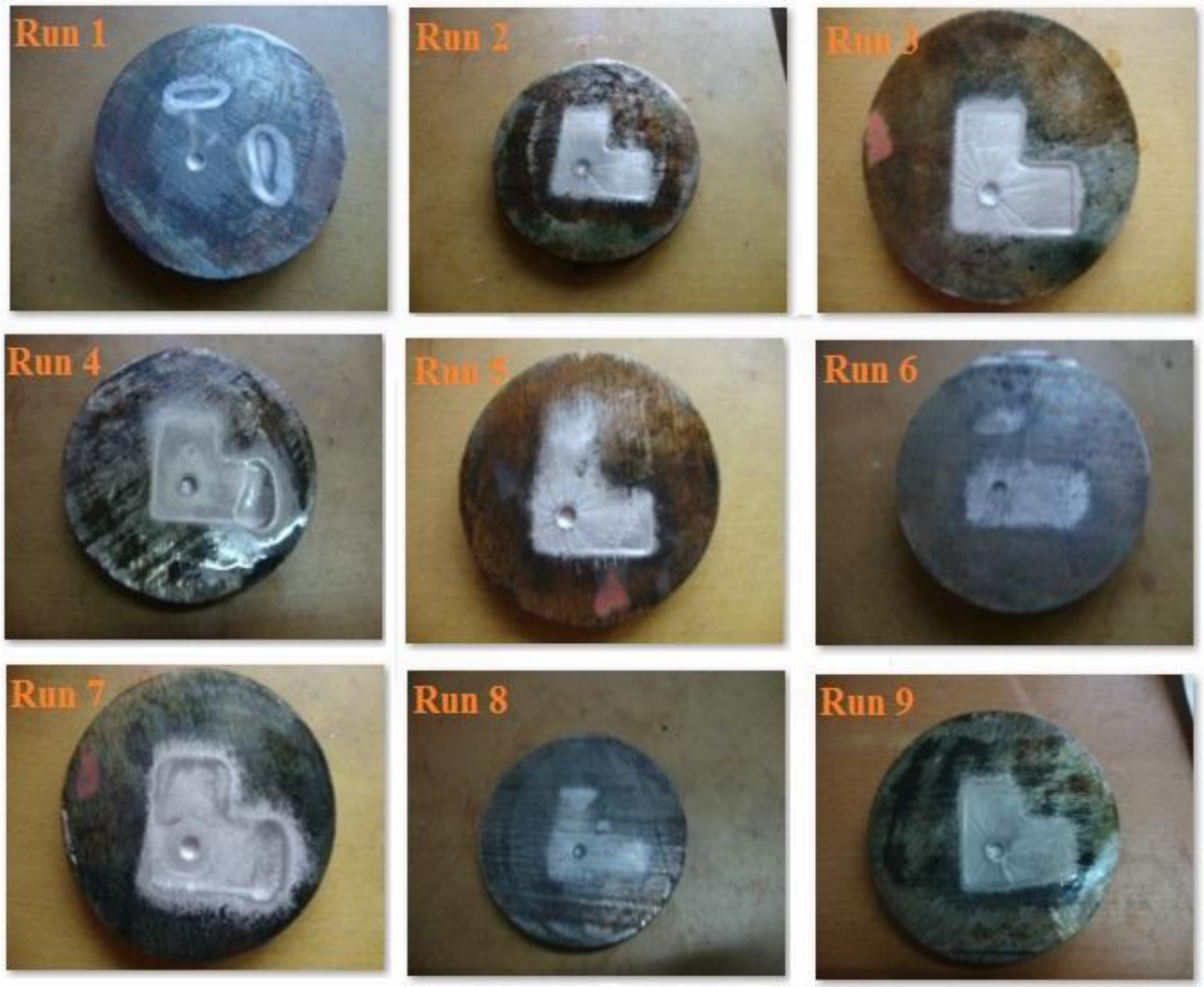

Fig. 4.12: Work-pieces after machining for Model 1

Fig. 4.13: Work-piece after machining for Model 2

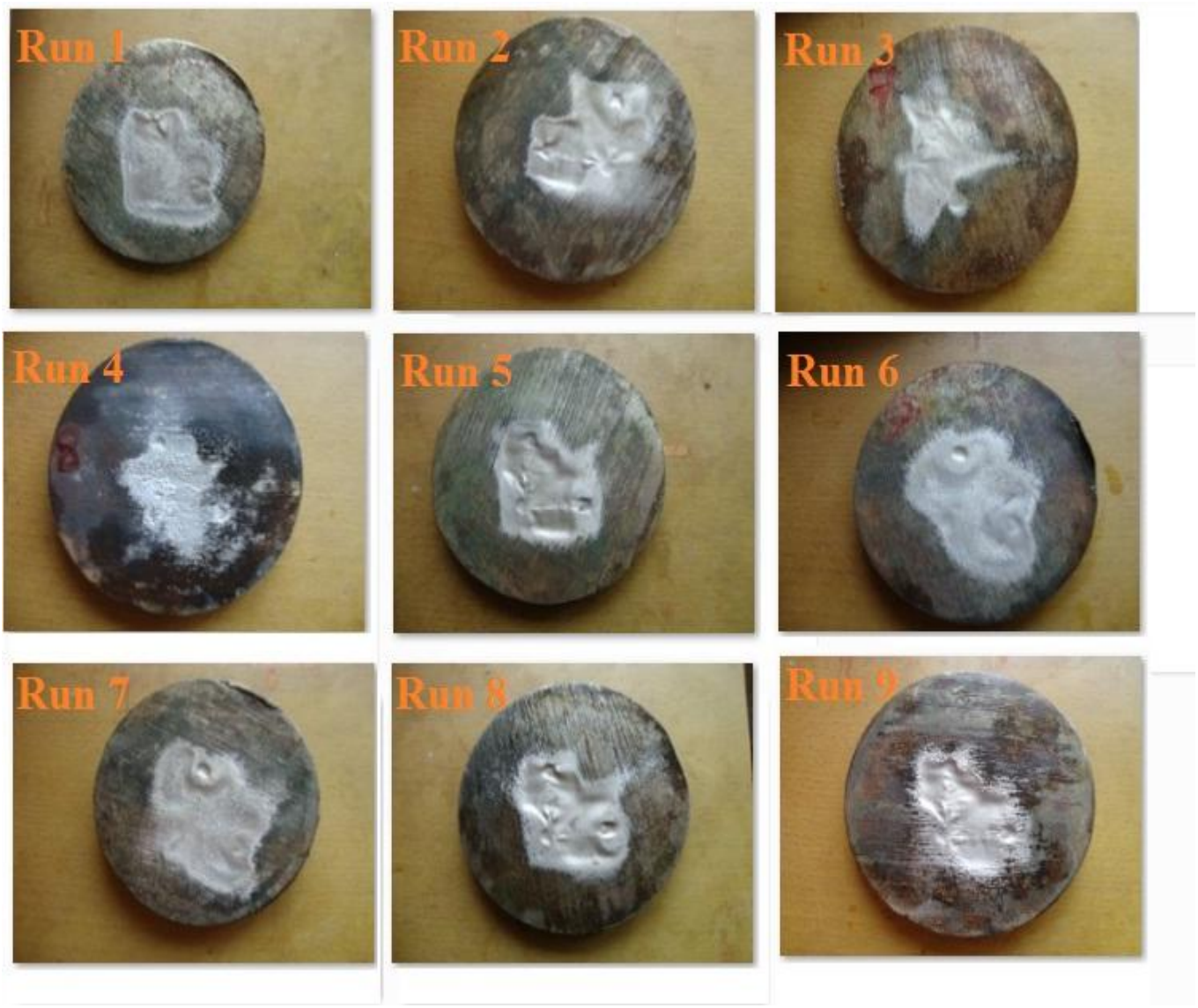

Fig. 4.14: Work-pieces after machining for Model 3

4.5 SUMMARY

The detailed specifications of ECM set up available in the laboratory are presented with figures. For carrying out the experiment, the three tool models were fabricated by using the facilities available in the production engineering laboratory and work shop. Experiments were conducted and the observations were tabulated as per the Taguchi L9 orthogonal array. Wok-piece shapes after machining were also presented.

CHAPTER 5
RESULTS AND DISSCUSSIONS

5.1 INTRODUCTION

This chapter deals with the analysis of the results and discussion of the three models generated in ANSYS CFX as per the chapter 3. It shows the crucial parameters affecting overall machining process of ECM in terms of contours from which we can predict the variation of these parameters in the IEG and their effects.

This chapter also describes the various experimental results we have obtained from the experiment carried out in ECM as per the chapter 4.

5.2 CRITICAL PARAMETERS ANALYSED IN SIMULATION

5.2.1 Volume Fraction Profile

Figures 5.1, 5.2, 5.3 shows the volume fraction profiles of the three models generated. The inlet velocity for this simulation study was taken as 40 m/s. The volume fraction contours shown are the volume fraction of brine in the homogenous mixture of continuous fluid brine and a dispersed fluid hydrogen bubble.

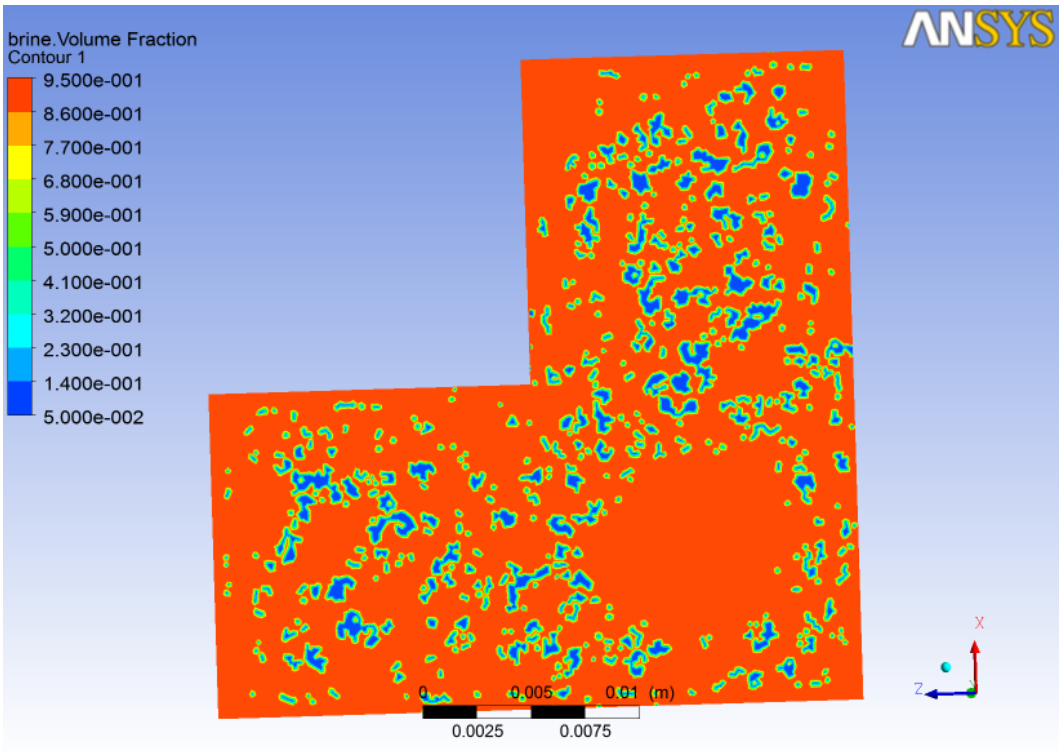

Fig. 5.1: Volume fraction profile for model 1

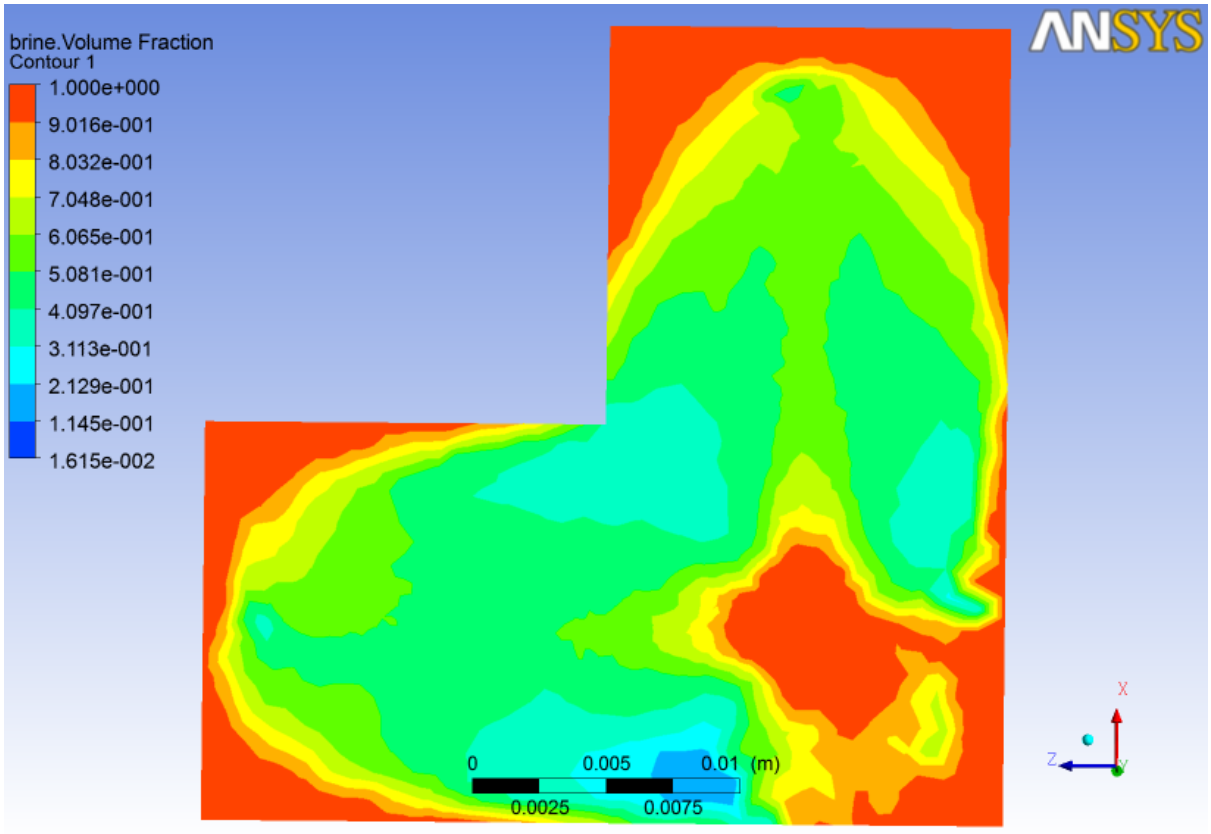

Fig. 5.2: Volume fraction profile for model 2

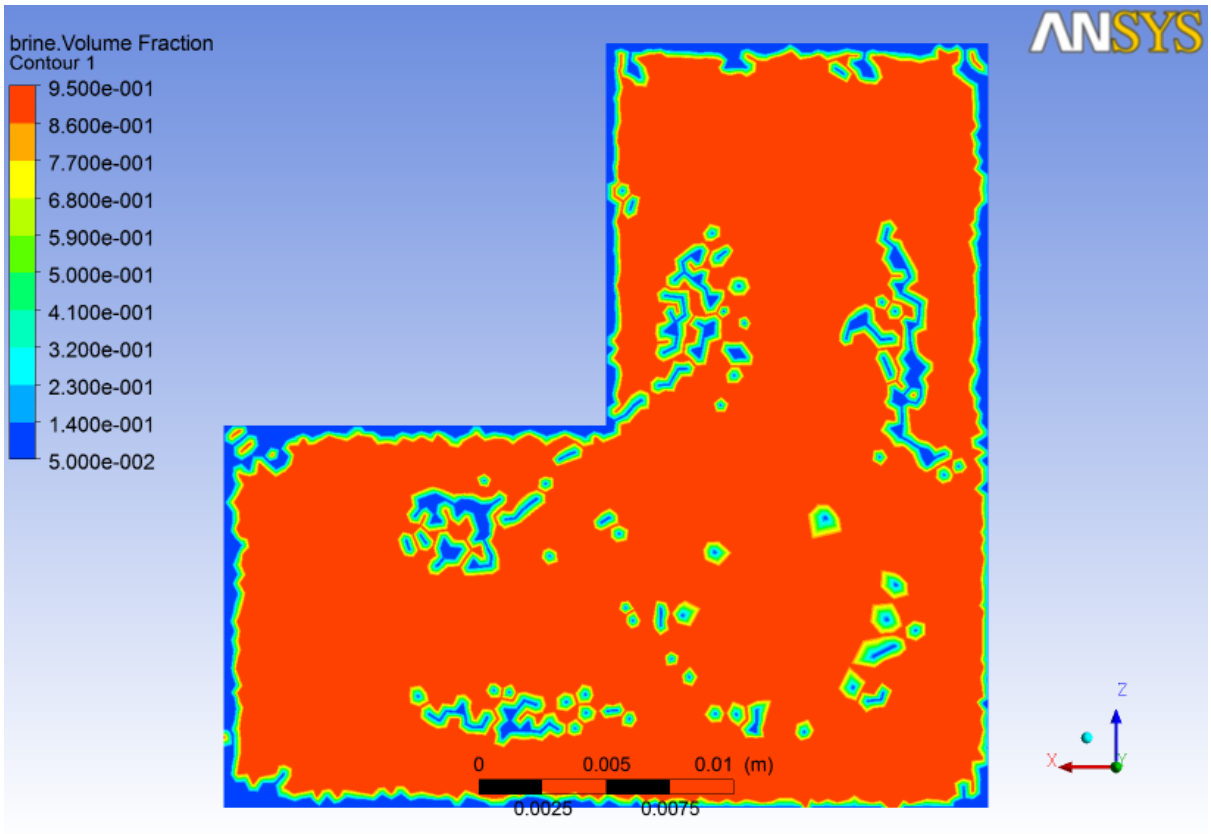

Fig. 5.3: Volume fraction profile for model 3

For model 1, the tool has a through groove within which the electrolyte flows and is supplied in the IEG between the tool and work-piece. Because of the generation of hydrogen bubbles near the cathode and it's flushing by the electrolyte flow, the amount of hydrogen bubbles go on increasing as we move from the groove outlet towards the outer boundaries as shown in Fig. 5.1. But for model 2, because of the slot on the tool bottom for the proper flow of electrolyte, the volume fraction pattern shows a different behavior from the pattern of model 1. The volume fraction of brine is highest at the groove outlet and also at the outer most boundaries. Because of the tool design, the volume fraction of brine for model 2 as shown in Fig. 5.2 is higher at each place than that of model 1. Again the volume fraction pattern for model 3 shows the best behavior as shown in Fig. 5.3. Because of proper flow of electrolyte throughout the L-shape, there are very tiny amount of hydrogen bubbles found in the machining area i.e. in the L-shape. Hence, from the volume fraction profile, model 3 is depicted as the best model.

5.2.2 Interphase Mass Transfer Profile

Figures 5.4, 5.5 and 5.6 show the interphase mass transfer profile for models 1, 2 and 3 respectively.

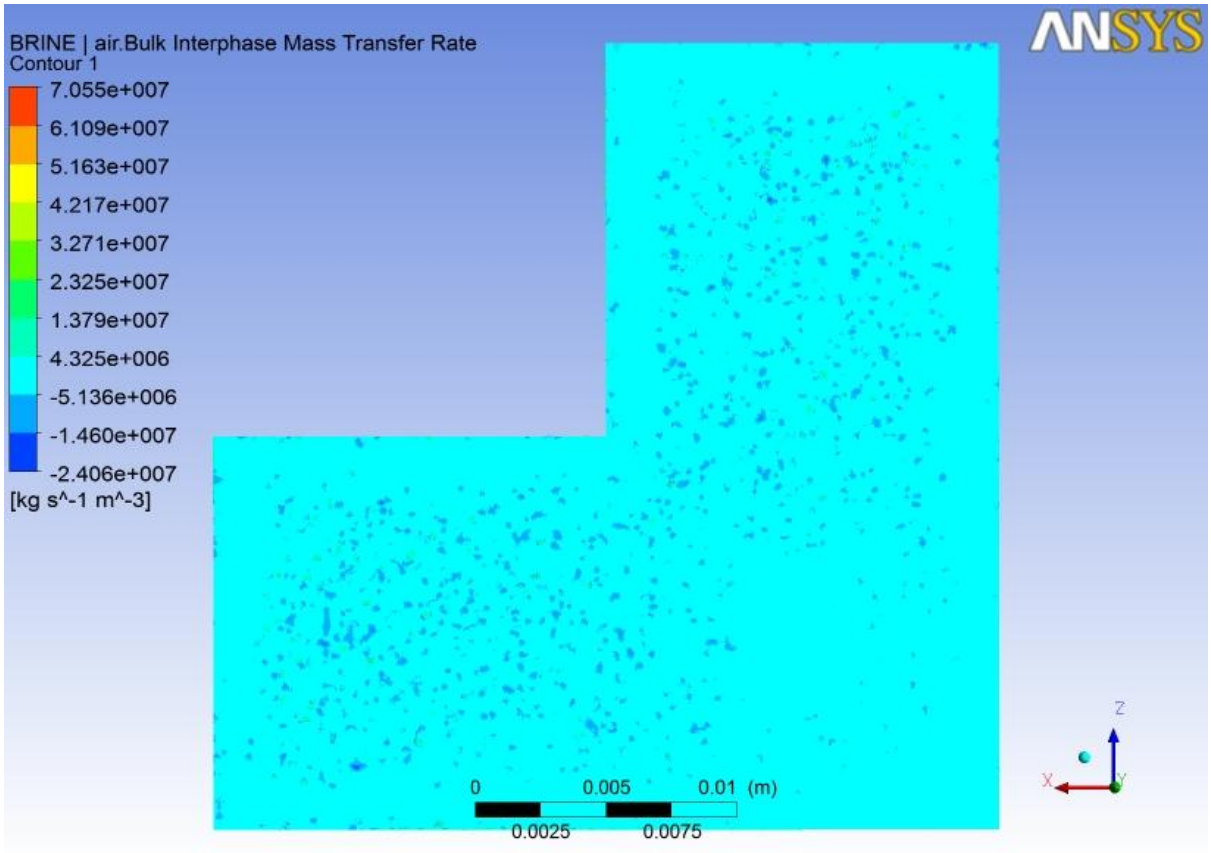

Fig. 5.4: Interphase mass transfer profile for model 1

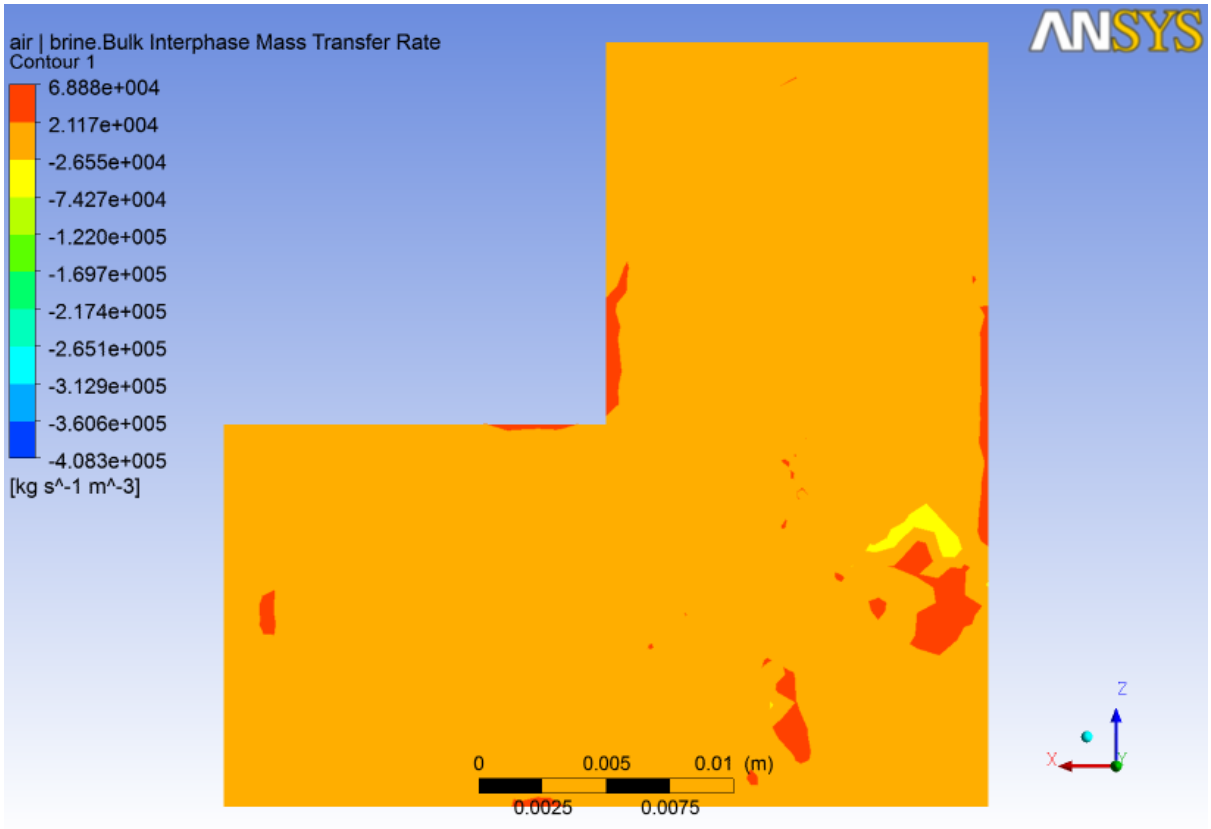

Fig. 5.5: Interphase mass transfer rate for model 2

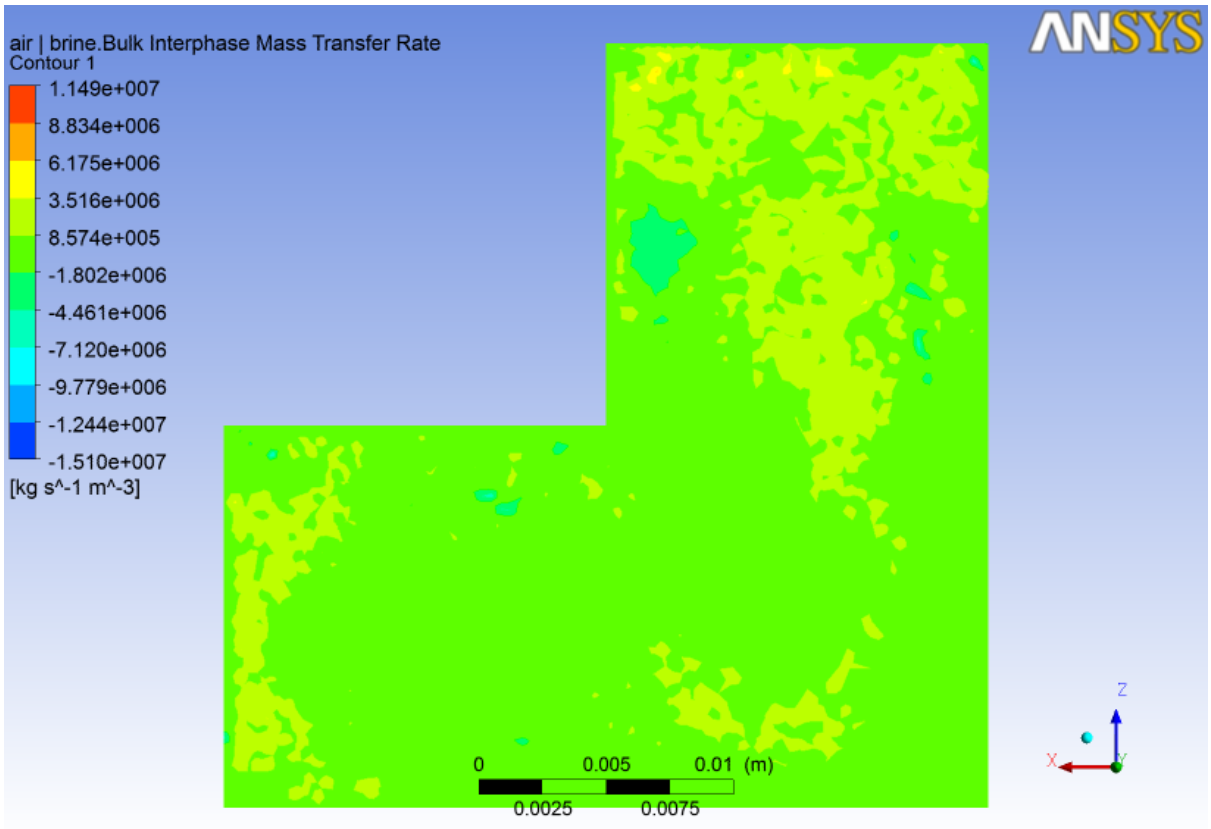

Fig. 5.6: Interphase mass transfer rate for model 3

Interphase mass transfer rate depicts the conversion of secondary phase from primary one. It may occur due to bubbling of brine and hence production of hydrogen bubbles. For model 1 as shown in Fig. 5.4, there is larger amount of conversion from brine to hydrogen and this conversion goes on increasing from the groove outlet towards the outer boundaries. This conversion can be described as nucleus sites formed randomly throughout the L-shape except at the groove outlet. But the interphase mass transfer profile for model 2 as shown in Fig. 5.5 and for model 3 as shown in Fig. 5.6 describes less amount of phase transfer concluding a better electrolyte flow and better tool shape.

5.2.3 Velocity Profile

Figures 5.7, 5.8 and 5.9 show the velocity profile for models 1, 2 and 3 respectively with an inlet velocity of 40 m/s.

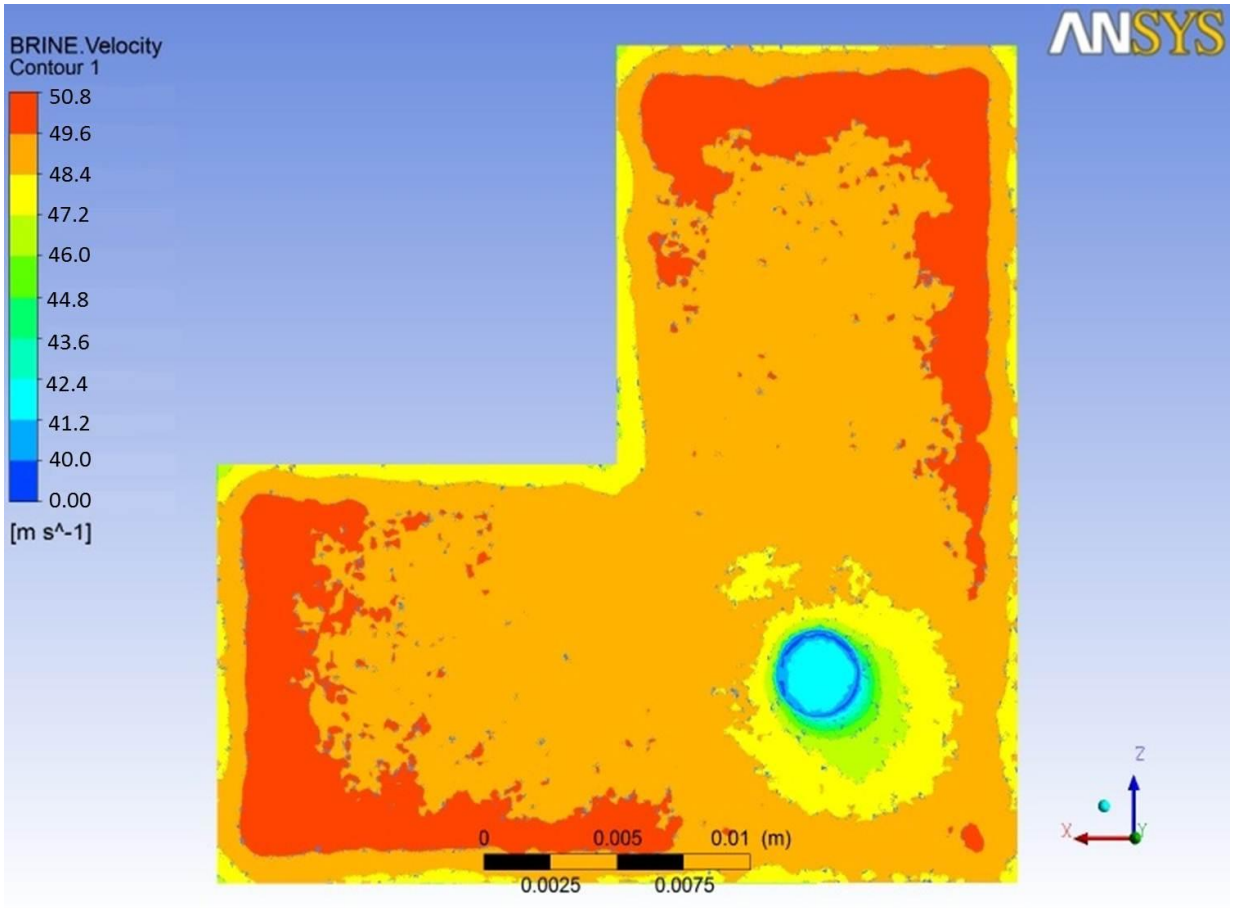

Fig. 5.7: Velocity profile for model 1

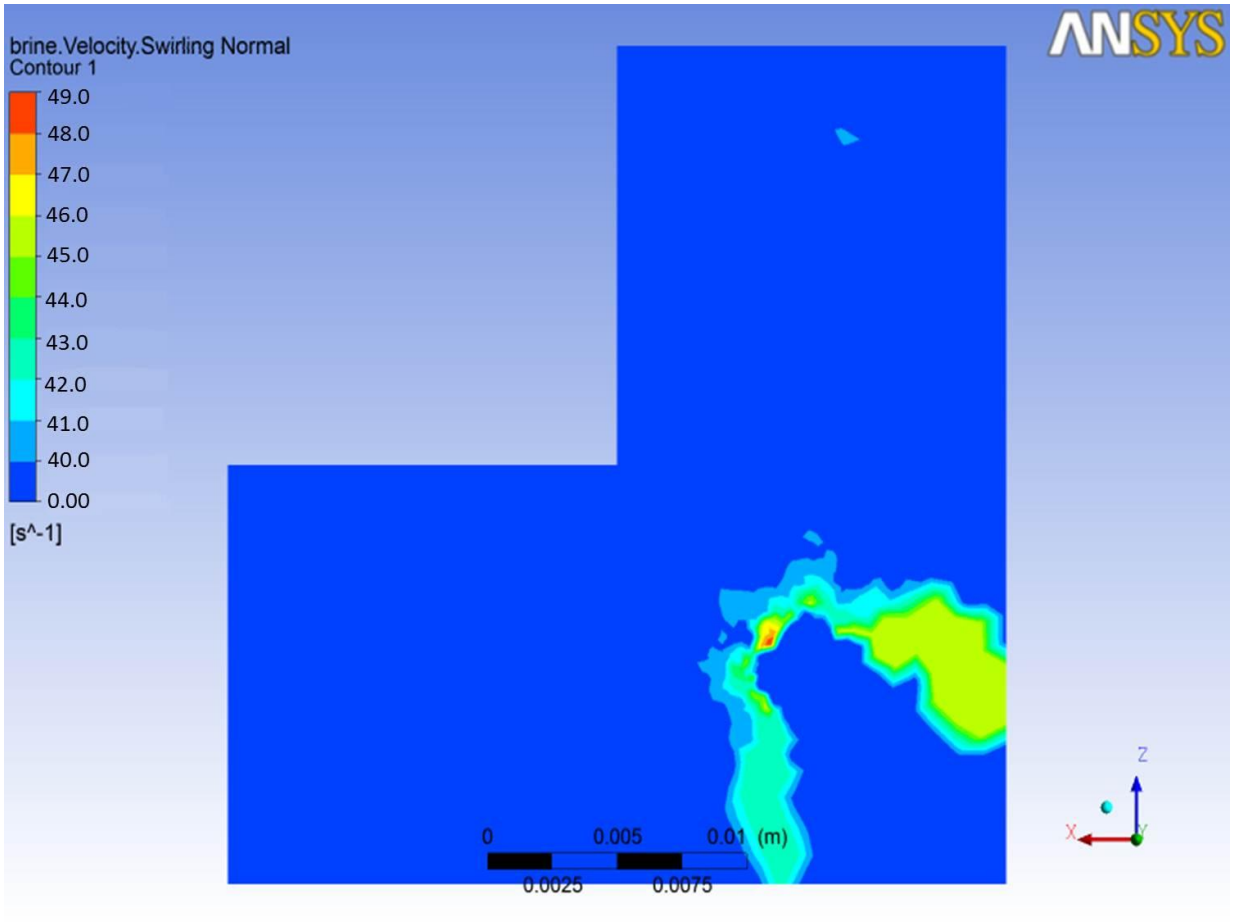

Fig. 5.8: Velocity profile for model 2

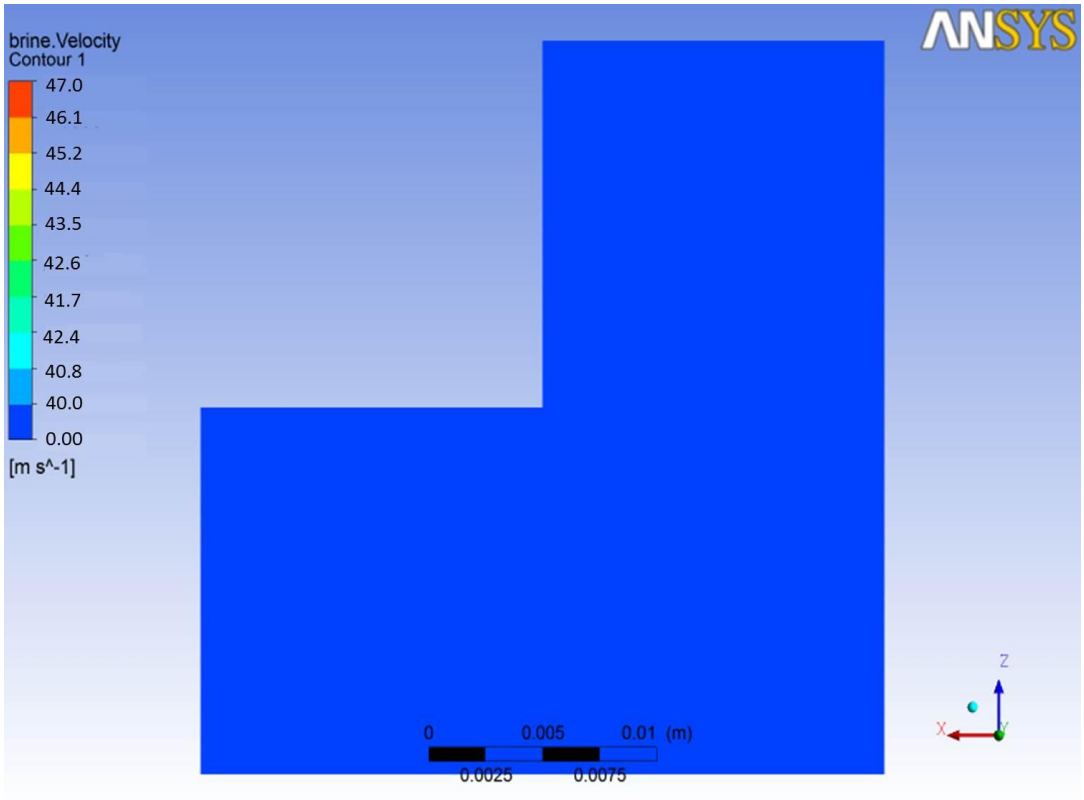

Fig. 5.9: Velocity profile for model 3

The velocity profile for model 1 is as shown in Fig. 5.7 which indicates that velocity of two phase electrolyte is increased from the groove to the boundary partly due to reduction in area of flow and partly due to formation of hydrogen bubbles resulting in more turbulence. But for model 2, due to large reduction in formation of hydrogen bubbles, there is very slight increase in velocity from the groove towards the boundary as shown in Fig. 5.8. But the velocity profile remains almost constant for model 3 as shown in Fig. 5.9.

5.2.4 PRESSURE PROFILE

Figures 5.10, 5.11 and 5.13 describes the pressure contours for model 1, 2, and 3 respectively in the inter electrode gap on the plane of work-piece.

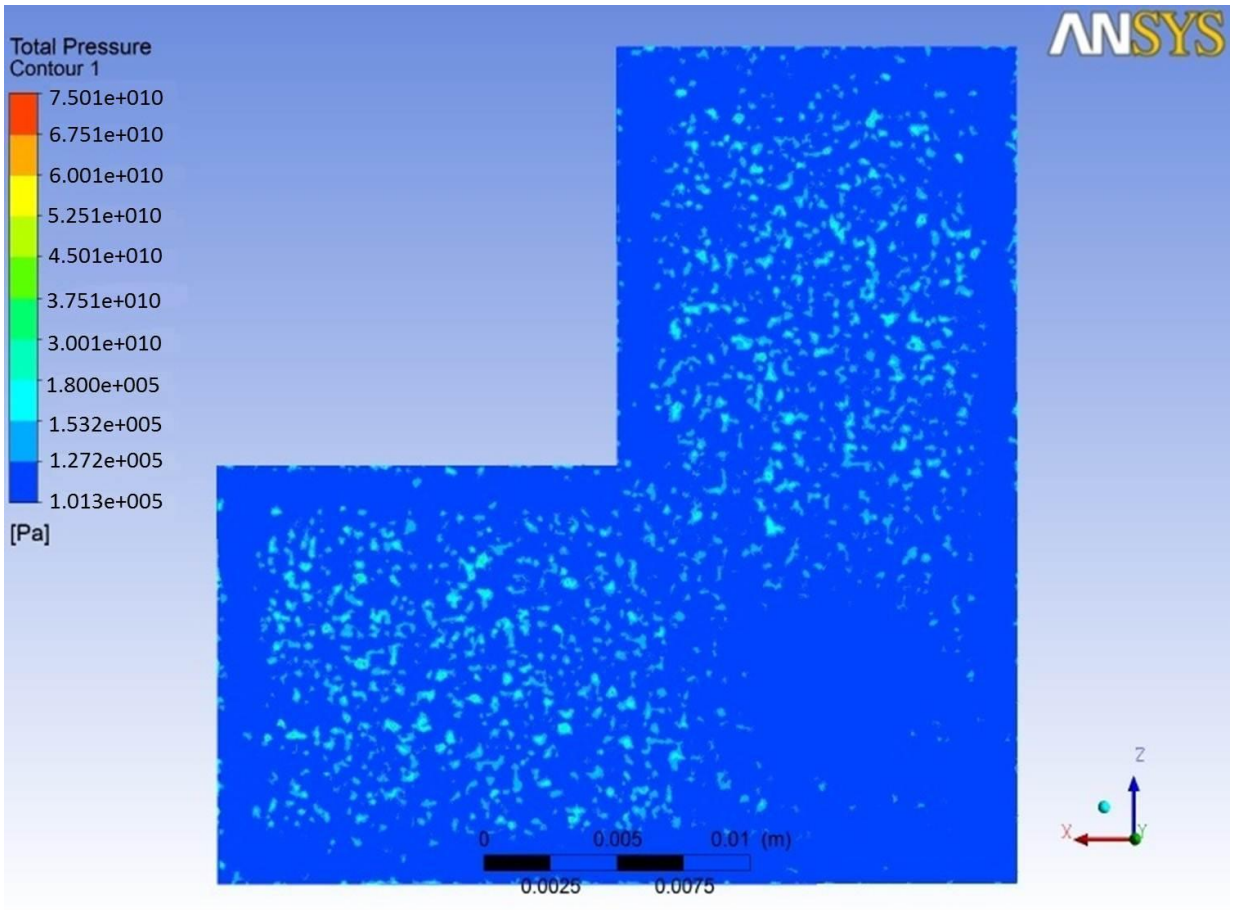

Fig. 5.10: Pressure profile for model 1

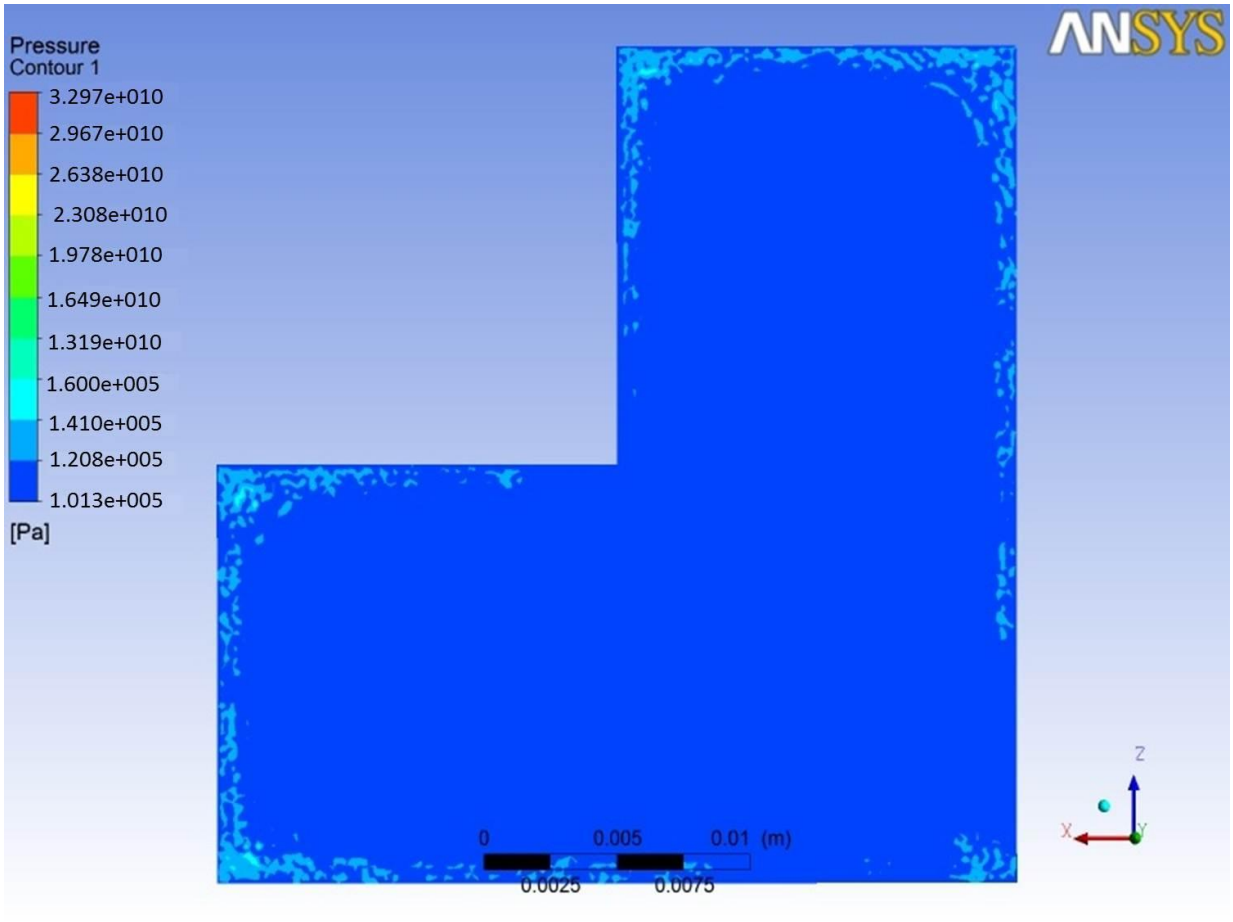

Fig. 5.11: Pressure profile for model 2

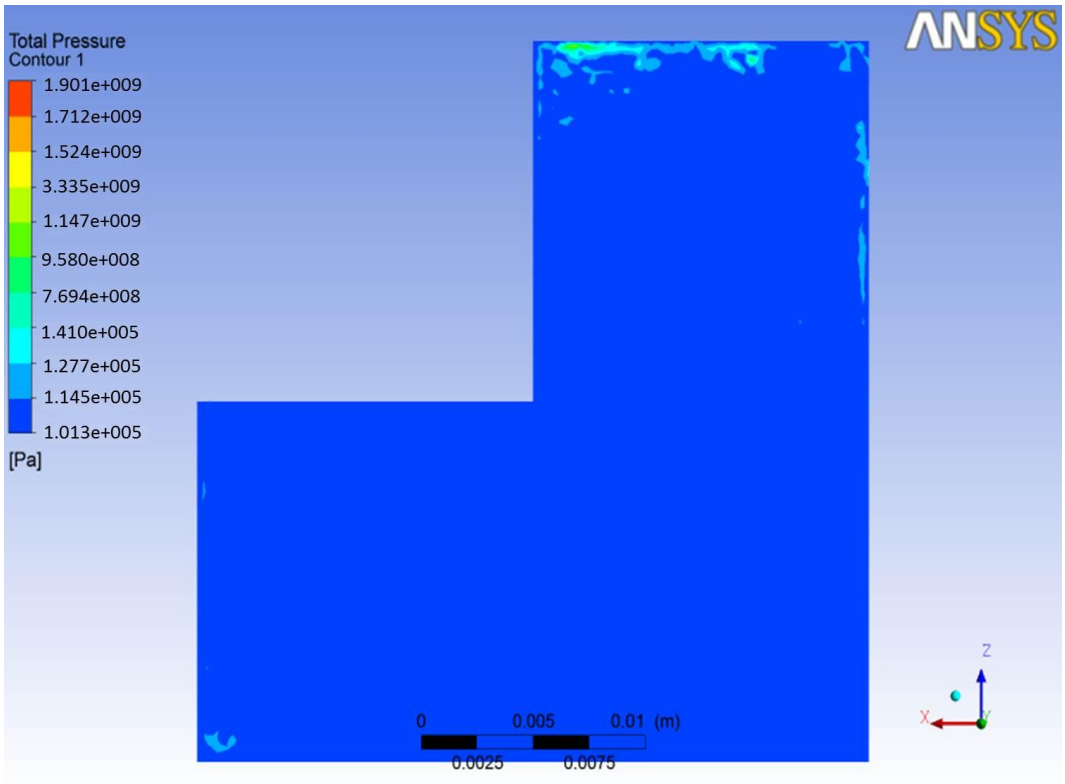

Fig. 5.12: Pressure profile for model 3

The above pressure profiles describe about the variation in pressure in the IEG on the plane of machining area. As in case of model 1, there is very large amount of production of hydrogen bubbles and because of cavitation effect, the pressure increases at a large number of nucleus sites from the groove outlet towards the outer boundaries showing the places of hydrogen bubbles and hence high pressure zones as shown in Fig. 5.10. But in case of model 2, there is very less chance of cavitation and hence the pressure does not increase from the groove towards the outer boundaries. But because of some hydrogen bubbles at the outermost boundaries, the pressure has a higher value at those places as shown in Fig. 5.11. Again, for model 3, where least amount of hydrogen bubbles are generated, pressure pattern remains also same except at a very few points at the outer most boundaries as depicted from Fig. 5.12.

5.2.5 TEMPERATURE PROFILE

Figures 5.13, 5.14, 5.15 demonstrate the temperature patterns for the generated models 1, 2 and 3 respectively.

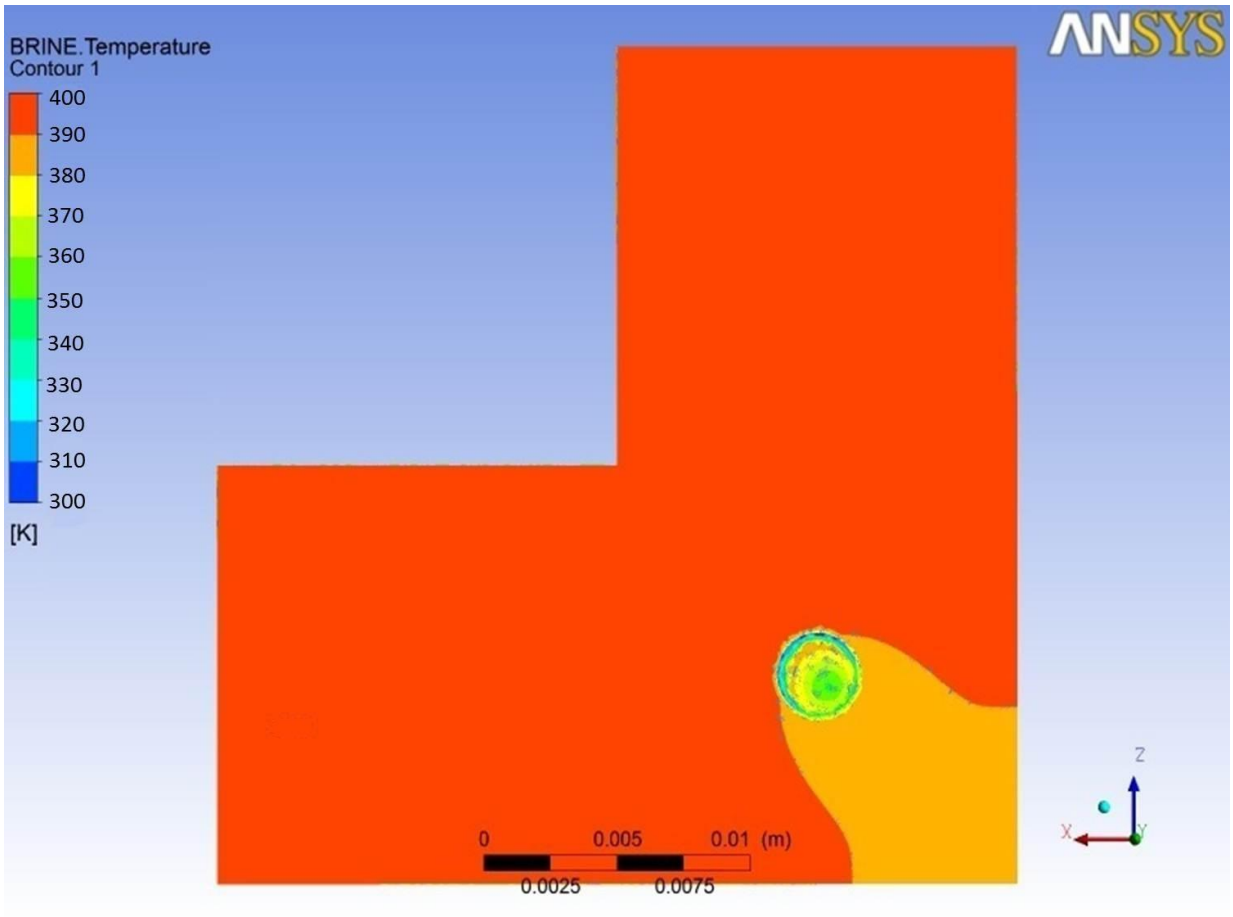

Fig. 5.13: Temperature pattern for model 1

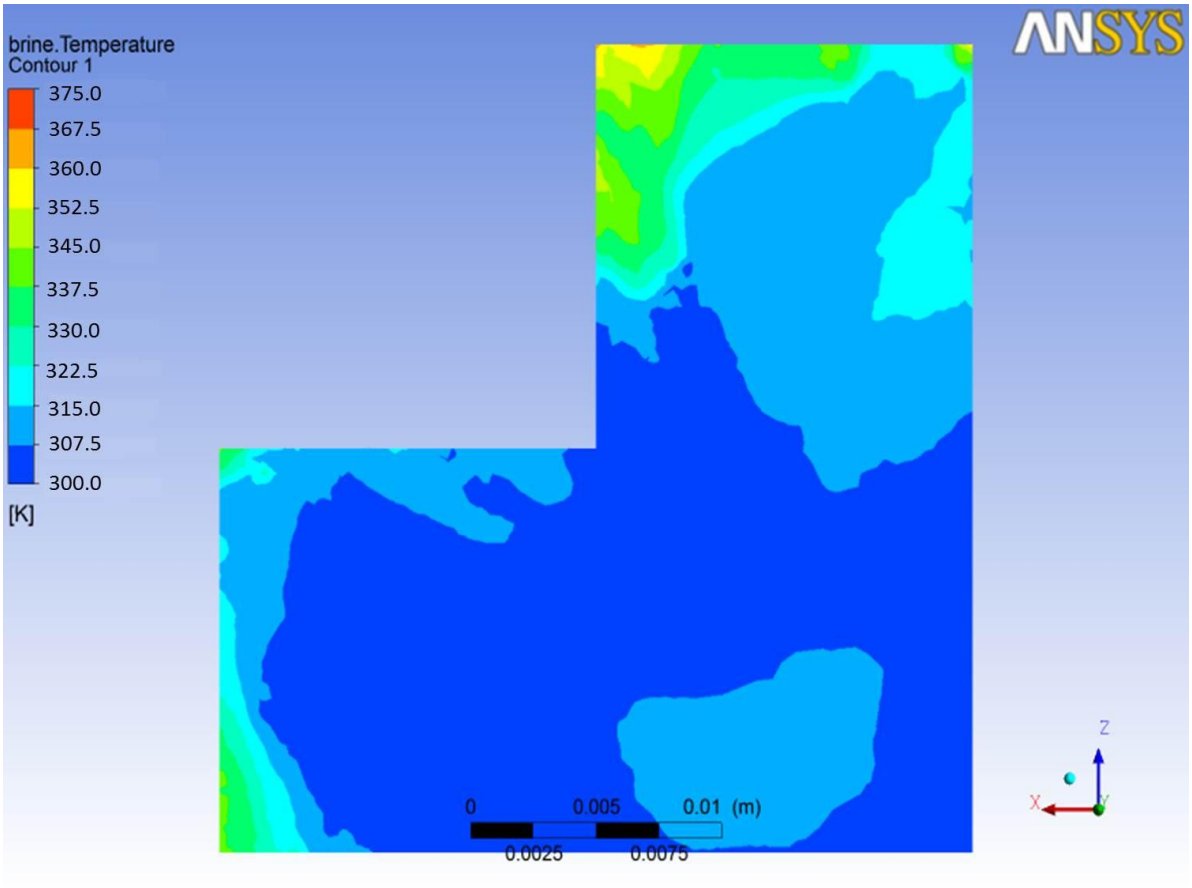

Fig. 5.14: Temperature pattern for model 2

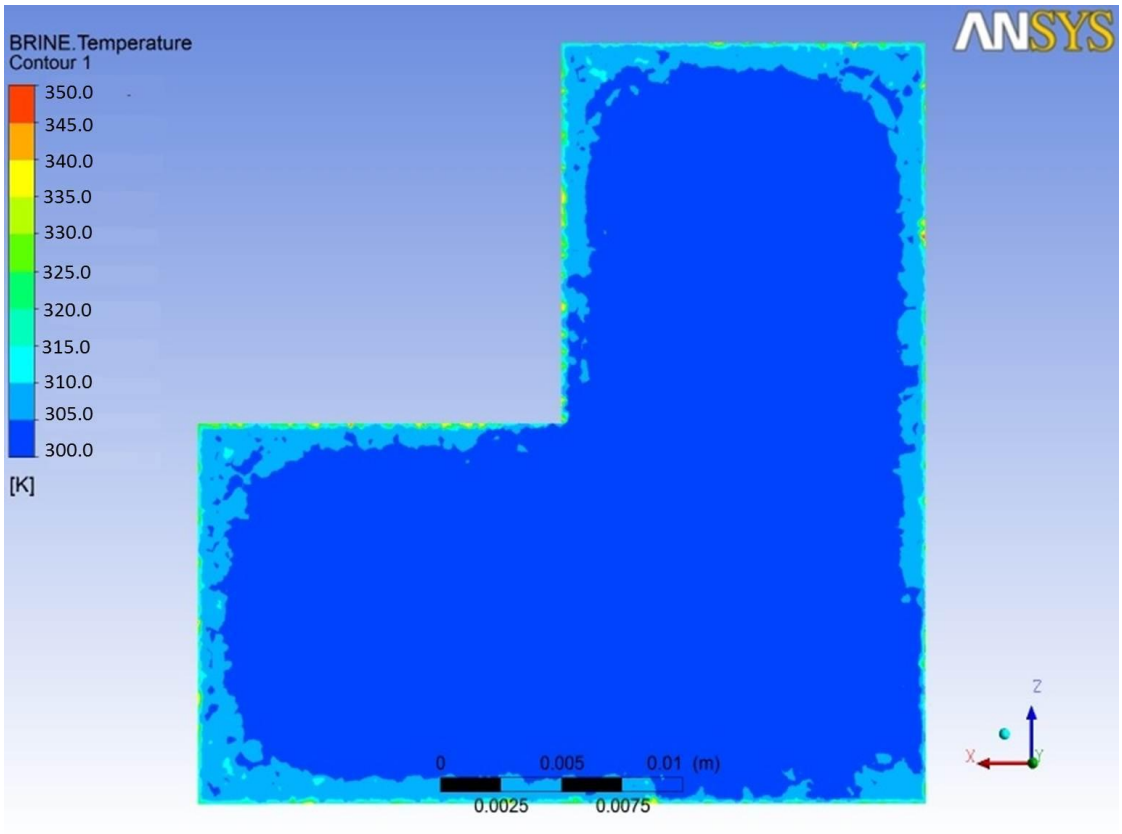

Fig. 5.15: Temperature pattern for model 3

Temperature pattern is a very crucial aspect for this study. As can be seen from the Fig. 5.13, the temperature is least at the groove outlet and goes on increasing rapidly as we move to outside for model 1. It crosses the boiling point of brine which in turn produces phase change and production of hydrogen bubbles as secondary dispersed phase. But for model 2, as shown in Fig. 5.14, the temperature is below the boiling point of brine at most of the points except at the boundaries and at very few inside points. For model 3, the temperature pattern shows the best behavior, as the temperature at every point remains almost constant below the boiling point of brine as shown in Fig. 5.15. The boiling point of brine exceeds only at the outermost boundaries.

5.2.6 Turbulent Kinetic Energy Profile

Figs. 5.16, 5.17 and 5.18 show the turbulent kinetic energy contour for models 1, 2 and 3 respectively.

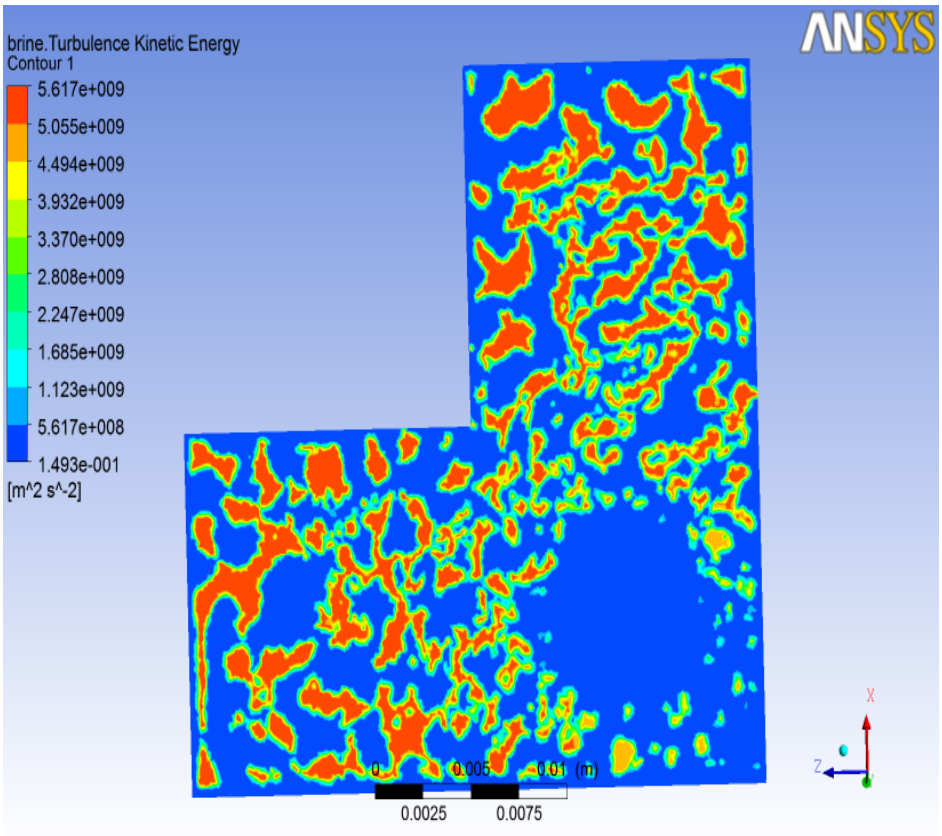

Fig. 5.16: Turbulent kinetic energy contour for model 1

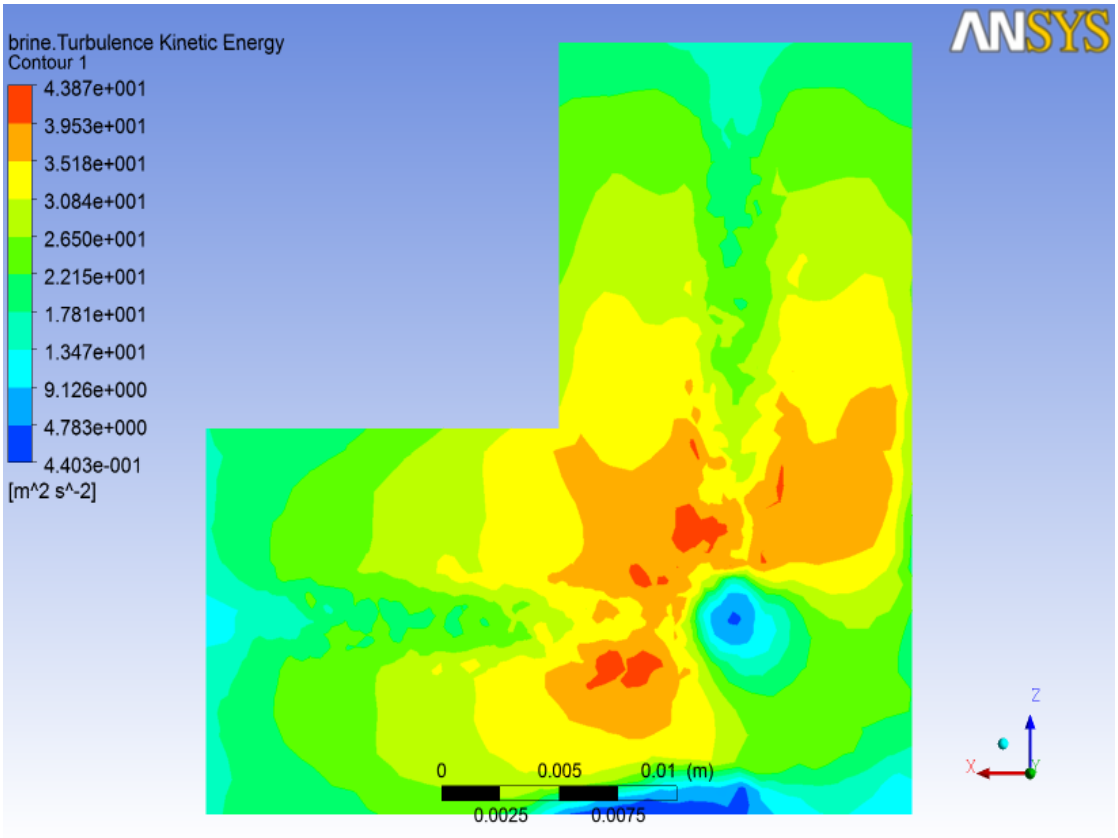

Fig. 5.17: Turbulent kinetic energy contour for model 2

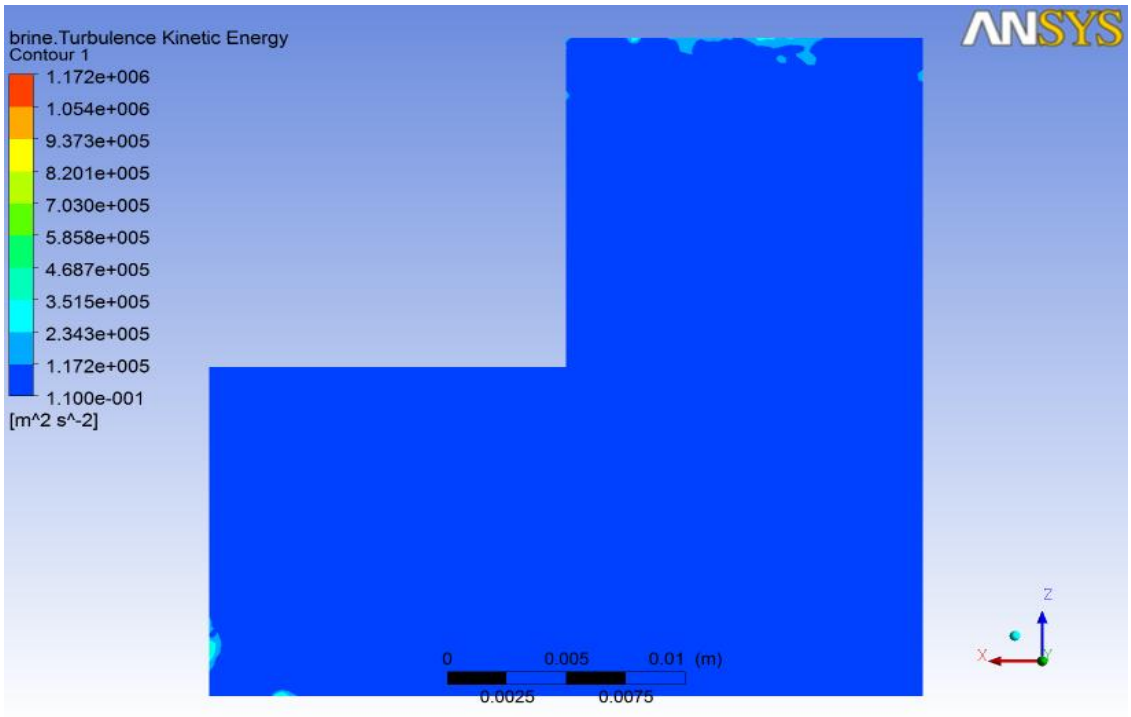

Fig. 5.18: Turbulent kinetic energy contour for model 3

As in this analysis, we have considered k-ϵ model for the turbulence, so there is a variation in k as well as in ϵ for a variation in the turbulence. Turbulence in the k- ε model depends on

turbulent kinetic energy (k) and turbulent eddy dissipation (ε). Roughness of the machined surface has a direct link with the turbulence. Turbulent kinetic energy depicts the energy in the turbulence. Turbulent kinetic energy is produced by fluid shear, friction or buoyancy or through external forces at low frequency eddy scale. For model 1, the turbulent kinetic energy value is lower near the groove outlet and increases towards the outer boundaries because of more turbulence which may be due to the formation of hydrogen bubbles. The minimum turbulent kinetic energy is $1.493 \times 10^{-1}\ {}^{m^2}/_{s^2}$ near the groove whereas maximum value is $5.617 \times 10^{9}\ {}^{m^2}/_{s^2}$ near the outer portions as depicted from the Fig. 5.16. But for model 2, because of the slot on the tool, there is larger turbulence and larger value of turbulent kinetic energy near the groove surrounding and this value reduce towards the outer boundaries. However, on the groove outlet, the turbulent kinetic energy has the minimum value. The minimum value of turbulent kinetic energy is $4.403 \times 10^{-1}\ {}^{m^2}/_{s^2}$ and maximum value is $4.387 \times 10^{1}\ {}^{m^2}/_{s^2}$ as depicted from Fig. 5.17. The turbulence is very less in case of model 3 and so as the turbulent kinetic energy. Turbulent kinetic energy is almost constant with a minimum value throughout the L-shape from the groove outlet towards the outer boundaries except at very few points at the outer most boundaries where the turbulent kinetic energy value is high. The minimum value is $1.100 \times 10^{-1}\ {}^{m^2}/_{s^2}$ and maximum value is $1.172 \times 10^{6}\ {}^{m^2}/_{s^2}$ as shown in Fig. 5.18.

5.2.7 Turbulent Eddy Dissipation Profile

Turbulent eddy dissipation gives the quantitative measurement of the turbulence. Figs. 5.19, 5.20 and 5.21 represent the profiles of turbulent eddy dissipation for models 1, 2 and 3 respectively.

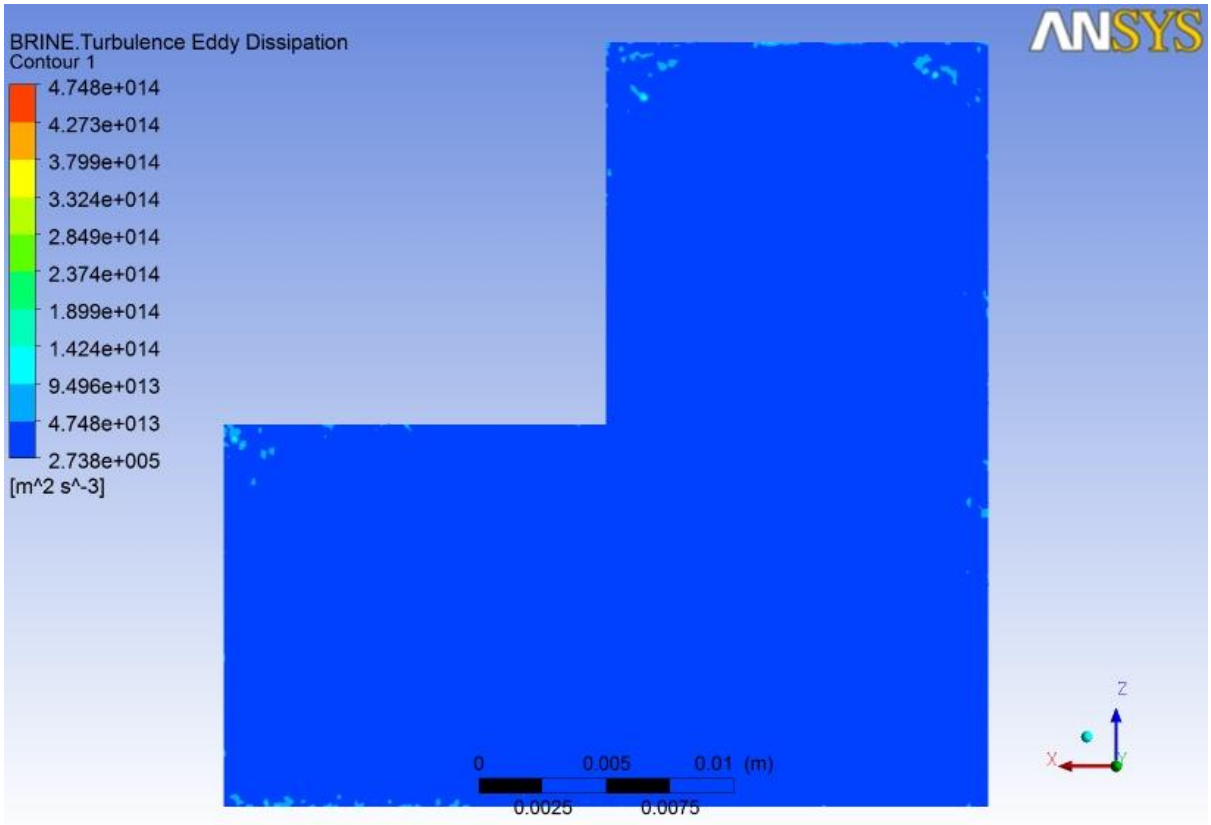

Fig. 5.19: Turbulent eddy dissipation contour for model 1

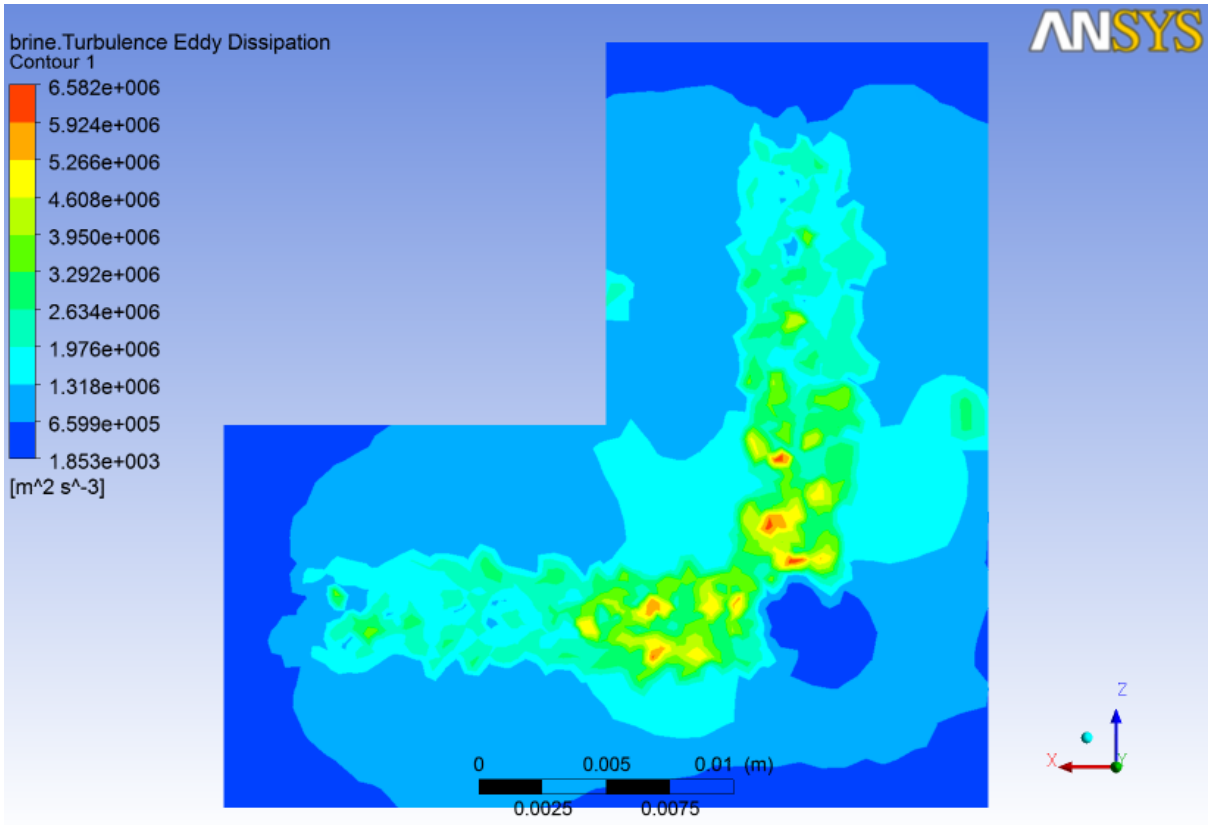

Fig. 5.20: Turbulent eddy dissipation contour for model 2

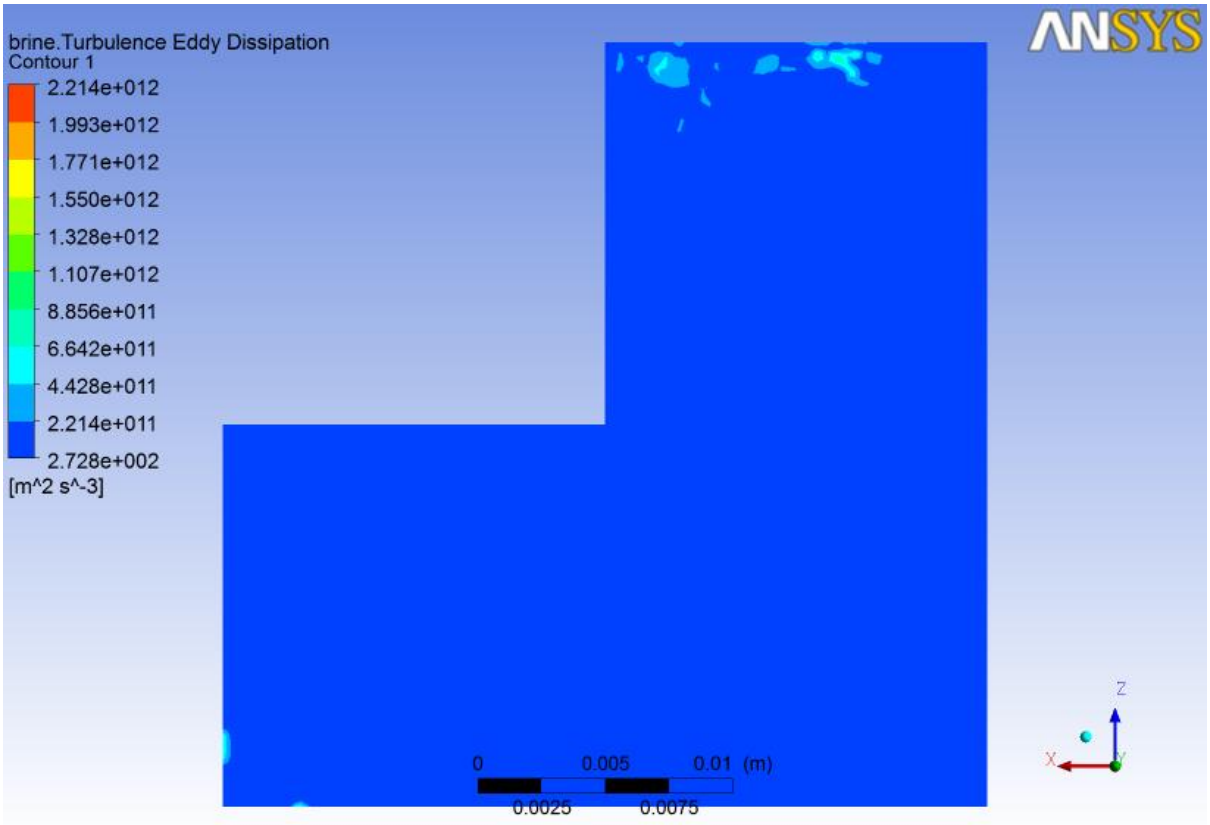

Fig. 5.21: Turbulent eddy dissipation contour for model 3

For model 1, as shown in Fig. 5.19, the value of turbulent eddy dissipation is very less near the groove outlet and has higher value at the boundaries. The minimum value of turbulent eddy dissipation is $2.738 \times 10^{5}\ {}^{m^2}/_{s^3}$ and maximum value is $4.748 \times 10^{14}\ {}^{m^2}/_{s^3}$ for model 1.

For model 2, the minimum value of turbulent eddy dissipation exists near the groove outlet. But, its value suddenly increases at the surrounding of the groove near the slot. However, at the extreme boundary, the value again reduces. The minimum value of turbulent eddy dissipation is $1.853 \times 10^{3}\ {}^{m^2}/_{s^3}$ and maximum value is $6.582 \times 10^{6}\ {}^{m^2}/_{s^3}$ for model 2 as shown in Fig. 5.20. For model 3, the value of turbulent eddy dissipation is the least among all the models. This value remains almost constant at $2.728 \times 10^{2}\ {}^{m^2}/_{s^3}$ which is the minimum value and only has a higher value of $6.642 \times 10^{11}\ {}^{m^2}/_{s^2}$ at few points near the extreme boundaries as shown in Fig. 5.21.

5.2.8 Heat Flux Pattern

Heat is generated in the IEG due to joule's heating. By appropriately designing tool shape, the heat generated and thus the overheating can be avoided. The figures 5.22, 5.23 and 5.24 describe the heat flus pattern for the models 1, 2 and 3 respectively.

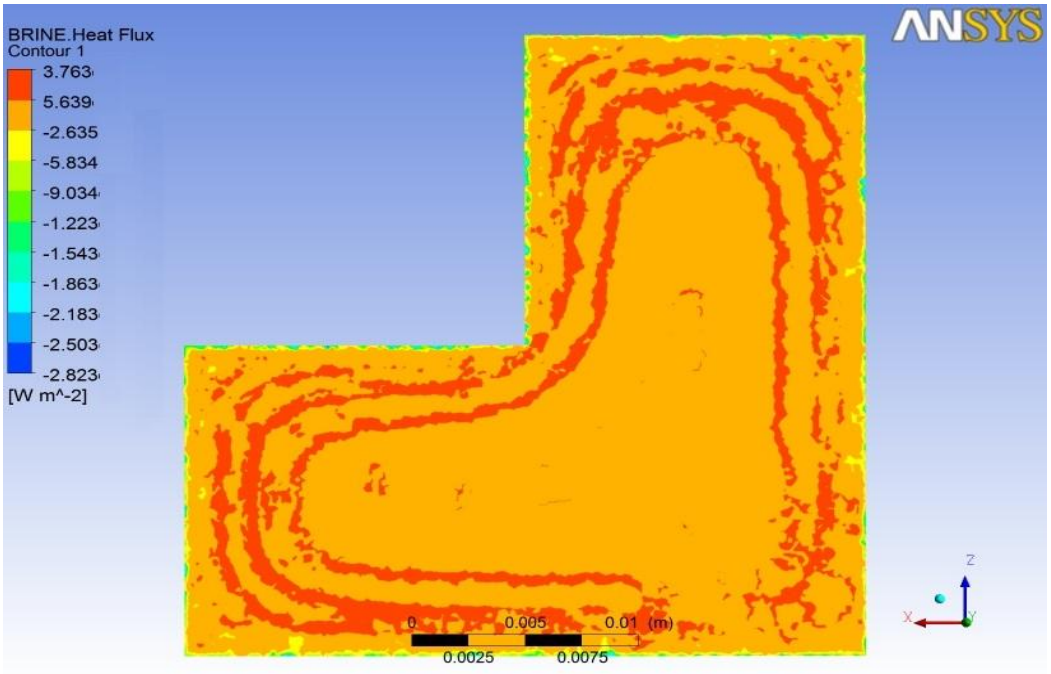

Fig. 5.22: Heat flux contour for model 1

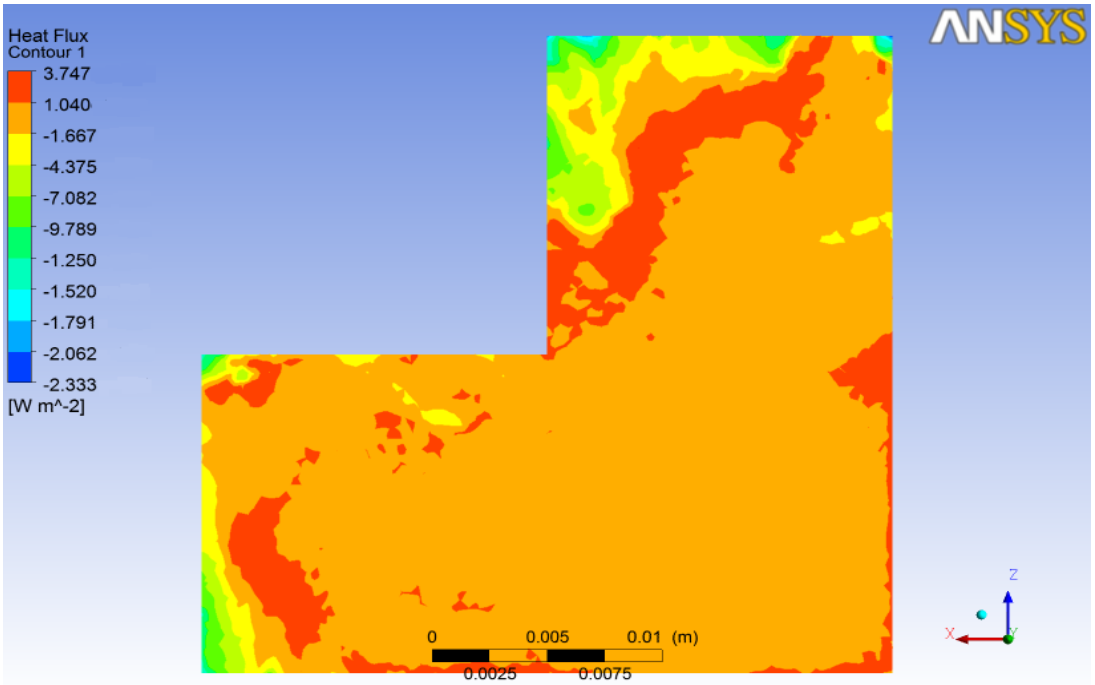

Fig. 5.23: Heat flux contour for model 2

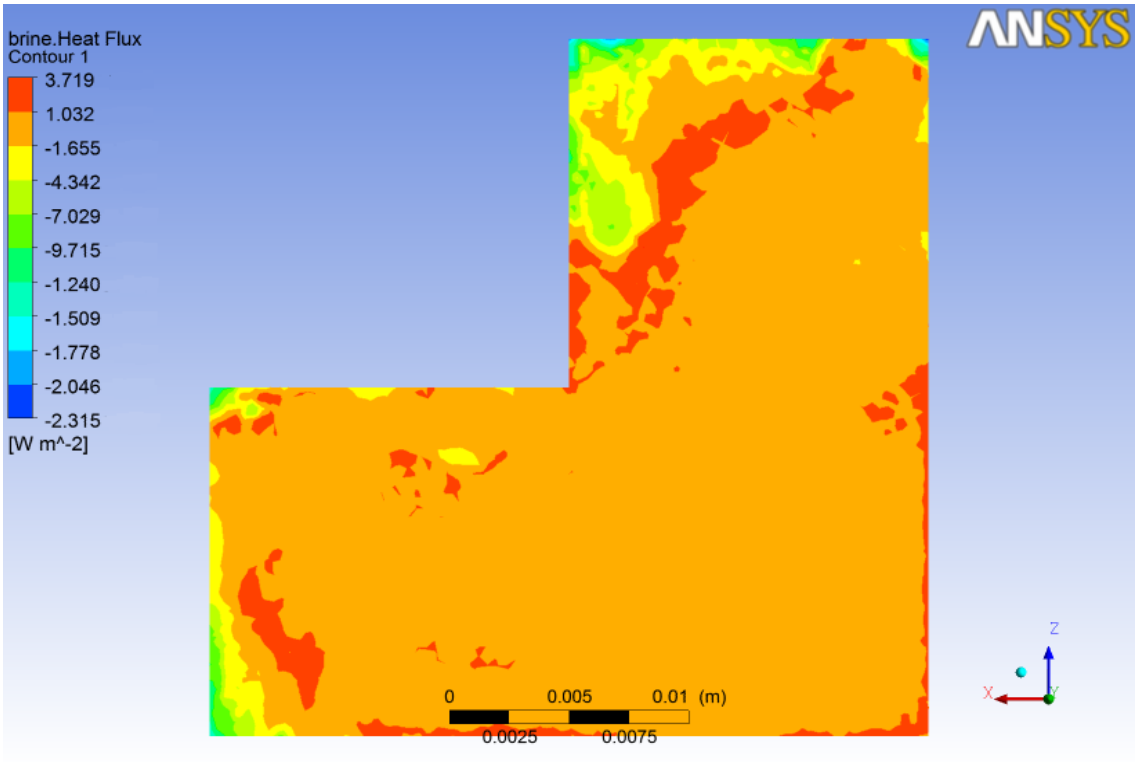

Fig. 5.24: Heat flux contour for model 3

In this simulation, we have assumed that the heat generated in the IEG is only due to Joule's heating. Heat flux is nothing but the heat generated per unit machining area. For model 1, the value is less near the groove outlet. But as we proceed towards the outer, the heat flux increases to a very high amount. This higher value of heat flux exists all over the outer boundary of L-shape in a comparatively larger area. The minimum amount of heat flux is $-2.823\ {}^{W}/_{m^2}$ and maximum amount is $3.763\ {}^{W}/_{m^2}$ for model 1 as depicted by the Fig. 5.22. Unlike the model 1, model 2 does not exhibit large amount heat flux except at fewer areas at the boundaries as shown in Fig. 5.23. The minimum value of heat flux is $-1.667\ {}^{W}/_{m^2}$ and maximum amount is $3.747\ {}^{W}/_{m^2}$ which indicates that there is very less chance of heat generation in model 2. Now, for model 3, which exhibit the least heat flux, the minimum heat flux value is $-1.655\ {}^{W}/_{m^2}$ and maximum value is $3.719\ {}^{W}/_{m^2}$ as shown by the Fig. 5.24. Hydrogen bubble generation is the reason for the high amount of heat flux. The area of the L-shape, where hydrogen bubble forms gives rise to higher resistance and in turn higher amount of heat as given by the Eq. 3.13.

5.3 EXPERIMENTAL RESULTS

5.3.1 Main Effect Plots

The main effect plots of MRR vs. V, MRR vs. F and MRR vs. C for all the three models obtained from MINITAB 16 are as shown in the Figs. 4.25, 4.26 and 4.27.

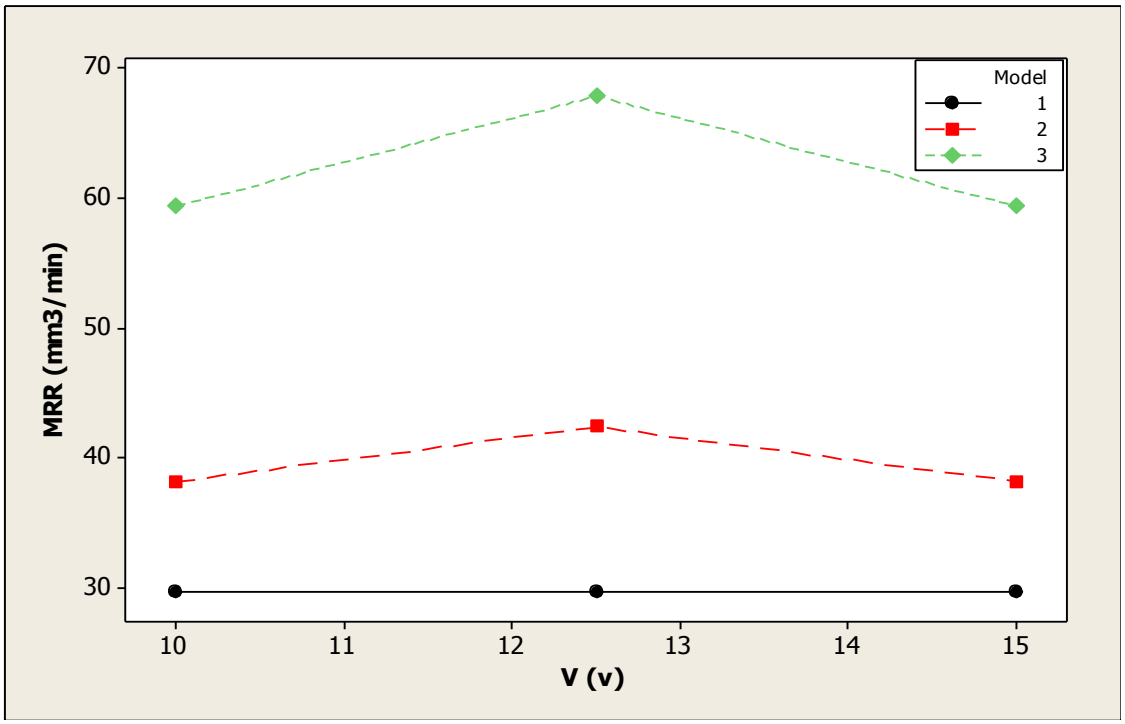

Fig. 5.25: Main effect plot of MRR vs. V

Here, from the main effect plot of MRR vs. V as shown in the Fig. 4.25, we can visualize that for Model 3, the MRR value is maximum, within the same range of voltage. From analysis of ANOVA, we found that V1 i.e. the voltage for model 1 is insignificant factor, whereas V2 and V3 has significance for the response MRR. So, from this plot we can conclude that Model 3 is the best Model in terms of MRR. This result obtained from MINITAB 16 is coming consistent with the results obtained from the simulation with the help of ANSYS 13.0 CFX as in both the cases we are getting, Model 3 as the best Model.

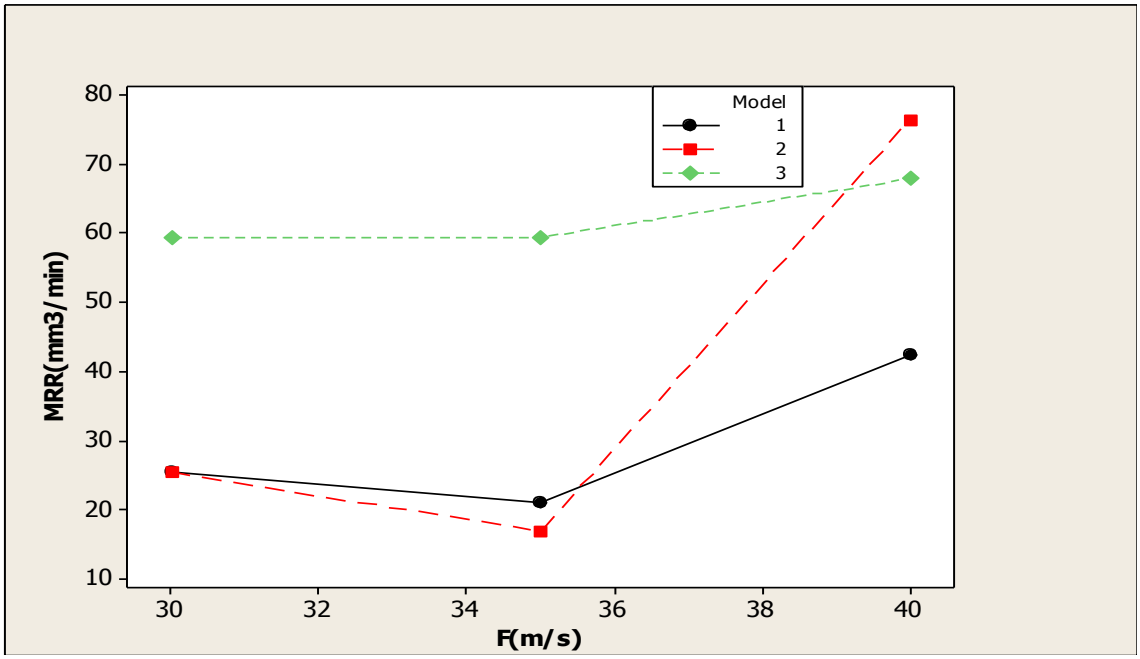

Fig. 5.26: Main effect plot of MRR vs. F

The main effect plot of MRR vs. F indicates the effect of flow rate on MRR for all the three Models. It shows that MRR is highest for Model 3 up to a flow rate of 39 m/s, after which the MRR of Model 2 increases than Model 3. Also, from the ANOVA table, we have found that F2 i.e. the flow rate for Model 2 is significant factor. This plot also comes in consistent with our simulation predicting that Model 3 is the best Model.

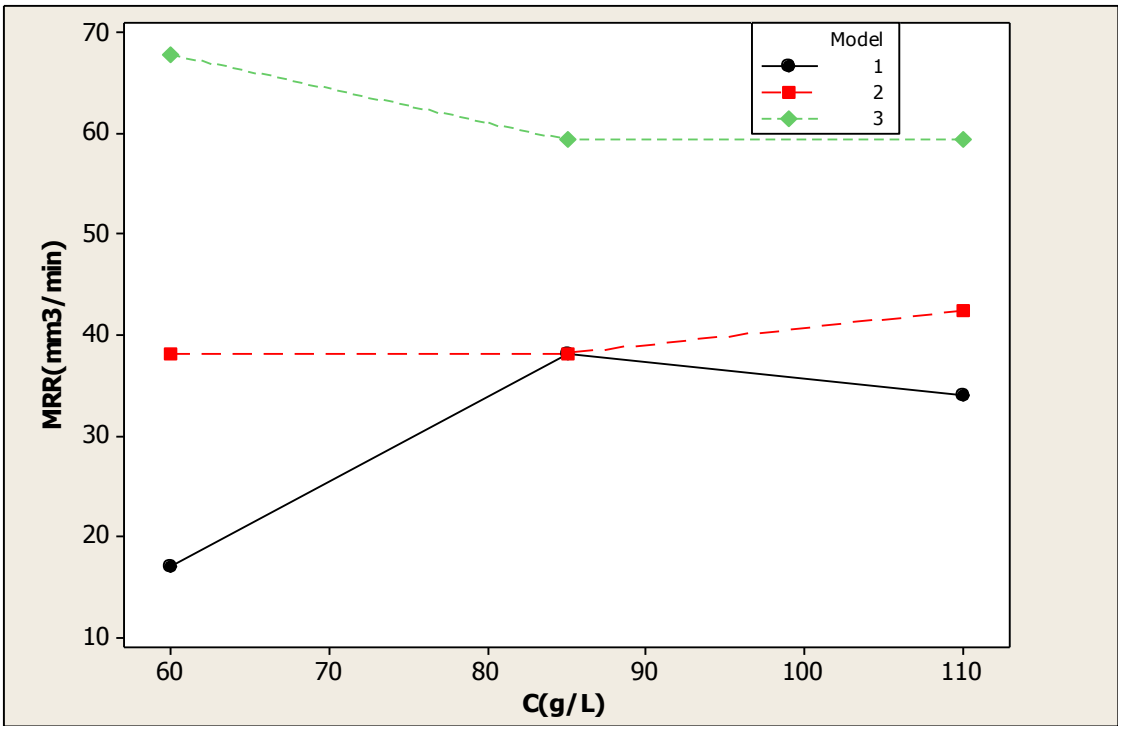

Fig. .27: Main effect plot of MRR vs. C

The main effect plot of MRR vs. C indicates the effect of electrolyte concentration on MRR. It is found that, MRR is coming higher for Model 3, but its value goes on decreasing after we increase the concentration. This erratic result may be due to the overheating of machine or due to the impurities present in the electrolyte solution as we had not taken fresh solution for each Model. So, it also indicates that Model 3 is the Best model giving higher MRR.

5.4 SUMMARY

All the critical parameters in the IEG were presented for all the Models. These parameters include volume fraction of brine, interphase mass transfer, velocity profile, pressure profile, temperature profile, turbulent kinetic energy profile, turbulent eddy dissipation profile and heat flux contour. The experimental results were also presented through the main effect plots of MRR vs. V, MRR vs. F and MRR vs. C.

CHAPTER 6

CONCLUSION

6.1 INTRODUCTION

Three dimensional two phase flow pattern analysis of electrochemical machining with L-shaped tool provides fundamental idea of velocity distribution, pressure pattern, temperature profile, turbulence etc. in the IEG. A cylindrical Iron work-piece, L-shaped Copper tool and 20% brine solution as electrolyte was considered in this analysis. Three tools with different slot designs were modelled using Design Modeller of ANSYS 13.0 CFX and subsequently analysed. To get consistent and good results, all the three Models were meshed with Fine mesh resolution. All models are analysed with inlet velocity of 40 m/s and with a residual target of1×10^{-4}. To validate the simulated result, experimentation was carried out in ECM by fabricating the three tool Models with the same dimension as in simulation. The experimental results were then analysed by using MINITAB 16 software.

6.2 MAJOR CONCLUSIONS DRAWN

1. Volume fraction profile for brine indicates that more hydrogen bubbles are generated in Model 1 and 2 whereas this tendency reduces in Model 3.
2. The velocity profile in Model 3 doesn't exhibit any inconsistency and remains constant throughout. Whereas, Model 1 and 2 indicate very high value at the outer side of groove due to the turbulence created because of the generation of hydrogen bubbles.
3. Pressure profile of Model 1 describes the pressure in the machining area and it has randomly generated high pressure spots throughout the machining area except at groove outlet because of the cavitation effect at the points of hydrogen bubbles generation. In Model 2, pressure variation is much less throughout the machining area except at the outer most boundaries. But Model 3 doesn't exhibit any variation and the pressure value remains uniform throughout.
4. Similarly, temperature pattern for Model 1 indicates boiling effect in the machining area resulting in the generation of hydrogen bubbles. Whereas, this effect reduces for Model 2 and 3. Model 3 exhibits a more uniform temperature throughout.

5. Turbulent kinetic energy and turbulent eddy dissipation energy profile exhibits higher value of turbulence for Model 1 and 2 whereas Model 3 has almost negligible turbulence.
6. Heat flux pattern has higher value for Model 1 and 2 and less value for Model 3 indicating that very less amount of heat generated in Model 3.
7. From the experimental analysis, it is observed that the MRR is higher with Model 3 than the other two models.
8. Hence, from the computational simulation and the experimental analysis, it was established that Model 3 is the best tool design.

6.3 SCOPE FOR FUTURE WORK

1. There is a future scope for the simulation by applying tool motion.

2. Three phase flow analysis (brine solution, hydrogen bubbles and metal precipitation) is another area of research in future.

REFERENCES

[1] Tsuboi, R. and Yamamoto, M. (2009) Modeling and applications of electrochemical machining process. *Proceedings of the ASME International Mechanical Engineering Congress & Exposition IMECE,* November 13-19, Lake Buena Vista, Florida, USA.

[2] Baburaj, M. CFD analysis of flow pattern in electrochemical machining for L-shaped tool. *M.Tech project report(2012).* National Institute of Technology, Rourkela, Odisha, India.

[3] Neto, J., Silva, E. and Silva, M. (2006) Intervening variables in electrochemical machining. *Journal of Materials Processing Technology,* Vol. 289, pp. 92-96.

[4] Mukherjee, S.K., Kumar, S., Srivastava, P.K. and Kumar, A. (2008) Effect of valency on material removal rate in electrochemical machining of aluminium. *Journal of materials processing technology,* Vol. 202, pp. 398-401.

[5] Jain, V.K., Kanetkar, Y. and Lal, G.K. (2005) Stray current attack and stagnation zones in electrochemical drilling. *International journal of advanced manufacturing technology,* Vol. 26, pp. 527-536.

[6] Davydov, A.D., Shaldaev, V.S., Malofeeva, A.N. and Savotin, I.V. (1997) Electrochemical dissolution of tungsten under pulsed conditions. *Journal of applied electrochemistry,* Vol. 27, pp. 351-354.

[7] Bilgi, D.S., Kumar, R., Jain, V.K. and Shekhar, R. (2008) Predicting radial overcut in deep holes drilled by shaped tube electrochemical machining. *International journal of advanced manufacturing technology,* Vol. 39, pp. 47-54.

[8] Hocheng, H., Sun, Y.H., Lin, S.C. and Kao, P.S. (2003) A material removal analysis of electrochemical machining using flat-end cathode. *Journal of Materials Processing Technology,* Vol. 140, pp. 264–268.

[9] Clifton, D., Mount, A.R., Alder, G.M. and Jardine, D. (2002) Ultrasonic measurement of the inter-electrode gap in electrochemical machining. *International Journal of Machine Tools & Manufacture*, Vol. 42, pp. 1259–1267.

[10] Smets, N., Damme, S.V., Wilde, D.D., Weyns, G. and Deconinck, J. (2009) Time-averaged concentration calculations in pulse electrochemical machining, spectral approach. *Journal of applied electrochemistry*, Vol. 39, pp. 2481-2488.

[11] Pa, P.S. (2007) Design of effective plate-shape electrode in ultrasonic electrochemical finishing. *International journal of advanced manufacturing technology*, Vol. 34, pp. 70-78.

[12] Zhitnikov, V.P., Fedorova, G.I., Sherykhalina, N.M. and Urakov, A.R. (2006) Numerical investigation of non-stationary electrochemical shaping based on an analytical solution of the Hele-Shaw problem. *Journal of engineering mathematics*, Vol. 55, pp. 255-276.

[13] Ramasawmy, H. and Blunt, L. (2007) Investigation of the effect of electrochemical polishing on EDM surfaces. *International journal of advanced manufacturing technology*, Vol. 31, pp. 1135-1147.

[14] Filatov, E.I. (2001) The numerical simulation of the unsteady ECM process. *Journal of Materials Processing Technology*, Vol. 109, pp. 327-332.

[15] Mount, A.R., Clifton, D., Howarth, P. and Sherlock, A. (2003) An integrated strategy for materials characterisation and process simulation in electrochemical machining. *Journal of Materials Processing Technology*, Vol. 138, pp. 449–454.

[16] Kozak, J (1998) Mathematical models for computer simulation of electrochemical machining processes. *Journal of Materials Processing Technology*, Vol. 76, pp. 170-175.

[17] Kozak, J., Chuchro, M., Ruszaj, A. and Karbowski, K. (2000) The computer aided simulation of electrochemical process with universal spherical electrodes when machining sculptured surfaces. *Journal of Materials Processing Technology*, Vol. 107, pp. 283-287.

[18] Purcar, M., Bortels, L., Bossche, B.V. and Deconinck, J. (2004) 3D electrochemical machining computer simulations. *Journal of Materials Processing Technology*, Vol. 149, pp. 472–478.

[19] Bortels, L., Purcar, M., Bossche, B.V. and Deconinck, J. (2004) A user-friendly simulation software tool for 3D ECM. *Journal of Materials Processing Technology*, 149, PP. 486–492.

[20] Pattavanitch, J., Hinduja, S. and Atkinson, J. (2010) Modelling of the electrochemical machining process by the boundary element method. *CIRP Annals - Manufacturing Technology*, Vol. 59, pp. 243–246.

[21] Labib, A.W., Keasberry, V.J., Atkinson, J. and Frost, H.W. (2011) Towards next generation electrochemical machining controllers: A fuzzy logic control approach to ECM. *Expert Systems with Applications*, Vol. 38, pp. 7486–7493.

[22] Hewidy, M.S., Ebeid, S.J., El-Taweel, T.A. and Youssef, A.H. (2007) Modelling the performance of ECM assisted by low frequency vibrations. *Journal of Materials Processing Technology*, Vol. 189, pp. 466–472.

[23] Ratkovich, N., Chan, C.C.V., Berube, P.R. and Nopens, I. (2009) Experimental study and CFD modelling of a two-phase slug flow for an airlift tubular membrane. *Chemical Engineering Science*, Vol. 64, pp. 3576 – 3584.

[24] Conner, M.E., Baglietto, E. and Elmahdi, A.M. (2010) CFD methodology and validation for single-phase flow in PWR fuel assemblies. *Nuclear Engineering and Design*, Vol. 240, pp. 2088–2095.

[25] Frank, T., Zwart, P.J., Krepper, E., Prasser, H.M. and Lucas, D. (2008) Validation of CFD models for mono- and polydisperse air–water two-phase flows in pipes. *Nuclear Engineering and Design*, Vol. 238, pp. 647–659.

[26] Li, X.G., Liu, D.X., Xu, S.M. and Li, H. (2009) CFD simulation of hydrodynamics of valve tray. *Chemical Engineering and Processing*, Vol. 48, pp. 145–151.

[27] Gerogiorgis, D.I. and Ydstie, B.E. (2005) Multiphysics cfd modelling for design and simulation of a multiphase chemical reactor. *Chemical Engineering Research and Design,* Vol. 83(A6), pp. 603–610.

[28] Kasat, G.R., Khopkar, A.R., Ranade, V.V. and Pandit, A.B. (2008) CFD simulation of liquid-phase mixing in solid--liquid stirred reactor. *Chemical Engineering Science,* Vol. 63, pp. 3877-3885.

[29] Mimouni, S., Boucker, M., Lavieville, J., Guelfi, A. and Bestion, D. (2008) Modelling and computation of cavitation and boiling bubbly flows with the NEPTUNE CFD code. *Nuclear Engineering and Design,* Vol. 238, pp. 680–692.

[30] Prasser, H.M. (2008) Novel experimental measuring techniques required to provide data for CFD validation. *Nuclear Engineering and Design,* Vol. 238, pp. 744–770.

[31] Schepper, S.C.K., Heynderickx, G.J. and Marin, G.B. (2008) CFD modeling of all gas–liquid and vapor–liquid flow regimes predicted by the Baker chart. *Chemical Engineering Journal,* Vol. 138, pp. 349–357.

[32] Vallee, C., Hohne, T., Prasser, H.M. and Suhnel T. (2008) Experimental investigation and CFD simulation of horizontal stratified two-phase flow phenomena. *Nuclear Engineering and Design,* Vol. 238, pp. 637–646.

[33] Wang, G., Yang, Y., Zhang, H. and Xia, W. (2007) 3-D model of thermo-fluid and electrochemical for planar SOFC. *Journal of Power Sources,* Vol. 167, pp. 398–405.

[34] Yun, B.J., Splawski, A., Lo, S. and Song, C.H. (2011) Prediction of a subcooled boiling flow with advanced two-phase flow models. *Nuclear Engineering and Design.* doi:10.1016/j.nucengdes.2011.08.067.

[35] Zahab, Z.E., Divo, E. and Kassab, A.J. (2009) A localized collocation meshless method (LCMM) for incompressible flows CFD modeling with applications to transient hemodynamics. *Engineering Analysis with Boundary Elements,* Vol. 33, pp. 1045–1061.

[36] Mcclesky, R.B. (2011). Electrical Conductivity of Electrolytes Found In Natural Waters from (5 to 90) °C. *Journal of Chemical and Engineering data*, Vol. 56, pp. 317-327.

[37] Sian, S. CFD analysis of flow pattern in electrochemical machining. *B.Tech. Project Report (2011),* National Institute of Technology Rourkela, Odisha, India.